USGS
science for a changing world

Geologic Map of Oldonyo Lengai (Oldoinyo Lengai) Volcano and Surroundings, Arusha Region, United Republic of Tanzania

By David R. Sherrod, Masota M. Magigita, and Shimba Kwelwa

Pamphlet to accompany
Open-File Report 2013-1306

2013

U.S. Department of the Interior
U.S. Geological Survey

U.S. Department of the Interior
SALLY JEWELL, Secretary

U.S. Geological Survey
Suzette M. Kimball, Acting Director

U.S. Geological Survey, Reston, Virginia: 2013

For product and ordering information:
World Wide Web: http://www.usgs.gov/pubprod
Telephone: 1-888-ASK-USGS

For more information on the USGS—the Federal source for science about the Earth,
its natural and living resources, natural hazards, and the environment:
World Wide Web: http://www.usgs.gov
Telephone: 1-888-ASK-USGS

Suggested citation:
Sherrod, D.R., Magitita, M.M., and Kwelwa, S., 2013, Geologic map of Oldonyo Lengai (Oldoinyo Lengai) and surroundings, Arusha Region, United Republic of Tanzania: U.S. Geological Survey Open-File Report 2013-1306, pamphlet 65 p., 1 sheet, scale 1:50,000, with GIS database, *http://dx.doi.org/10.3133/ofr20131306*.

ISSN 2331-1258

Contents

Figures

Tables

Geologic Map of Oldonyo Lengai (Oldoinyo Lengai) Volcano and Surroundings, Arusha Region, United Republic of Tanzania

By David R. Sherrod[1], Masota M. Magigita[2], and Shimba Kwelwa[3]

Introduction

Described herein is the geology of Oldonyo Lengai volcano and the southernmost Lake Natron basin, a part of the East African rift system (fig. 1). Rift-related volcanism has proceeded southward as the African continent is being torn into the Nubian and Somalian plates, west and east respectively. Rifting commenced in Ethiopia about 30 Ma, in Kenya about 12 Ma, and began in northern Tanzania only about 8 Ma (summarized in Dawson, 1992; Dawson, 2008, chap. 1). The vast rift basins have also been centers for sedimentation. Modeling of GPS and oceanic plate motions suggest the Somalian plate is moving eastward relative to the Nubian plate at about 6–7 mm per year in the Ethiopian rift segment. The rate diminishes to about 2–3 mm per year in the Gregory rift segment and the area of the Lake Natron basin (fig. 1; Stamps and others, 2008).

The southern Lake Natron basin lies between Gelai volcano to the east and a major range-bounding fault system of the East African rift to the west (figs. 2, 3). The basin's best-known geographic feature, however, is Oldonyo Lengai, an active explosive volcano that erupted most recently in 2007–08 (fig. 3*B*). The volcano, prominently visible throughout the basin, is famous for its sporadic eruptions of carbonatite, an unusual CO_2-laden lava.

This explanatory pamphlet discusses several features of stratigraphy and structure in the map area, proceeding generally from oldest to youngest. The topical treatment is uneven owing to the variable detail uncovered in our reconnaissance mapping and the level of knowledge extant in other publications. Our goal is to place our findings into the framework of previous investigations while highlighting gaps in knowledge. In this way questions are raised and challenges proposed to future workers. Additional information about the making of the map is found in appendix 1. Our use of geographic names is discussed in appendix 2.

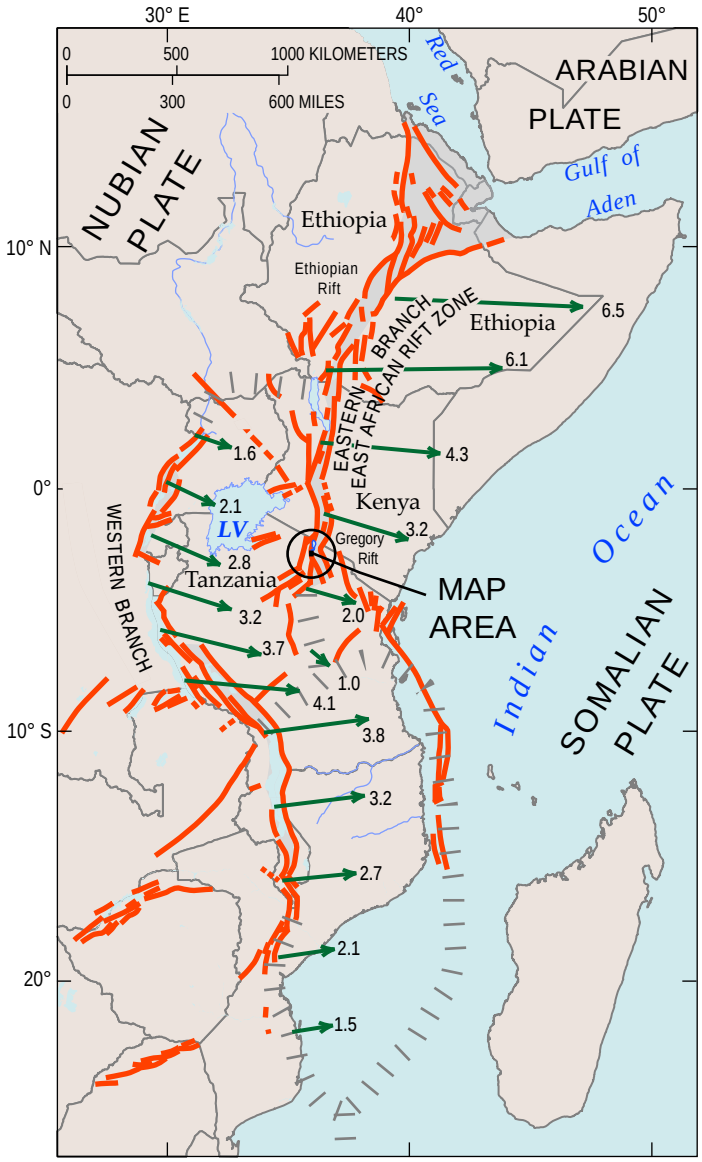

Figure 1. East African rift zone. Structural grain shown by Miocene to Holocene faults (red lines, from Chorowicz and Sorlien, 1992) Hachured gray lines show inferred boundaries of two microplates, Victoria and Rovuma (from Stamps and others, 2008). Axial depressions emphasized by gray shading along eastern branch of the rift zone, whereas deep rift-zone lakes provide same effect along western branch. Modeled plate velocity vectors (green arrows, scaled proportionately) show motion, in millimeters per year, of the Somalian plate relative to the Nubian plate (Stamps and others, 2008). Oldonyo Lengai lies in the Gregory rift of the East African rift zone's eastern branch, just south of the Kenya-Tanzania border 280 km southeast of Lake Victoria (LV, broad lake near center of map). Mercator conformal projection.

Brief Geologic History of the Southernmost Lake Natron Basin

Setting the Stage

The Lake Natron basin has a protracted history of volcanism, sedimentation, and faulting. Within the map area, sedimentary deposits began accumulating before about 2 million years

[1]U.S. Geological Survey, 1300 SE Cardinal Court, Vancouver, WA 98683, USA
[2]Geological Survey of Tanzania, P.O. Box 903, Dodoma, United Republic of Tanzania
[3]Department of Geology, University of Dar es Salaam, P.O. Box 35091, Dar Es Salaam, United Republic of Tanzania; now at Mineral Resources Institute, P.O. Box 1696, Dodoma, Tanzania

ago (mega-annums, Ma). These deposits, where exposed in the Natron escarpment (mapping of Isaac, 1967), are entirely Quaternary in age. They grade upward from the deltaic Humbu Formation to lake deposits of the Moinik Formation. Their extent indicates a much larger ancestral Lake Natron. Radiometric ages from these stratigraphic units indicate the Humbu and Moinik Formations were deposited between about 1.8 and 1.1 Ma (Isaac and Curtis, 1974; Foster and others, 1997; Manega, 1993). Little is known about the full extent of ancient Lake Natron, some part of which likely extended east and south of the map area but is now buried by Gelai volcano and younger volcanic rocks.

Renewed faulting along the Natron fault after about 1.1 Ma created the major escarpment that bounds the southernmost Lake Natron basin today (Macintyre and others, 1974; Foster and others, 1997). Kerimasi volcano, which forms the south end of the Lake Natron basin, is built against this escarpment and appears only little faulted. Gelai volcano, on the east side of the basin, probably was active about 1.0 Ma (Evans and others, 1971).

Displacement across the Natron fault in the map area is at least 600 m, simply to account for the topographic relief between range front and valley floors north and south of Oldonyo Lengai. Total offset is larger, and the basin floor is buried by infilling sedimentary and volcanic rocks. Farther north, the fill in the Lake Natron basin may be as thick as 1.6 km on the basis of Bouguer gravity anomalies (Ebinger and others, 1997).

Enter the Youngest Volcano

It is in this geographic setting where Oldonyo Lengai, Tanzania's most active volcano of the past several thousand years, built its volcanic edifice. Oldonyo Lengai is a steep-sided stratovolcano, with most eruptions centered near the present-day summit. Consequently the volcano is fairly symmetrical. Dotting the lower flanks are a few tephra cones and tuff rings, some of which presumably are related to the magmatic system that has built Oldonyo Lengai.

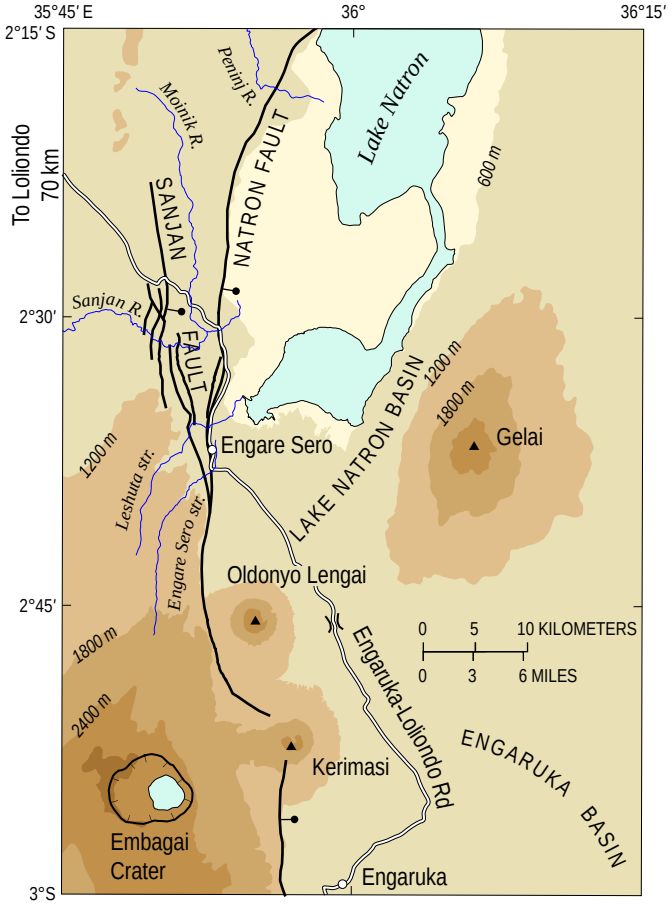

Figure 2. Geographic setting of southern Lake Natron basin and adjacent terrain. Tint depicts land altitudes in 600-m intervals. Ball-and-bar shows downthrown side of fault. Base from 1:50,000-scale topographic quadrangle maps of the Tanzania Division of Lands and Surveys: Binini (27/4), 1966; Gelai (40/1), 1990; Kitumbeine West (40/3), 1990; Lake Natron East (28/3), 1990; Mosonik (38/2), 1990; and Oldonyo Lengai (39/4), 1990.

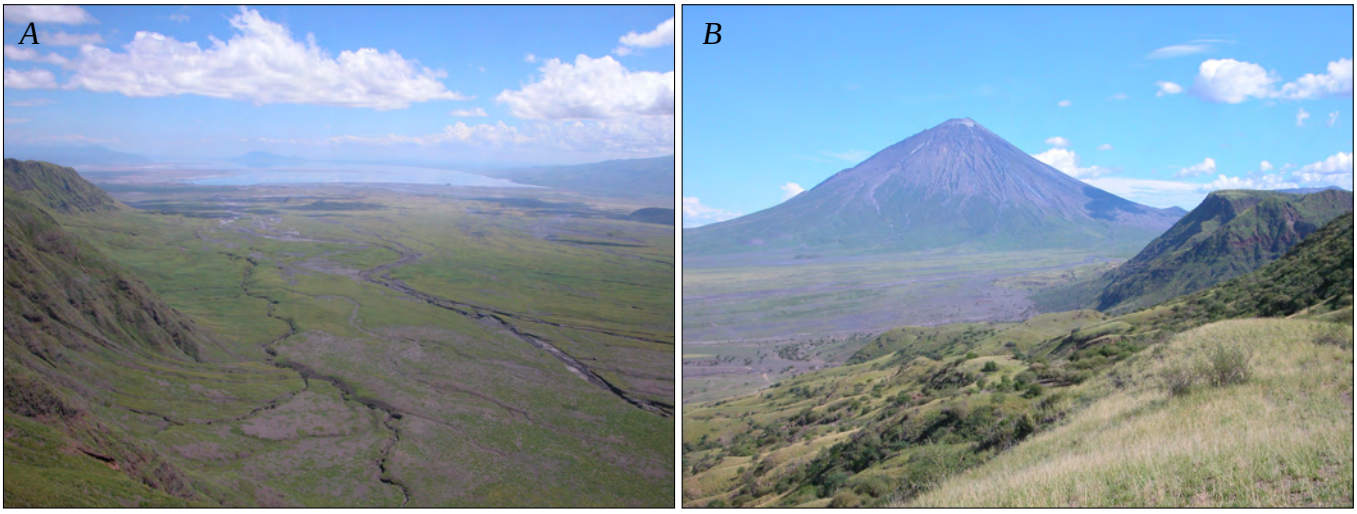

Figure 3. Southernmost Lake Natron basin. *A*, View northeast along rift basin from Natron escarpment west of Oldonyo Lengai. Lake Natron shimmers 20 km in distance. Cloud shadows in middle ground are in area of extensive debris-avalanche deposits. Photo 0077, March 17, 2010. *B*, View south-southeast to Oldonyo Lengai, 17 km distant, from above Engare Sero village. Natron escarpment on right (west). Photo 7680, March 7, 2010.

Oldonyo Lengai's eruptions are chiefly explosive, producing fallout tephra, pyroclastic flows, and lahars. Lava flows form less than 10 percent of the exposed cone, to judge from the geologic map by Dawson (1962), and lava domes are absent. Oldonyo Lengai is moderately incised; typical exposures are 30–50 m deep in gullies around the volcano's flanks. The east and southeast flanks are slightly more deeply incised than the other flanks, in part because the southern summit crater has been inactive for at least the past 100 years but also because prevailing winds favor the deposition of fallout tephra onto the west and northwest flanks. Maximum depth of exposure is about 300 m in the Eastern Chasm, a large landslide scar on the east flank.

Beyond the main cone, Oldonyo Lengai's debris has been shed mostly northward toward Lake Natron, because volcanic and tectonic highlands hem in the volcano on its other sides. Runoff during seasonally intense rain reworks all this material downslope toward Lake Natron, sporadically eroding and aggrading a broad floodplain.

Debris-Avalanche Deposits

Volcanologists who cross into the Lake Natron basin recognize immediately the hummocky terrain north of Oldonyo Lengai as an indicator of one or more large debris avalanches that likely originated by partial collapse of the volcano in the past. Debris-avalanche deposits extend 24 km northward from Oldonyo Lengai, reaching the shore of Lake Natron and along the foot of the escarpment west of it. Indeed, much of the southern lake basin is surfaced today by debris-avalanche deposits. The village of Engare Sero, 17 km from the volcano's summit, sits atop these debris-avalanche deposits.

Stratigraphic and Structural Features of the Natron Escarpment

Natron Escarpment and Area West of It Expose Oldest Rocks in Map Area

Lava flows in the Natron escarpment and, farther west, the partly buried Mosonik volcano, are the oldest rocks in the map area, probably all younger than 5 Ma. East of the escarpment, volcanic and sedimentary deposits younger than 1 Ma bury the southern part of the Natron basin.

Mosonik Volcano

Mosonik is a stratovolcano formed mostly of volcaniclastic strata (Dawson, 2008, chap. 7). Its composition ranges from basanite to nephelinite (fig. 4 and table 1; Guest and others, 1961; Paslick and others, 1996). Minor carbonatite dikes and breccia are also reported (M.S. Garson in Dawson, 2008, chap. 7).

We mapped and sampled only the eastern edge of Mosonik, where its deposits dip beneath younger strata along a north-trending reach of Leshuta stream, west of the Natron fault (see geologic map). The Mosonik beds (unit Tmv) are volcaniclastic in that area, composed of pyroxene-bearing phonotephrite clasts within a devitrified ashy matrix. Many beds are monolithologic or nearly so, giving us some confidence that the clasts sampled for chemical analysis are representative of magma erupted from Mosonik and not the reworked detritus of other volcanoes. The matrix has undergone a pervasive, secondary alteration to reddish-brown indurated clay.

A few streaky nonvesicular lava flows(?) are layered concordantly with the volcaniclastic beds in the Leshuta stream exposures. The area is cut by a nexus of faults, however, and the lava may have been emplaced as sills. Matrix oxidation of the enclosing volcaniclastic beds precluded the use of baked horizons as a criterion for judging whether the "lava" was emplaced as flows or intrusions, although the absence of vesiculation may be evidence for sills. The lava lacks associated flow breccia such as characterizes ʻaʻā.

The age of Mosonik volcanic beds is known only by reference to nephelinite lava flows north and northeast of the volcano's topographic center (unit Tnnm). Ages from these lava flows are 3.53±0.06 and 3.26±0.08 Ma (Isaac and Curtis, 1974; and Manega, 1993, respectively). As mapped by Isaac (1967) and shown in the northwest corner of our map, these lava flows overlie a sequence of basalt at least 200 m thick, the Sambu and Hajaro Basalts, placing them high in that part of the stratigraphic section. In contrast, the Mosonik volcaniclastic strata we sampled, only 2–3 km south in Leshuta stream, are at the base of the exposed stratigraphic section. Geologic mapping of the intervening area (Guest and others, 1961) is too generalized to resolve the stratigraphic relation between Mosonik volcano and the dated nephelinite lava flows. With that correlation still uncertain, we consider the nephelinite lava age a minimum age for Mosonik volcano, 3.6 to 3.2 Ma, and the volcano may be substantially older.

Mosonik volcanic beds in Leshuta stream are overlain by a thick sequence of conglomerate (unit Tmc). The conglomerate is composed entirely of volcaniclastic cobbles, pebbles, sand, and silt that vary widely in textural diversity and composition. Intervening sandy layers contain abundant evidence for fluvial deposition.

Escarpment Volcanic and Sedimentary Rocks

The Natron escarpment, which overlooks Lake Natron, is the prominent north-trending range front in the map area. The escarpment formed by normal faulting along the Natron fault and, farther west, the Sanjan fault (fig. 2). These two faults converge in the area of Engare Sero village. Well-layered Tertiary and lower Quaternary volcanic rocks form most of the escarpment south of Engare Sero stream. Sedimentary beds increase in abundance northward and are locally predominant in the north part of the map area, where a sedimentary sequence that marks the early history of Lake Natron is found in the Humbu and Moinik Formations of the Peninj Group.

Volcanic Rocks

Lava flows predominate among the volcanic rocks. Sometimes referred to casually as flood lava, the escarpment lava flows (unit QTel) lack the vast extent or large volume that characterizes individual lava flows in flood-basalt provinces of the world. Instead, the escarpment lava flows likely issued from numerous scoria cones and short fissures and then spread across a few to tens of square kilometers. Such vent deposits are mapped in the escarpment sequence 6–7 km northwest of Oldonyo

Lengai (unit QTev). Although some vents in the province built shield volcanoes of moderate size (Gelai volcano to the east, or Oldonyo Sambu volcano 35 km north), in which the layering of lava flows steepens as the flows pile up, lava flows exposed in the escarpment are nearly flat lying. No major volcanic edifices are recognized among the escarpment exposures of the map area.

Mapped separately is the lava of Endukai Kiti, a sequence of near-vent deposits, lava flows, and fine-grained intrusions exposed at the base of the escarpment lava sequence on both sides of the Engare Sero canyon. These rocks are also known as the Waterfall sequence in the report of Neukirchen and others (2010), who mapped them and several other recognizable stratigraphic units on oblique-photo maps (Neukirchen and others, 2010). The waterfall, a popular scenic attraction low in the Engare Sero canyon, spills over the lava of Endukai Kiti.

The lava of Endukai Kiti is notable for being the oldest stratigraphic unit exposed along the face of the escarpment in the map area. We sought samples suitable for dating, but none were sufficiently fresh; thus no age relation is established for the lava of Endukai Kiti and the Mosonik volcanic beds.

Embalulu Sekenge

Embalulu Sekenge (Sekenge crater) is a tuff ring near the top of the escarpment west of Engare Sero village. It is 850–900 m in diameter and today has a depth of 30 m from lowest rim point

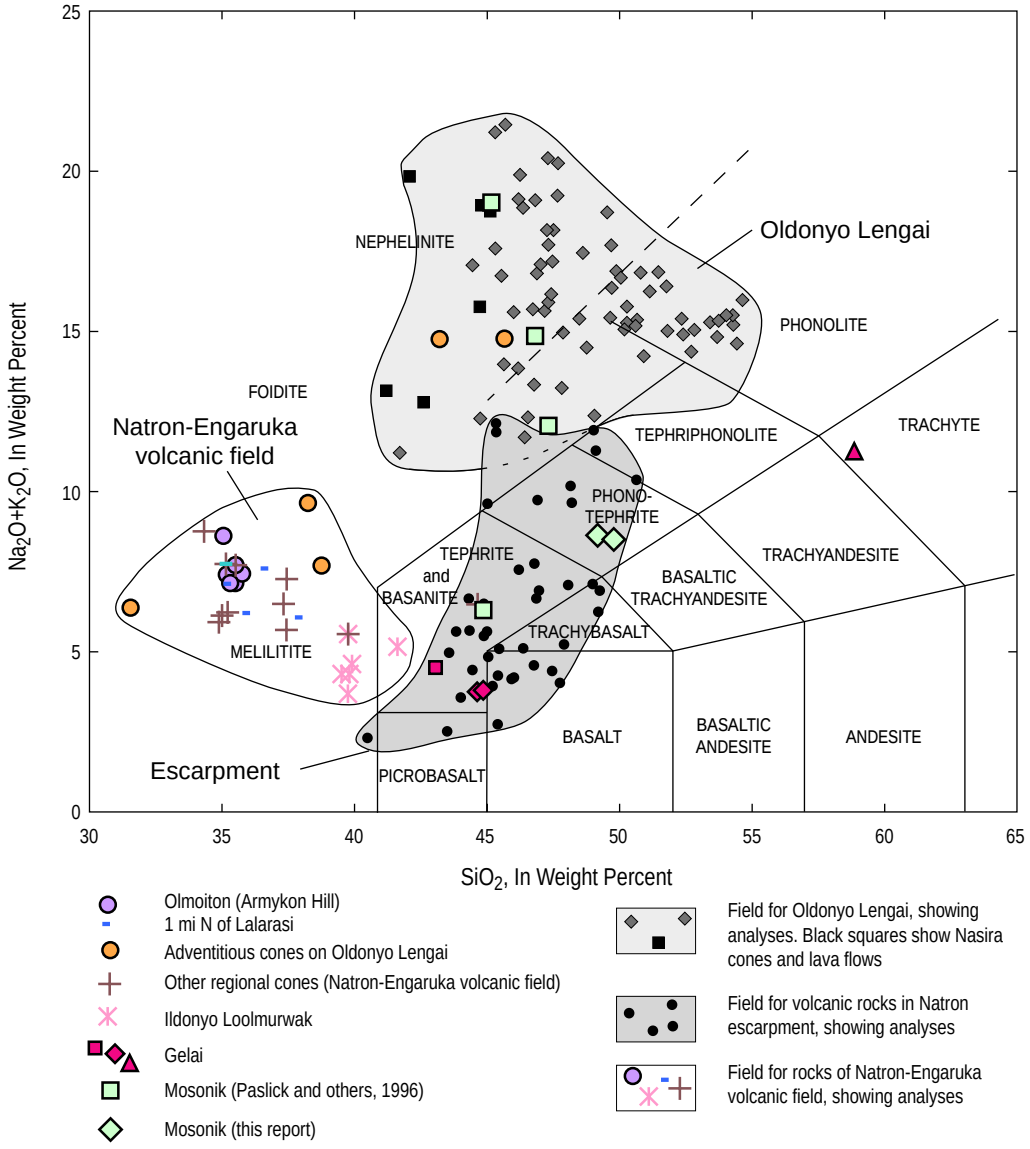

Figure 4. Alkali-silica (Na_2O+K_2O vs. SiO_2) diagram for the volcanic rocks of the southernmost Lake Natron basin and its margins. All analyses normalized to 100 percent, volatile free. Rock grid from Le Maitre (2002). Dashed line terminates the phonolite field against nephelinite (Klaudius and Keller, 2006) along approximately the same low-silica limit as that of Cox and others (1979, p. 14). See appendix 3 for information about analytical geochemistry used for this publication. Escarpment data from Neukirchen and others (2010) and F. Neukirchen (written commun., 2011). Oldonyo Lengai analyses from Donaldson and others (1987; 19 analyses), Peterson (1989; 6 analyses), Keller and Krafft (1990; 1 analysis); Keller and others (2006; 4 analyses), Klaudius and Keller (2006; 22 analyses), and this report (33 analyses).

Table 1. Whole-rock major and trace element chemical analyses from Mosonik and Gelai volcanoes.

[Dashes, no data. Major-element analyses are shown normalized to 100 percent, volatile free. FeO*, all iron as FeO. Also shown are original oxide totals and values for loss on ignition, for completeness. Data compiled and available in electronic spreadsheet format as part of this publication. References: 1, Paslick and others, 1996; 2, this report; 3, Guest, 1953, and Dawson, 2008 appendix 2. For analytical methods see source references or, for this report, appendix 3]

Table 1 No.	1	2	3	4	5	6	7	8	9	10
Volcanic center	Mosonik						Gelai			
Sample No.	MO93-1	MO93-3	MO93-5	MR93-2	S10-L196	S10-L195	JG923	S10-L161	G93-1	G93-2
Rock type	Foidite	Basanite	Foidite	Foidite	Phonotephrite	Phonotephrite	Trachyte	Tephrite	Tephrite	Tephrite
Reference	1	1	1	1	2	2	3	2	1	1
Major-element analyses, normalized water-free (weight percent)										
SiO_2	47.32	44.86	45.16	46.82	49.17	49.77	58.85	43.06	44.63	44.85
TiO_2	3.48	3.22	2.21	2.51	2.00	1.96	0.32	3.58	3.40	3.33
Al_2O_3	14.00	12.56	18.19	19.28	15.19	14.92	21.09	11.67	12.60	12.65
FeO*	11.84	11.87	8.77	9.58	12.15	11.99	4.91	14.91	13.72	13.47
MnO	0.48	0.21	0.34	0.35	0.21	0.19	0.47	0.22	0.23	0.22
MgO	2.40	7.74	1.33	1.50	4.10	3.99	0.80	9.74	9.45	9.40
CaO	7.86	12.46	4.44	4.70	7.98	8.12	2.29	11.67	11.47	11.54
Na_2O	9.13	4.48	12.63	10.06	5.36	4.76	7.59	3.34	2.68	2.71
K_2O	2.92	1.82	6.39	4.79	3.29	3.75	3.67	1.16	1.07	1.08
P_2O_5	0.56	0.77	0.54	0.39	0.56	0.56	0.00	0.65	0.76	0.73
Loss on ignition	5.84	4.36	0.64	4.44	3.72	5.25	2.10	2.46	1.49	1.64
Original oxide total	99.40	99.06	97.96	99.35	98.67	98.70	99.72	96.57	99.49	99.96
Trace-element analyses (parts per million)										
Ni	5.2	21.5	3.9	6.6	25	25	--	210	21.1	180.8
Cr	0	18.6	0.2	0	8	7	--	269	19.8	291.5
Sc	0	17.8	0	0	12	11	--	20	12.8	16.8
V	296.7	186.7	176.2	194.6	235	229	--	275	150.3	246.9
Ba	4170.3	590.8	2803	3196.5	966	1159	--	624	717.3	493.8
Rb	109.7	33.3	178.8	138.4	65	79	--	34	47.1	25.3
Sr	2537.8	683.2	2213.2	1573	1143	2038	--	1047	818	1122.2
Zr	887.9	302.9	646.4	523	188	175	--	217	303.7	164.8
Y	62.2	44.9	55.1	54.9	22	23	--	28	32.5	28.3
Nb	275.3	56.4	311.2	314.2	65	61	--	70	65.5	52.4
Ga	--	--	--	--	23	20	--	21	--	--
Cu	179.7	24.8	92.3	108.9	111	111	--	124	25.7	63.5
Zn	303.9	124.5	235.7	238.7	128	124	--	140	98.8	110.6
Pb	17.7	4.1	14.6	13.3	9	10	--	3	9.9	4.5
La	106.7	52.8	126.1	152.4	60	54	--	54	67	37.1
Ce	171.7	105.1	171.5	220	113	105	--	112	137.2	95.9
Th	12.7	8.5	25.1	26.7	9	8	--	6	9.4	7.8
Nd	60.4	61.2	56.5	76.3	38	39	--	52	62.3	51.3
U	--	--	--	--	4	1	--	2	--	--
Isotopic ratios										
$^{87}Sr/^{86}Sr$	0.704148	0.704049	0.704243	0.704308	--	--	--	--	0.704002	0.704002
$^{143}Nd/^{144}Nd$	0.512729	0.512731	0.512701	0.512682	--	--	--	--	0.512703	0.512792
ε_{Nd}	1.78	1.81	1.23	0.86	--	--	--	--	1.27	3.01
$^{206}Pb/^{204}Pb$	--	20.031	19.843	19.912	--	--	--	--	20.049	20.112
$^{207}Pb/^{204}Pb$	--	15.634	15.653	15.679	--	--	--	--	15.664	15.707
$^{208}Pb/^{204}Pb$	--	39.876	39.962	40.061	--	--	--	--	39.747	39.879

to alluviated crater floor. The tuff ring deposits are described in greater detail by Neukirchen and others (2010).

Faults of the Sanjan fault system slice through the crater, displacing the western crater walls to expose the full thickness of the vent's lapilli tuff beds (about 35–40 m) and also 170 m of underlying escarpment lava flows. This contact—between Sekenge crater deposits (unit Qsk) and pre-crater lava flows—steps down to the east along these faults until, at the crater's east rim, only Sekenge lapilli tuff is exposed. The crater's circular shape is preserved, an indication that faulting has been essentially extension (pure dip slip) on steep faults, with no strike-slip movement. Net strain across the crater is less than 5 percent. We disagree with the interpretation by Neukirchen and others (2010) that the crater is younger than faulting in the area.

Despite the faulting, the crater remains a closed basin now floored by sand and silt washed from the crater walls. A gaping crack, on strike with a minor fault of the Sanjan fault system, crosses the crater floor. The crack is as wide as 1.4 m midway along its length, where central keystone blocks have subsided. In this area one may descend about 7 m into the crack. The crack's walls expose weakly indurated, fine-grained fluviolacustrine beds (in unit Qa_1). Displacement is horizontal opening only; no vertical separation is seen at the current level of exposure. The crack's alignment with range-front faults suggest it is the shallow expression of a fault still active in Holocene time.

Sedimentary Rocks in the Area of Mto Wa Mbagai

Sedimentary rocks form a conspicuous part of the escarpment strata in the northwest corner of the map area. The geologic map portrayal is from the work of Glynn L. Isaac as it appeared on a page-size map (scale approximately 1:200,000; Isaac, 1967[1]). The presentation here of this legacy mapping serves several purposes. It emphasizes the short distance within which sedimentary rocks become a prominent part of the escarpment's stratigraphic sequence. It provides geologic setting for several radiometric ages important to understanding the timing of the Natron escarpment. And it makes available, on topographic base, map data that otherwise have limited distribution, thereby perhaps spurring further study of the escarpment's structure and stratigraphy. Farther north, Isaac's mapping is included as part of the Loliondo geologic map (Dundas and Adwalla, 1999).

Sedimentary rocks in this part of the escarpment were assigned by Isaac (1967) to the Humbu and Moinik Formations of the Peninj Group (Pleistocene). Through time the depositional setting for these beds changed from deltaic (coarser-grained, Humbu Formation) to lacustrine (finer-grained, Moinik Formation) as the basin deepened and a central lake expanded or shifted its depocenter. Our only traverse, ascending a prominent canyon, passed through the lower part of the Moinik Formation. From it we offer two comments that contrast with a description of the Moinik as simply lacustrine strata. Lava flows are more abundant than shown on the map, although they form less than 25 percent of the stratigraphic sequence. Also, the Moinik along our traverse contains much sandstone and conglomerate that is subaerial, not lacustrine, in origin, judging from grain size and sedimentary structure. This area is at the southern limit of Isaac's (1967) mapping. Our observations suggest that careful remapping may uncover many structural and stratigraphic details that bear on the development of the Lake Natron basin. Our only modification in the area of Isaac's (1967) map is to show debris-avalanche deposits (unit $Qoda_5$) from Oldonyo Lengai, which are plastered along the range front.

Several radiometric ages have been reported from lava flows and crystal tuff in the Humbu and Moinik Formations (table 2). Early efforts at dating were aimed at better understanding the age of deposits that enclose hominid artifacts in the Peninj delta, 22 km north of the map area (Isaac and Curtis, 1974); and determining the age of tectonic development by dating across the major escarpments (Macintyre and others, 1974). Subsequent dating (Manega, 1993; Foster and others, 1997) has concentrated more on the timing of rift-zone structural evolution.

The ages are displayed graphically in a time-depositional framework (fig. 5). In this illustration, the presumed stratigraphic sequence progresses from youngest to oldest across the horizontal axis, whereas age increases downward along the vertical axis. Ages from the Moinik range from 1.5 to 1.1 Ma; the few outliers were reported with large error (Foster and others, 1997). Ages from the Humbu have greater scatter, although one of the oldest, a weighted mean age of about 1.7 Ma, is from crystals in a basal Humbu tuff (table 2, No. 16). This Humbu tuff age makes sense stratigraphically when compared with a slightly older age from pre-Humbu lava, about 1.8 Ma (table 2, No. 18). On this basis the Humbu Formation was deposited between 1.8 and 1.5 Ma. The scatter among the Humbu ages relative to the Moinik may be explained by the difficulty in finding fresh samples for dating, but conceivably the Humbu and Moinik Formations interfinger along their extent, which could also produce the overlapping radiometric age relations—a matter to be resolved by future workers.

Escarpment Structure and the Timing of Range-Front Faulting

A single main fault trace characterizes the Natron escarpment from Engare Sero canyon southward to Oldonyo Lengai. The downthrown side is buried by the basin-filling deposits, and any structural complexities are lost from view. The upthrown side exposes roughly 460 m of lava flows and vent deposits near the canyon mouth, the thickest single exposure in the map area.

Northward from Engare Sero canyon, the Natron fault is marked by closely spaced faults that slice the upthrown block near the basin margin. The slivers are, for the most part, displaced successively down to the east, so that the face of each downthrown block obscures the face of the adjacent, structurally higher block. In consequence, exposed strata are nowhere more than 100 m thick.

The slivered fault blocks preserve evidence of normal drag folding, expressed by flexural tilting of the lava flows toward the basin. If total offset were small—only a few meters or tens of meters—the escarpment might instead appear as a monoclinal flexure. As faulting proceeds, the flexures fail and the fault escarpments become the prominent physiographic feature. As the basin widens, the slivered fault blocks subside on the downthrown side of a single major fault, taking with them the visual evidence of flexural-slip folding.

[1]An earlier article (Isaac, 1965) described preliminary results, but the later (1967) publication formalized the stratigraphic names and became the authoritative version of the map.

Gelai Volcano Forms Eastside Basin Boundary

The east side of the southernmost Lake Natron basin is bounded by the prominent Gelai shield volcano. Gelai is large, 25–30 km across and 50 km long in a north-northeast direction. Its western slopes ascend gently from the ~600-m shoreline of Lake Natron to the summit, about 2,940 m altitude (Gelai topographic quadrangle map 40/1, 1990). Cumulative volcano height must be greater, however, because the base of the volcano is in the subsurface. Its volume is in excess of 600 km^3, conservatively estimated by using a 600-m contour interval (fig. 2, for example), base altitude about 600 m (Lake Natron shoreline), and exposed extent. The estimate could be 30–50 percent too low depending on buried extent and thickness of the volcano's apron. Gelai is built chiefly by lava flows of vesicular alkali basalt and basanite. Minor trachyte is reported from the upper slopes of the volcano (table 1, No. 7; Guest and Pickering, 1966a, b; Dawson, 2008).

The span of Gelai's eruptive history is poorly known. A single Gelai lava flow has been dated, yielding an age of 1.00±0.02 Ma (table 2, No. 5; from Evans and others, 1971). The volcano could have been built in less than 100,000 years if lava were emplaced at rates characteristic of oceanic shield volcanoes. Gelai's radiometric age and the inferred age of major offset along the Natron fault are similar, so conceivably some Gelai lava may have encroached far enough westward to interfinger with lava flows near the top of the Natron escarpment, before faulting trapped the volcano in the basin. No effort at petrographic or geochemical correlation between Gelai and the escarpment lava flows was undertaken to test this hypothesis.

Normal-polarity magnetization was measured by fluxgate magnetometer on three lava flows of the lower southwest flank of Gelai volcano in the map area. This finding might be expected, inasmuch as Gelai's 1-Ma radiometric age corresponds to the Jaramillo Normal-Polarity Subchron (0.988–1.072 Ma; see chart on right side of Correlation of Map Units, geologic map). Alternatively, Gelai volcano may have a lengthy eruptive history that spans at least the early part of the Brunhes Normal-Polarity Chron (younger than 0.78 Ma).

Natron-Engaruka Volcanic Field

Scattered tuff rings, tephra cones, and a few lava flows dot the area from Lake Natron southward to Engaruka, 17 km south of the map area. This smattering of vents was first described by Dawson and Powell (1969) as the Natron-Engaruka explosion crater area. A detailed study was published during the preparation of this map (Mattsson and Tripoli, 2011). We modify the original name in a minor way to encompass the diversity of features found in this volcanic field.

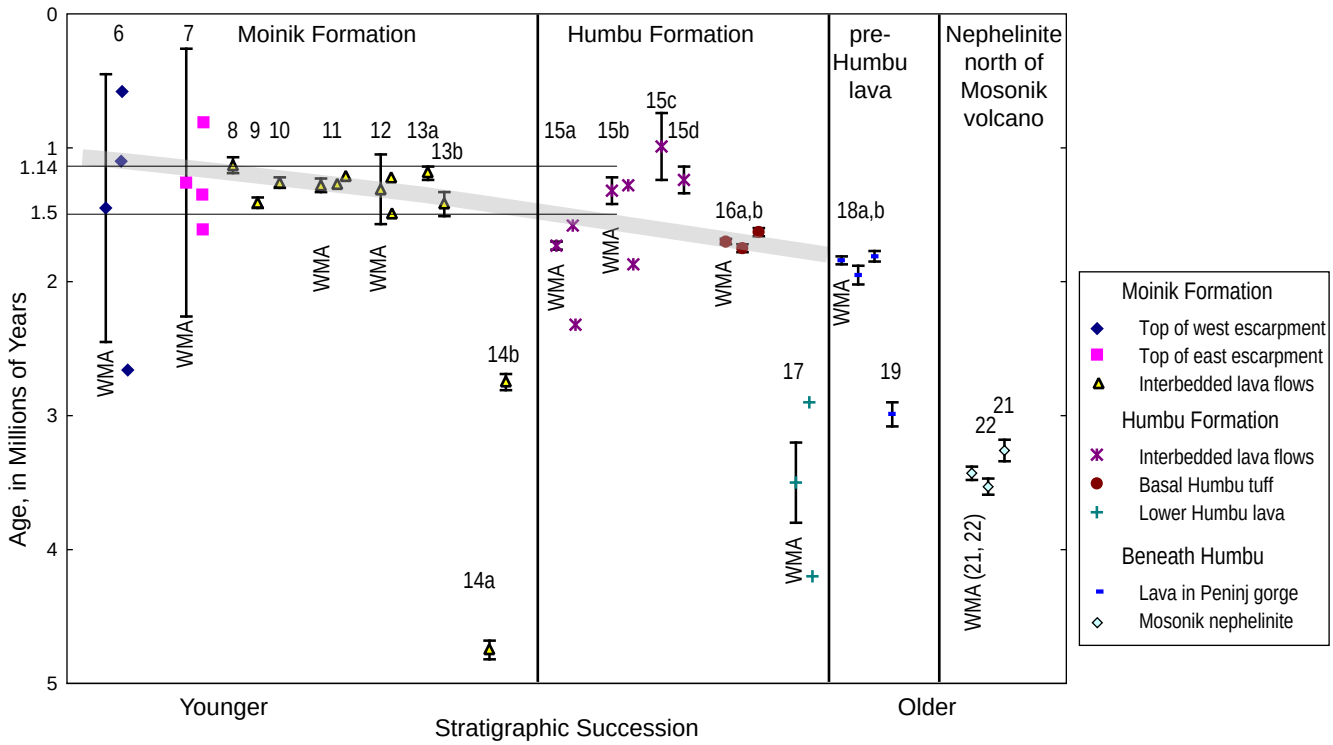

Figure 5. Time-depositional framework for dated samples from Peninj Group and other rocks in the map area. Vertical bars show age and 1-sigma error, if known, for previously published ages in table 2; numbers above bars indicate entry number in table 2. Samples grouped by stratigraphic formation (Moinik, Humbu, and so on) and arranged generally from youngest to oldest. WMA, weighted mean age and 1-sigma error for multiple determinations. Gray band sloping across graph indicates a likely succession, visually estimated, that assumes the Moinik Formation overlies the Humbu Formation with no interfingering. In this interpretation, the age of the Moinik is 1.1–1.5 Ma and that of the Humbu 1.5–1.8 Ma. Not shown but in table 2 are Nos. 1–4 (known to postdate the Moinik Formation), No. 5 (Gelai volcano), and No. 20 (a sample far enough away that its stratigraphic position relative to the other samples is unknown).

Table 2. Previously published K-Ar and $^{40}Ar/^{39}Ar$ ages from map area and vicinity.

[Data from source publications converted, where necessary, to K_2O (percent) and $^{40}Ar_{rad}$, mol per gm $x10^{-11}$. Ages in bold are considered stratigraphically meaningful and used herein (text and illustrations). WR, whole rock. SCLF, single-crystal laser fusion. Dashes indicate data not used ($^{40}Ar/^{39}Ar$ ages). n.r., data not reported; do and Do., ditto. Ages published before 1976 are recalculated using international standards for the isotopic abundance and decay rates (Steiger and Jäger, 1977), as listed in column Recalculated Age. Mean ages are weighted by the inverse of the variance of individual runs (Taylor, 1982). See appendix 4 for geographic coordinates]

Table No.	Sample No. [1]	Volcano or geographic locality	Material dated	K_2O, wt. percent	$^{40}Ar_{rad}$, mol per g $x10^{-11}$	$^{40}Ar_{rad}$, percent	Reported age and 1σ error, Ma	Recal-culated age, Ma	Age and 1σ error used herein, Ma	Reference
1	11301	Near Oldonyo Lengai	WR, phonolite	n.r.	n.r.	n.r.	0.15±0.02	0.15 [2]	**0.15±0.02**	Bagdasaryan and others, 1973
2	105	Ildonyo Loolmurwak	WR, olivine nephelinite	1.64	0.0357	1.4	0.14±0.12	0.15	**0.15±0.12**	Macintyre and others, 1974
3	891	Loolmurwak crater	Phlogopite	9.23	0.727	5.6	0.53±0.10	0.55	**0.36±0.05** [3]	Macintyre and others, 1974 [4]
	Do.	do	do	do	0.558	4.3	0.41±0.10	0.42		Do.
	Do.	do	do	do	0.263	2.7	0.19±0.08	0.20		Do.
4	3	Kisitei crater	Phlogopite	9.04	0.763	4.1	0.57±0.15	0.59	**0.37±0.11** [3]	Macintyre and others, 1974
	Do.	do	do	do	0.187	1.0	0.14±0.15	0.14		Do.
5	138	Gelai volcano, south flank	WR	2.39	0.338	29.6	0.96±0.03	0.98	**1.00±0.02** [3]	Evans and others, 1971
	Do.	do	do	do	0.349	31.2	0.99±0.03	1.01		
6	S9/6	Top of westernmost escarpment	WR, basalt	0.477	0.0401	1.4	1.45± large error [5]	0.58	**1.45±** large error	Foster and others, 1997
	Do.		do	do	0.0758	2.7		1.10		
	Do.		do	do	0.1829	6.0		2.66		
7	S10/10	100 m below top of eastern escarpment	WR, basalt	0.806	0.1874	3.0	1.26± large error [5]	1.61	**1.26±** large error	Foster and others, 1997
	Do.		do	do	0.0937	1.8		0.81		
	Do.		do	do	0.1562	2.4		1.35		

Table 2. Continued

Table No.	Sample No. [1]	Volcano or geographic locality	Material dated	K_2O, wt. percent	$^{40}Ar_{rad}$, mol per g x10^{-11}	$^{40}Ar_{rad}$, percent	Reported age and 1σ error, Ma	Recal-culated age, Ma	Age and 1σ error used herein, Ma	Reference
8	NAT90-01 (KA1187)	Intra-Moinik lava flow	WR	0.780	0.1258	3.18	1.13±0.06	1.12	**1.13±0.06** [6]	Manega, 1993
9	NAT90-12 (KA1186)	Intra-Moinik lava flow	WR	0.790	0.1593	4.42	1.41±0.04	1.40	**1.41±0.04** [6]	Manega, 1993
10	BPT-NAT	Birdprint tuff in Moinik Fm.	SCLF	--	--	--	1.26±0.04	--	**1.26±0.04**	Manega, 1993
11	S11/4	Lava flow in Moinik Fm [7]	WR, nephelinite	5.61	1.0264	23.3	1.28±0.05	1.27	**1.28±0.05** [8]	Foster and others, 1997
	Do.	do	do	do	0.9773	22.1		1.21		Do.
12	S11/6	Interbedded in upper Moinik Fm.	WR	4.84	0.8479	6.1	1.31±0.26	1.22	**1.31±0.26** [9]	Foster and others, 1997
	Do.	do	do	do	1.0353	6.8		1.49		Do.
13a	KA2410	Intra-Moinik lava flow	WR, basalt	1.23	0.210	14.4	1.33±0.05	1.19	**1.19±0.05** [10]	Isaac and Curtis, 1974
13b	KA2589	Intra-Moinik lava flow	WR, basalt	1.22	0.249	10.6	1.38±0.09	1.42	**1.42±0.09** [10]	Isaac and Curtis, 1974
14a	KA1814	Intra-Moinik lava flow	WR, nephelinite	7.04	4.82	40.3	4.60±0.07	4.75	4.75±0.07 [11]	Isaac and Curtis, 1974
14b	KA2250	Intra-Moinik lava flow	WR, nephelinite	7.56	2.99	49.4	2.68±0.06	2.75	2.75±0.06 [11]	Isaac and Curtis, 1974
15a	KA1754	Lava flow in Humbu Fm.	WR, basalt	0.878	0.200	26.0	1.55±0.03	1.58	**1.73±0.03** [12]	Isaac and Curtis, 1974
15a	KA1754R	do	do	0.878	0.294	10.7	2.27±0.06	2.32		Do.
15b	KA2382	do	do	0.978	0.181	5.7	0.96±0.10	1.28	**1.32±0.10** [13]	Do.
15b	KA2382R	do	do	0.817	0.220	2.1	1.21±0.36	1.87		Do.
15c	KA2578	do	do	0.922	0.132	2.7	0.97±0.25	0.99	**0.99±0.25**	Do.
15d	KA2646	do	do	0.904	0.161	6.9	1.21±0.10	1.24	**1.24±0.10**	Do.
16a	NAT90-07	Basal Humbu tuff	SCLF, feldspar	--	--	--	1.75±0.03	--	**1.70±0.02** [14]	Manega, 1993
16b	NAT90-08	do	do				1.63±0.03			Manega, 1993
17	S10/11	Lava flow in lower Humbu Fm.	WR	0.560	0.3392	3.1	3.5±0.3	4.2	**3.5±0.3** [15]	Foster and others, 1997
	Do.	do	do	do	0.2365	2.3		2.9		Do.

Table 2. Continued

Table No.	Sample No. [1]	Volcano or geographic locality	Material dated	K_2O, wt. percent	$^{40}Ar_{rad}$, mol per g x10^{-11}	$^{40}Ar_{rad}$, percent	Reported age and 1σ error, Ma	Recal-culated age, Ma	Age and 1σ error used herein, Ma	Reference
18a	KA1755	Beneath Humbu Fm., Peninj gorge	WR	1.144	0.321	15.4	1.90±0.07	1.95	**1.84±0.03** [3]	Isaac and Curtis, 1974
18b	KA1755R	do	do	do	0.298	18.6	1.77±0.04	1.81		Do.
19	NATM89-01 (KA1185)	Beneath Humbu Fm.	WR	0.590	0.2539	6.97	2.99±0.09	2.99	**2.99±0.09**	Manega, 1993
20	KA2570	Lava flow in Malambo gorge [16]	WR, basalt	0.698	0.361	4.9	3.50±0.46	3.59	**3.59±0.46**	Isaac and Curtis, 1974
21	NATM89-07	Mosonik, lava flow	WR	4.431	2.254	35.12	3.53±0.06	3.53	**3.53±0.06**	Manega, 1993
22	KA1757	Mosonik lava flow	Biotite	8.27	3.88	18.4	3.18±0.08	3.26	**3.26±0.08**	Isaac and Curtis, 1974

[1] Sample numbers except for those reported by Isaac and Curtis, which are laboratory run numbers.

[2] Recalculated by method of Dalrymple (1979, his table 3) for Russian constants, although this age is so young that it remains unchanged at the reported precision of two significant figures.

[3] Weighted mean age of the recalculated ages, using standard deviation reported in original publication.

[4] A "best estimate" of 0.37 Ma was described in original report (Macintyre and others, 1974, p. 356). That age was incorrectly credited to Bagdasaryan and others (1973) by Klaudius and Keller (2006).

[5] Arithmetic mean age of the recalculated ages (original publication described "large error").

[6] These two ages are from discrete sample locations lying about 7 km apart (Manega's [1993] localities 3 and 6 on his fig. 3.28) but were deemed the same lava flow; on this basis Manega (1993) reported a weighted mean age 1.33±0.03 Ma.

[7] No. 11. Described in original publication as having flowed from Mosonik volcano. Geographic coordinates place it high in Moinik Formation, in agreement with radiometric age, and we discount Mosonik volcano as eruptive source.

[8] Arithmetic mean is 1.24 Ma but age from original publication is used here.

[9] Arithmetic mean is 1.36 Ma.

[10] Unclear in original report if two wholly different samples were used or if the same sample was used for two gas extractions (and repeated K_2O analyses).

[11] Original report describes these ages as grossly inconsistent with stratigraphic setting. Unclear in original report if two wholly different samples were used or if the same sample was used for two gas extractions (and repeated K_2O analyses).

[12] Weighted mean age of KA1754 and KA1754R.

[13] Weighted mean age of KA2382 and KA2382R.

[14] Weighted mean age of originally reported ages and their 1σ errors.

[15] Arithmetic mean is 3.6 Ma.

[16] Malambo gorge is 35 km west of the Lake Natron escarpment, and the dated lava flow is difficult to correlate with any stratigraphic units in map area. Its inclusion here is for completeness.

Tuff Rings

Tuff rings (explosion craters) are perhaps the most memorable features in the Natron-Engaruka volcanic field. The rings have low rims and broad craters whose floors lie below what would have been the ground surface during eruption. Several have great breadth. For example, Loolmurwak crater (southeast part of map area) is a circular depression 850 m across; the crater is 100–120 m deep, two-thirds of which is carved into underlying bedrock. The crater's initial depth is speculative, since its floor, like other tuff rings in the area, is covered by modern alluvium. Pre-crater wall rocks at Loolmurwak were assigned to Kerimasi volcano (Dawson and Powell, 1969) and described in more detail by Hay (1983).

Loolmurwak tuff deposits include phlogopite books as large as 10 cm across. Similar phlogopite megacrysts occur at Deeti, a tephra cone 5 km southeast of Loolmurwak crater. As described and interpreted by Johnson and others (1997), the large megacrysts at Deeti must have formed in a melt under ideal fluxing conditions, such as those of pegmatites. In their interpretation, an alkaline silicate melt, probably melilititic in composition, stalled at depths of 60–90 km (2–3 GPa; lithospheric upper mantle) to allow for mineral growth before erupting. The magmatic setting for Loolmurwak likely is similar.

At Loolmurwak crater we dated a phlogopite megacryst, obtaining a $^{40}Ar/^{39}Ar$ plateau age of 0.92±0.07 Ma (table 3). In contrast is a previously published phlogopite K-Ar age of 0.36±0.05 Ma (table 2, No. 3; Macintyre and others, 1974). The disparate ages leave unanswered the question of actual emplacement age—ours is perhaps too old because of excess argon, or the Macintyre age too young because of argon loss, incomplete sample degassing, or some other reason.

Two tuff rings are embedded within the cone of Oldonyo Lengai, presumably a fortuitous geographic aspect and not necessarily indicating a close relation to the Oldonyo Lengai magmatic system. One of them, Embalulu Oltatwa, has been dated. It is discussed more fully in the section on Oldonyo Lengai ("Lava flows and vents on the lower flanks").

Tephra Cones

Tephra cones are the more common vent of the Natron-Engaruka volcanic field, both within the map area and probably throughout the volcanic field (Dawson and Powell, 1969, their fig. 2; Mattsson and Tripoli, 2011). Most are built of small lapilli and ash and might be termed tuff cones. Spatter or scoria cones, such as those that characterize many volcanic arcs and oceanic island volcanoes, are few.

A relative age criterion among the tephra cones may be found in the amount of erosional rilling of their flanks. For example, the tephra cone east of Oldonyo Lengai ("Lalarasi" on the geologic map) is so deeply rilled that the Maasai refer to it as Olorok Kimojik, or "black fingers," in reference to its furrowed slopes. We made some effort to subdivide the unit of tephra cones (Qnc) into older and younger parts by the extent of rilling, a plan frustrated by the many cones that proved difficult to assign. The scheme may prove useful, however, in future, more detailed mapping.

Widespread Extensive Tuff

The growth of numerous, dispersed tuff rings and tephra cones in the Natron-Engaruka volcanic field resulted in a widespread extensive unit of tuff and lapilli tuff (unit Qnet) that blankets much of the divide between Oldonyo Lengai and Gelai volcano. The tuff and lapilli tuff typically crop out as poorly sorted beds 50 cm to 2 m thick. The matrix is devitrified. Some beds have subangular to subrounded pebbles or cobbles broadly basaltic (foiditic) in composition that produce layering internal to specific beds, whereas others lack internal layering. None of the beds shows color variation from bottom to top, such as might form when hot material is oxidized at its upper surface after emplacement. Columnar jointing is absent. No bed was traced far in our reconnaissance, so nothing is known about variation downslope in a single bed.

The widespread extensive tuff is the amalgam of numerous small emplacement units, probably many of them by pyroclastic flows emanating beyond the tuff rings. A few are clearly fallout

Table 3. New $^{40}Ar/^{39}Ar$ radiometric ages from Natron-Engaruka volcanic field.

[Preferred ages are plateau ages, shown in bold. Errors are estimates of analytical precision at the 95-percent confidence level. MSWD, mean square of weighted deviates (York, 1969). $^{40}/_{36}$ i, $^{40}Ar/^{36}Ar$ isochron intercept. See appendix 5 for argon plateau and isochron diagrams]

			Plateau age				Total-gas age	Isochron age			
	Sample No.	Material	%^{39}Ar (steps)		Age (ka)	Error (2σ)	(ka)	Age (ka)	Error (2σ)	MSWD	$^{40}/_{36}$i
Oremit											
1.	S10-L9 [1]	Groundmass [2]	85.1	(6 of 8)	**340**	**85**	713±160	339	177	0.01	295.5±1.9

			Plateau age				Total-gas age	Isochron age			
			%^{39}Ar (steps)		Age (Ma)	Error (2σ)	(Ma)	Age (Ma)	Error (2σ)	MSWD	$^{40}/_{36}$i
Loolmurwak crater											
2.	S10-L40 [1]	Phlogopite	90.1	(7 of 11)	**0.92**	**0.07**	0.84±0.08	0.88	1.21	0.05	296.7±43.4

[1] Locations (WGS84):
S10-L9 lat −2.7283° long 35.9829°.
S10-L40 lat −2.7985° long 35.9798°.

tephra, whereas others are probably lahars. Devitrification has obscured textural features, and at many outcrops we puzzled over the origin by hot or cold processes. Beds that are clearly sedimentary in origin, such as sandstone or conglomerate, are sparse.

Lava Flows

The only four lava flows among the vents of the Natron-Engaruka volcanic field (Dawson and Powell, 1969) are within the area of our geologic map. Three have some fame in the geologic literature owing to their relative ease of access and freshness of the lava. Their freshness makes them preferred targets for dating and geochemical analysis compared to the tuff rings and tephra cones.

Ildonyo Loolmurwak

The most southerly of these lava flows in the map area is a melilitite that flanks the south and southeast sides of Ildonyo Loolmurwak, a tephra cone in the southeast corner of the map area. The lava flow has a K-Ar age of 0.15±0.12 Ma (table 2, No. 2; Macintyre and others, 1974), although the low radiogenic ^{40}Ar component (1.4 percent) results in such large analytical error that its emplacement age is known no more precisely than sometime in the past 0.3 m.y. The Ildonyo Loolmurwak lava flow lies beyond the area impacted by debris-avalanche deposits from Oldonyo Lengai, so it has limited usefulness as a stratigraphic marker for understanding the relative age of south-flank debris avalanches from Oldonyo Lengai. The Ildonyo Loolmurwak melilitite is relatively primitive, with Mg number about 70 and Ni content 250–400 ppm (chemical analysis in table 4); thus it was identified as a likely composition for mantle-derived primitive parental melt in this part of the East African rift (Dawson and others, 1985; Dawson 1998).

Olmoiton (Armykon Hill)

Olmoiton, east of Engare Sero village, is another vent of the Natron-Engaruka volcanic field that has erupted lava flows (chemical analyses in table 5). The flows are found on the south side of the cone and eastward across a broad alluvial floor. The eastern lava flow lacks obvious physical connection to the Olmoiton vent, but we found no evidence that it was erupted locally from a separate fissure. A small inferred graben must have formed after lava-flow emplacement to separate the flow from Olmoiton. Only a few meters of subsidence along the graben, and then infilling by sediment from Engare Sero stream, would be sufficient to mask the critical link to the presumed vent at Olmoiton.

The graben interpretation is supported, in part, by the abrupt termination of the eastern lava flow where its edge forms a 6-m-high topographic escarpment against the alluvial plain. Other small normal faults cut the eastern lava, as shown on the geologic map. Displacement on the most prominent of them is down on the west, 4–6 m, and the upthrown side exposes two or three lava flows. The lowest flow is at least 5 m thick, but the exposure does not reach the base of the flow, frustrating our search for charcoal in the underlying soil for radiocarbon dating.

In terms of relative ages, the eastern lava is younger than the main sheet of debris-avalanche deposits from Oldonyo Lengai (unit $Qoda_5$), because it laps onto a tiny mound of those deposits. The lava flow may be younger than about 11,500 calibrated years B.P., because a traverse across the northern reach of the lava flow failed to find evidence of ancestral shoreline deposits described by Hillaire-Marcel and others (1987; shoreline trace shown on geologic map). The northern end of the Olmoiton (Armykon) vent itself, not visited, may be a more suitable setting for erosion by wave fetch and deposition of rounded pebbles by shoreline processes; therefore we urge a more careful examination than given in our reconnaissance to test the age relation between the Olmoiton vent and past shorelines of Lake Natron.

Elsewhere upslope toward Oldonyo Lengai, several of the vents and lava flows of the Natron-Engaruka volcanic field are older than adjacent debris-avalanche deposits. The debris-avalanche deposits along the basin formed during several emplacement episodes, so inferences from relative age relations will prove mostly of local importance.

Oremit ("One Mile North of Lalarasi")

A third lava flow lies east of Oldonyo Lengai. It is named here informally as the lava of Oremit, the Maasai name for this area where the oremit tree is common. This lava, a fresh olivine melilitite (table 4), is sometimes called the Lalarasi flow (Dawson and Powell, 1969) or Lalarasi Sinja Eledoi (Keller and others, 2006, their table 1) for its position about 2 km north-northeast of the Lalarasi tephra cone. (In older sample descriptions it is described as "one mile north of Lalarasi.")

The lava of Oremit has a ^{40}Ar/^{39}Ar plateau age of 340±85 ka (table 3). This lava flow is of interest stratigraphically because it has been overrun by a young debris avalanche (deposits of unit $Qoda_2$) but itself is younger than a more extensive debris avalanche (deposits of unit $Qoda_5$). This latter relation is based on presence of debris-avalanche deposits 0.5 to 2.5 km downslope of the lava on trend away from the volcano. The lava flow may have erupted from one of the three tephra cones almost completely buried by the younger debris avalanche (deposits of unit $Qoda_2$). Conceivably the lava issued from a fissure connecting the three cones, given the broad convex-outward shape of its margin in map view.

Five Kilometers North of Lalarasi

The fourth mapped lava flow, also olivine melilitite (table 6, No. 6), lies 5 km north of Lalarasi (3 km north of lava flow 3, the Oremit lava) and east of Sidan Indare (Sinja Ndare) stream. The 'a'ā lava erupted from a small cone at the basin's edge, on the west margin of Gelai volcano. Mantling the edge of the lava flow are debris-avalanche deposits, probably part of the main sheet of debris avalanche ($Qoda_5$). Thus, although the strata are not directly superimposed, the following oldest-to-youngest stratigraphic relation is suggested for these events north and east of Oldonyo Lengai: lava flow 4, debris-avalanche deposits ($Qoda_5$), lava flow 3 (Oremit), debris-avalanche deposits ($Qoda_2$).

The lava flows and vent deposits of the Natron-Engaruka volcanic field have some of the lowest SiO_2 contents of any silicate volcanic rocks in the area (fig. 4). Consequently they are distinct from volcanic rocks in the Natron escarpment (units QTel, QTev, and Tek) (Dawson, 2008; Neukirchen and others,

Table 4. Whole-rock major and trace element chemical analyses from lava flows at Ildonyo Loolmurwak and Oremit ("1 mile N of Lalarasi").

[Dashes, no data. Major-element analyses are shown normalized to 100 percent, volatile free. Also shown are original oxide totals and values for loss on ignition, for completeness. Data compiled and available in a spreadsheet that accompanies this publication. References: 1, Dawson and others, 1985; 2, this report; 3, Keller and others, 2006. For analytical methods see source references or, for this report, appendix 3]

Volcanic center	Ildonyo Loolmurwak					Oremit			
Sample No.	BD105	S10-L37	OL199	OL342	OL141	BD25	S10-L9	OL350	OL352
Rock type	Foidite	Foidite	Foidite	Foidite	Foidite	Melilitite	Melilitite	Melilitite	Melilitite
Reference	1	2	3	3	3	1	2	3	3
Major-element analyses, normalized water-free (weight percent)									
SiO_2	39.51	39.76	39.80	39.90	39.75	35.10	35.14	35.81	37.79
TiO_2	4.12	4.51	4.08	3.93	3.94	5.47	5.43	5.42	4.44
Al_2O_3	7.30	7.96	7.50	7.60	7.54	7.33	7.48	7.70	7.80
FeO*	14.03	13.53	13.79	13.74	14.08	14.37	14.62	14.56	13.27
MnO	0.24	0.21	0.21	0.22	0.22	0.26	0.25	0.25	0.22
MgO	15.87	12.50	15.98	15.30	15.90	10.16	9.59	10.35	15.50
CaO	13.66	14.86	13.38	13.74	13.96	18.82	18.39	18.41	13.99
Na_2O	2.65	3.33	2.77	2.80	2.28	4.55	4.97	3.91	3.62
K_2O	1.66	2.23	1.54	1.82	1.41	2.57	2.78	2.30	2.45
P_2O_5	0.97	1.12	0.95	0.94	0.92	1.37	1.35	1.27	0.92
Loss on ignition	3.03 [1]	3.72	1.74 [2]	2.88 [2]	2.21 [2]	3.97 [1]	3.25	0.68 [2]	0.76 [2]
Original oxide total	98.69	94.77	98.83	99.73	99.18	98.81	94.73	98.25	98.59
Trace-element analyses (parts per million)									
Ni	356	254	368	374	399	92	81	89	296
Cr	698	513	722	620	654	125	118	112	481
Sc	--	26	22	27	26	--	33	37	34
V	276	282	300	228	265	347	355	337	264
Ba	617	763	673	780	747	851	1002	1257	1168
Rb	48	58	37.1	42	36	55	61	49	51
Sr	845	1220	973	1087	1672	1602	1586	1364	1189
Zr	326	435	395	373	369	420	512	454	349
Y	28	32	28.1	33	34	33	36	43	29
Nb	97	113	101	104	99	168	187	156	118
Ga	--	18	19.4	17	15	--	20	16	16
Cu	114	124	126	131	127	194	218	232	176
Zn	117	132	142	133	131	125	137	132	119
Pb	8	5	5.3	6	7	30	8	9	6
La	--	89	83.1	--	--	--	136	--	--
Ce	--	184	167	--	--	--	255	--	--
Th	--	10	10	5	<5	--	15	11	6
Nd	--	86	--	--	--	--	111	--	--
U	--	3	2.53	<3	<5	--	5	<3	<3
Isotopic ratios									
$^{87}Sr/^{86}Sr$	--	--	0.703689	--	--	--	--	--	--
$^{143}Nd/^{144}Nd$	--	--	0.512759	--	--	--	--	--	--
ε_{Nd}	--	--	--	--	--	--	--	--	--
$^{206}Pb/^{204}Pb$	--	--	20.047	--	--	--	--	--	--
$^{207}Pb/^{204}Pb$	--	--	15.706	--	--	--	--	--	--
$^{208}Pb/^{204}Pb$	--	--	39.962	40.061	--	--	--	--	39.747

[1] Sum of H_2O^+ and CO_2.
[2] Sum of H_2O^+, $H2O^-$, and CO_2.

Table 5. Whole-rock major and trace element chemical analyses from lava flows at Olmoiton (Armykon hill).

[Dashes, no data. Major-element analyses are shown normalized to 100 percent, volatile free. Also shown are original oxide totals and values for loss on ignition, for completeness. Data compiled and available in a spreadsheet that accompanies this publication. References: 1, Keller and others, 2006; 2, Dawson and others, 1985; 3, Dawson and Powell, 1969; 4, this report, sample collected from lava flow 0.5 km east of hill. For analytical methods see source references or, for this report, appendix 3]

Sample No.	OL336	OL12/99	OL12/2K	JG958	JG958 (?)	S10-L3
Volcanic center	Olmoiton					
Rock type	Melilitite	Melilitite	Melilitite	Melilitite	Melilitite	Melilitite
Reference	1	1	1	2	3	4
Major-element analyses, normalized water-free (weight percent)						
SiO_2	35.18	35.50	35.05	35.76	35.31	35.51
TiO_2	6.02	6.03	6.00	6.19	4.97	6.23
Al_2O_3	7.56	7.31	7.12	7.16	9.41	7.05
FeO*	14.49	14.58	14.37	14.42	14.61	14.65
MnO	0.24	0.24	0.23	0.24	0.25	0.23
MgO	10.00	10.24	10.08	9.99	10.07	10.17
CaO	17.70	17.38	16.94	17.21	16.96	16.90
Na_2O	4.59	4.45	5.45	4.52	4.56	4.86
K_2O	2.82	2.69	3.17	2.92	2.58	2.84
P_2O_5	1.40	1.57	1.60	1.60	1.29	1.57
Loss on ignition	0.60 [1]	1.57 [1]	0.75 [1]	3.19 [2]	2.02 [1]	0.78
Original oxide total	98.17	98.78	99.00	99.21	100.23	97.35
Trace-element analyses (parts per million)						
Ni	104	139	128	117	--	125
Cr	110	161	218	168	--	205
Sc	39	29	30	--	--	31
V	311	289	375	383	--	382
Ba	1103	919	908	875	--	963
Rb	49	54	61.2	66	--	61
Sr	1427	1579	1479	1511	--	1562
Zr	576	605	567	549	--	628
Y	44	55	36.6	35	--	38
Nb	158	153	167	169	--	184
Ga	20	17	21.8	--	--	18
Cu	191	247	197	180	--	196
Zn	106	140	167	123	--	139
Pb	12	7	8.78	14	--	8
La	--	--	124	--	--	131
Ce	--	--	249	--	--	268
Th	8	nil	13.5	--	--	13
Nd	--	--	--	--	--	123
U	<3	<5	3.63	--	--	5
Isotopic ratios						
$^{87}Sr/^{86}Sr$	--	0.703641	0.703638	--	--	--
$^{143}Nd/^{144}Nd$	--	0.512773	0.512773	--	--	--
ε_{Nd}	--	--	--	--	--	--
$^{206}Pb/^{204}Pb$	--	19.932	--	--	--	--
$^{207}Pb/^{204}Pb$	--	15.669	--	--	--	--
$^{208}Pb/^{204}Pb$	--	39.739	--	--	--	--

[1] Sum of H_2O^+, H_2O^-, and CO_2.
[2] Sum of H_2O^+ and CO_2.

2010), which are higher in SiO_2 although with similar total alkali content. The low silica and other geochemical features also distinguish the Natron-Engaruka rocks from the volcanic rocks of Oldonyo Lengai (Keller and others, 2006).

Phonolite Lava Dome 10 km Northeast of Summit

A massive phonolite lava 80–100 m thick forms a prominent hill northeast of the Engaruka-Loliondo road, 10 km northeast of Oldonyo Lengai's summit. The lava has been smothered by debris-avalanche deposits, so exposures are found only on the side leeward of Oldonyo Lengai. Given its circular outline (900-m diameter), the phonolite likely is a volcanic dome with vent near the center of the circular mass. No associated explosive deposits are recognized.

Could the outcrops instead be the distal snout of a lava flow originating from Oldonyo Lengai? In that case, it would probably prove fairly old because it is topographically distinct; that is, it stands higher than surrounding terrain, so any geomorphic tie back to the volcano has been destroyed. It is appealing to

Table 6. Whole-rock major and trace element chemical analyses from miscellaneous lava flows and scoria of Natron-Engaruka volcanic field.

[Major-element analyses normalized to 100 percent, volatile free. Also shown are original oxide totals and values for loss on ignition, for completeness. Data compiled and available in a spreadsheet that accompanies this publication. For analytical methods see appendix 3]

Table No.	1	2	3	4	5	6	7	8	9	10
Sample No.	S10-L210	S10-L77	S10-L172	S10-L15	S10-L164	S10-L117	S10-L118	S10-L67	S10-L238	S10-L310
Rock type	Melilitite	Melilitite	Melilitite	Melilitite	Basanite	Melilitite	Melilitite	Melilitite	Phonolite	Basanite
Major-element analyses, normalized water-free (weight percent)										
SiO_2	34.99	34.32	37.32	37.44	44.65	34.88	35.21	37.43	54.67	46.97
TiO_2	5.80	4.59	3.66	5.10	3.13	5.21	5.08	3.49	0.65	1.96
Al_2O_3	7.20	8.00	8.21	9.01	14.07	7.56	7.57	9.87	20.29	14.81
FeO*	14.69	14.08	13.67	14.91	13.08	14.96	14.77	11.94	4.64	11.56
MnO	0.24	0.26	0.25	0.26	0.22	0.27	0.26	0.22	0.18	0.18
MgO	11.19	9.72	14.20	8.78	6.39	10.18	10.29	17.85	0.56	5.15
CaO	18.19	18.83	14.96	15.99	11.22	19.64	19.11	12.85	2.84	12.06
Na_2O	3.34	5.22	4.43	4.44	4.53	3.95	4.20	2.92	10.58	5.36
K_2O	2.79	3.54	2.07	2.84	1.96	1.98	2.04	2.77	5.42	1.55
P_2O_5	1.55	1.44	1.22	1.24	0.76	1.37	1.48	0.67	0.16	0.38
Loss on ignition	10.37	15.58	5.43	3.84	3.92	3.13	2.70	14.79	2.58	7.69
Original oxide total	87.76	82.85	92.87	94.27	94.85	94.97	95.30	83.86	95.49	91.74
Trace-element analyses (parts per million)										
Ni	123	83	234	78	131	103	91	200	5	84
Cr	260	118	473	105	111	156	156	756	3	127
Sc	29	23	23	24	13	31	30	25	1	34
V	319	199	263	301	202	283	330	80	54	268
Ba	1008	766	953	938	767	1009	1026	715	1252	477
Rb	84	62	42	57	45	49	49	94	107	51
Sr	1646	1960	1447	1638	1322	1812	1815	830	1323	736
Zr	522	446	387	443	268	534	527	173	700	103
Y	33	30	31	33	34	38	39	20	27	22
Nb	165	167	157	166	90	202	198	88	202	20
Ga	17	14	15	20	24	20	20	11	30	15
Cu	170	145	143	181	214	220	222	154	4	93
Zn	119	120	125	144	139	141	143	85	158	78
Pb	10	7	6	9	4	5	5	5	30	1
La	124	126	129	123	74	143	137	61	83	20
Ce	252	247	248	251	147	275	264	114	153	39
Th	14	13	15	13	8	17	14	7	33	1
Nd	114	103	102	108	63	114	112	47	49	23
U	3	3	5	4	3	6	5	1	7	1

associate this lava with Oldonyo Lengai, because its phonolitic composition (table 6, No. 9) makes it unusual compared to other lava flows and domes of the Natron-Engaruka volcanic field.

Not ruled out is the unlikely possibility that the lava moved downslope, as a megablock in a debris avalanche, from a site originally closer to the volcano's north flank. One line of evidence that might support whole-block displacement would be proof that it rotated; that test would come from knowledge of its paleomagnetic directions. (A handheld fluxgate magnetometer, such as we carried, is insufficient for such measurements.) Another feature to be expected, if the unit is of megablock origin, is internal dislocation along small faults as the blocks became segmented during transport. Some local shearing was seen along fractures on the northwest cliff exposures, but displacements appeared insignificant and are likely volcanic emplacement features. The monolithic aspect of the lava and lack of internal contacts hampered the effort to quantify the magnitude of displacement among the exposed fractures. Thus, for the present, we prefer a locally erupted origin for the phonolite.

In closing is this note about geographic names. The phonolite lava dome forms an unnamed hill on topographic quadrangle maps. The hill bears the name Olorgogorie on the geologic map of Guest (1953). Maasai residents in our acquaintance refer to it as Lalarasi, a name they say is wrongly assigned on topographic quadrangle maps to a large tephra cone (their Olorok Kimojik) located 9 km south-southeast (Mosonik quadrangle, sheet 39/4, 1990). The issue has crept into the Earth science literature because geologists name major rock units by geographic names. Thus, some geologists have coined new geographic names and refer to the phonolite dome as Oldonyo Lalarasi (for example, Kervyn and others, 2008a) and the distant tephra cone as Sinja Lalarasi (Keller and others, 2006). We prefer to see geographic names originate among a local people. For that reason we use an awkward but descriptive informal name, "phonolite dome 10 km northeast of summit" (of Oldonyo Lengai), until geographic names are resolved.

Ancient Lake Natron Beds on the Basin Floor

Thin-bedded gray sandstone and white siltstone (unit Ql_3) are exposed across 11 km^2 at the 620–640-m altitude along the east margin of the map area, 3–6 km south of Lake Natron. A few seams of freshwater limestone are interbedded in the siltstone. Blocks of carbonate, likely stromatolitic in origin, are scattered across the area of exposure. A lacustrine origin for the sandstone and siltstone is certain. Previously unmapped, these lacustrine deposits are the most southerly outcrops of late Pleistocene Lake Natron known to us, although the lake may once have extended as far south as the Engaruka basin (Dawson, 2008, p. 23).

Several aspects of the lacustrine beds are puzzling. The sequence is highly deformed. Bedding dips range from 20° to vertical (fig. 6). The folding is abrupt and discontinuous; indeed, in one place, gently dipping beds were traced into vertical orientation across 30 m distance (one of the most extensive outcrops found). The carbonate blocks abound as rubble across the landscape. Their placement is what might be expected when a resistant, capping layer, stripped back by erosion, leaves its remnants as slope-mantling blocks above softer, more easily eroded beds—but no such capping carbonate layers were ever found intact. The lacustrine sequence is at least 6–8 m thick, but its base is not exposed and the unit could be substantially thicker.

Interspersed with the sandstone and siltstone are a few large debris-avalanche blocks 50–200 m across (unit $Qoda_6$) and several blocks too small to map. They are mantled by the lacustrine beds but also may be embedded within the lacustrine sequence, an irresolvable stratigraphic relation owing to the shallow depth of exposure and low relief of the area. The entire sequence is overlain unconformably by 2–3 m of grayish-red sandstone of the Gelai alluvial fan (unit Qa_4), the basal 20 cm of which is commonly riddled with now-infilled worm(?) burrows. The Gelai alluvial fan deposits are undeformed.

Figure 6. Typical exposures of the ancient lake deposits south of Lake Natron. Masota Magigita stands on a ribbon of thin-bedded sandstone and siltstone, turned up on end. The slopes around him are littered with angular limestone blocks and fragments of sedimentary rocks. Large dark blocks are bits of debris-avalanche deposit found scattered among these highly disrupted beds. Photo 7640, March 6, 2010.

Several explanations might explain the complex structural and stratigraphic relations in this part of the map area. In our view, a debris avalanche from Oldonyo Lengai ripped into preexisting lake sediment, deforming and disrupting it. Competent carbonate layers shattered, but the thin-bedded siltstone and sandstone folded. This explanation accounts for the juxtaposition of debris-avalanche blocks and lacustrine sediment, the deformation, and the landscape littered with carbonate—a terrain described succinctly by one of us (MM) as "if a bomb had gone off." Subsequent or continued lacustrine deposition would explain the few well-exposed mantling relations. An alternative three-step interpretation requires emplacement of debris-avalanche deposits, deposition of lacustrine beds, and then intense tectonic deformation affecting at least the area of present-day outcrop. A tectonic explanation would require shallow thrust or strike-slip faulting to create the discontinuous, locally intense deformation seen in the lacustrine sequence; whereas the Lake Natron basin formed by normal faulting, a process that continues today along the East African rift.

We suggest a tentative correlation of these lacustrine beds with paleo-highstands of Lake Natron sometime between 240,000 and 135,000 years ago. This interpretation is based on U/Th ages from stromatolite that marks a shoreline altitude of 655 m (Hillaire-Marcel and others, 1986). The deformed lacustrine sequence must predate the debris-avalanche blocks found within it (unit $Qoda_6$) and the main sheet of debris avalanche (unit $Qoda_5$). Otherwise, how can one explain the complete absence of any of the lacustrine beds westward and northwestward across the main-sheet debris-avalanche deposits?

A minimum age of 11,500 years (cal B.P.) can be assigned to the deformed lacustrine sequence, although it has little instructive value if the aforementioned age range of 240,000–135,000 years is correct. The minimum age is derived from still-younger shoreline deposits (Hillaire-Marcel and others, 1987) that form a thin discontinuous veneer on the main sheet of debris-avalanche deposits (unit $Qoda_5$) northwest of the deformed lacustrine sequence.

Remnant Erosion Surfaces and Gelai Alluvial Fan Overlie the Ancient Lake Natron Beds

Two distinct geomorphic surfaces have formed above the ancient Lake Natron beds. The higher (older) is associated with sandy gravel that forms a layer less than 1 m thick (in unit Qa_5). The gravel is composed of subrounded to well-rounded clasts 1–6 cm in diameter; pebbles are of volcanic rocks compositionally similar to those found in nearby debris-avalanche deposits (Oldonyo Lengai source). Few of the clasts are vesicular basalt or basanite that might have originated from nearby Gelai volcano. The upper part of the sandy gravel is cemented by pedogenic calcium carbonate 2–5 cm thick with pebbles embedded in it. Its upper surface slopes gently into the basin and stands 7–8 m above the surrounding alluvial plain (fig. 7). Though nearly obliterated by erosion, the sandy gravel and its capping surface are preserved as five small patches, the largest only 0.5 ha in extent and the group of them amassing only 1 ha.

The lower (younger) surface is atop a light-reddish-brown sand informally named the Gelai sandstone, for nearby Gelai school. Where exposed at its westward limit, the Gelai sandstone (Qa_4) is a 3–6-m-thick sequence of poorly sorted sandstone and sandy soils (figs. 8, 9). Though only weakly indurated, the sandstone maintains bluffs along its western exposures.

The Gelai sandstone lacks a pebbly component, although it is overlain by a basalt-cobble lag that thickens eastward toward Gelai volcano. The sand component probably originated by erosion of the extensive tuff deposits of the Natron-Engaruka volcanic field (unit Qnet) and the one nearby tephra cone, Esoit Ondulali (in unit Qnc). Thus the sandstone may have accumulated fairly quickly owing to the fortuitous supply of fine-grained material to the southeast, along the margin of the southernmost Lake Natron basin. If the Gelai sandstone is from such a source, then its deposition must have been dominated by downbasin transport of material (sand carried by an ancestral Sidan Indare stream). In contrast is the later basalt-cobble lag that spread westward from the mouths of streams on the west side of

Figure 7. View west to erosional surface carved into deformed ancestral lake beds of the basin floor. Shimba Kwelwa stands atop the erosion surface, which dips gently northward toward Lake Natron (to right). In middle distance is the upthrown block of the Natron fault escarpment. Mosonik volcano, 20 km distant on skyline, is part of the upthrown block. Photo 7044, February 10, 2010.

Gelai volcano. The lack of basalt cobbles in the Gelai sandstone may be in part a consequence of differing climatic conditions in the past, so that streams draining Gelai volcano lacked the carrying capacity of modern intermittent flash floods.

The geomorphic surface above the Gelai sandstone projects into the basin at slightly lower altitude than the older surface (associated with Qa_5 sandy gravel) discussed earlier in this section. Additional evidence that the two surfaces mark different erosion-aggradation events is the common occurrence of pebbles in deposits associated with the older surface and lack of pebbles in or above the Gelai sandstone alluvial fan. The basalt-cobble lag atop the Gelai fan is not correlative with the sandy gravel of the older surface, because vesicular basalt clasts are lacking or only sparsely present in the sandy gravel, yet they are the only component in the basalt-cobble lag.

An interpretive depositional and erosional sequence of events is illustrated (fig. 10). In it, lacustrine sedimentation of ancestral Lake Natron continues for some period of time following incursion of debris avalanche into the area, but ultimately the lake recedes and an alluvial pebbly sand is layered across the slope. Erosion isolates this pebble-armored surface, perhaps because the basin center to the north subsides more greatly than the southern margin where these outcrops lie. The encroaching Gelai sandstone blankets the area; but then it too erodes back, to form the setting found today.

Figure 8. Red Gelai sandstone of the Gelai alluvial fan. Black basalt cobbles on stream floor have been transported from Gelai volcano, as near as 1.5 km to the east, along streams that flood the top of the alluvial fan deposits and incise into them. Surprisingly, the alluvial fan deposits lack these cobbles. Photo 7032, February 10, 2010.

Figure 9. View east to the red Gelai sandstone of the Gelai alluvial fan, the edge of which is exposed along the east bank of a dry stream bed in the middle ground. In the foreground are disrupted strata of the deformed ancient lake beds; in distance is the flank of Gelai volcano. Photo 7634, March 6, 2010.

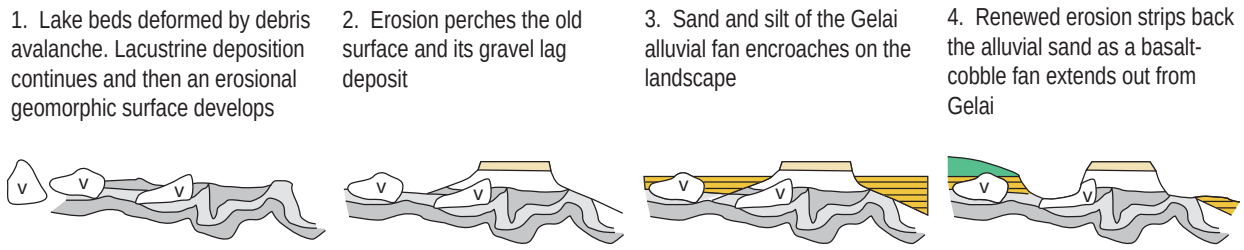

Figure 10. Sequential steps of deposition and erosion to produce the sedimentary deposits and geomorphic surfaces in the southernmost Lake Natron basin adjacent to Gelai volcano. Panel 1 likely corresponds to a time when lake shoreline was at least as high as 650 m altitude, which is known to have occurred most recently between about 240,000 and 130,000 years ago. The debris-avalanche deposits (v) in panel 1 (unit $Qoda_6$ on geologic map) predate the widespread unit of debris-avalanche deposits ($Qoda_5$), which probably was emplaced after Gelai alluvial fan time (after panel 3).

Oldonyo Lengai

Oldonyo Lengai is a classic stratovolcano: a steeply sloped cone comprising alternating layers of lava, lithified ash, and coarser explosion debris ejected by eruptions. Its summit altitude is 2,952 m (Anderson, 2005)[2], about 2,000 m above the adjacent plain. The volcano has a basal diameter of about 6 km. Most eruptions are centered near the present-day summit, giving the volcano a symmetrical profile. (A contour-interval change in the zone 1,800 to 2,800 m altitude on topographic quadrangle maps makes the upper flanks appear to flatten.) A few tephra cones and two tuff rings dot the lower flanks (Dawson, 1962), a few of which presumably are related to the magma system that built the main volcanic edifice (Keller and others, 2006).

Oldonyo Lengai's eruptions are chiefly explosive, producing fallout tephra, pyroclastic flows, and debris flows. Lava flows form less than 10 percent of the exposed cone, to judge from the geologic map by Dawson (1962) (fig. 11). The volcano is only mildly incised, with typical exposures 30–50 m deep in gullies on most flanks. The east and southeast flanks are more deeply eroded than the other flanks, mainly because the central vent has shifted slightly northward in the past several thousands of years but also because prevailing winds favor the deposition of fallout tephra onto the west and northwest flanks. A large landslide from the east flank hollowed a scar about 300 m deep, creating what is now known as the Eastern Chasm (Dawson, 1962; Kervyn and others, 2008a).

Oldonyo Lengai chiefly erupts nephelinite and phonolite (fig. 4). The rocks are peralkaline, with total alkali content of 12–22 percent for silica contents of 40 to 55 percent (tables 7, 8, 9, and 10[3]; all analyses normalized to 100 percent, volatile free, and total iron as FeO). Characteristic mineralogy and approximate paragenetic sequence are illustrated in figure 12. Rocks even lower in silica have issued from lower-flank tephra cones and tuff rings: for example, olivine melilitite (SiO_2 31–40 percent, reported by Keller and others, 2006). The lower-flank vents have an unclear magmatic relation to the volcano, inasmuch as olivine melilitite is common across the wider region of the Natron-Engaruka volcanic field. Carbonatite lava forms only a small part of Oldonyo Lengai. Estimates of its proportion range from less than 5 percent (Klaudius and Keller, 2006) to less than 1 percent (Donaldson and others, 1987). We favor the more restrictive estimate.

Our fundamental understanding of Oldonyo Lengai's geology originates in the work of J. Barry Dawson (1962). He divided the main-cone volcaniclastic rocks into two stratigraphic units: (1) yellow tuff and agglomerate (YTA), which forms almost the entire cone, and (2) black tuff and agglomerate (BTA), which caps the sequence (fig. 11). As the names suggest, Dawson's (1962) yellow and black units are similar lithologically, aside from color. From a field perspective, the difference between them is the degree of alteration. Glass has altered so fully to zeolite and clay minerals (palagonite) in the older unit (yellow tuff and agglomerate) that hand sample and outcrop are now dominated by grayish yellow to brownish yellow hues. In contrast, black tuff and agglomerate is less altered, and its fresher, glassy ash component lends a dark-gray aspect to outcrop and hand sample. The degree of alteration is a time-dependent process and therefore can be a useful indicator of relative stratigraphic age. Indeed, many geochemical analyses from Oldonyo Lengai are coded by their assignment to the yellow or black stratigraphic units (for example, Donaldson and others, 1987), a procedure that proves helpful when reexamining previously published data. Although our geologic map unit for main-cone strata (Qom) does not distinguish between the yellow or black tuff-agglomerate units, we utilize the distinction to aid discussion in this pamphlet.

According to Dawson (1962), a sharp erosional contact separates the yellow from the black tuff-and-agglomerate units. We found this true at some sites, but in other places the boundary was difficult to place owing to a transitional zone that ranged from a few meters to tens of meters in thickness. The nature of the contact between the older (yellow) and younger (black) volcaniclastic beds of the main cone warrants deeper examination than we could give to it, because its volcano-wide presence would indicate that Oldonyo Lengai was inactive for a lengthy period of time in its past. Also unresolved by us is the approximate age range marked by the boundary, regardless of its abrupt or transitional character.

To avoid confusion we retain the term "agglomerate" when referring specifically to the black or yellow tuff-and-agglomerate units, although, in modern terminology, most of the poorly

[2]Orthometric altitude, above mean sea level. The highest topographic contour on Oldonyo Lengai quadrangle (1990, sheet 39/4) is 2,940 m, and no spot measurement marks the peak, so summit altitude determined by map inspection could be known only as lying between 2,940 and 2,960 m.

[3]Tables 7 through 10 appear beginning on page 22.

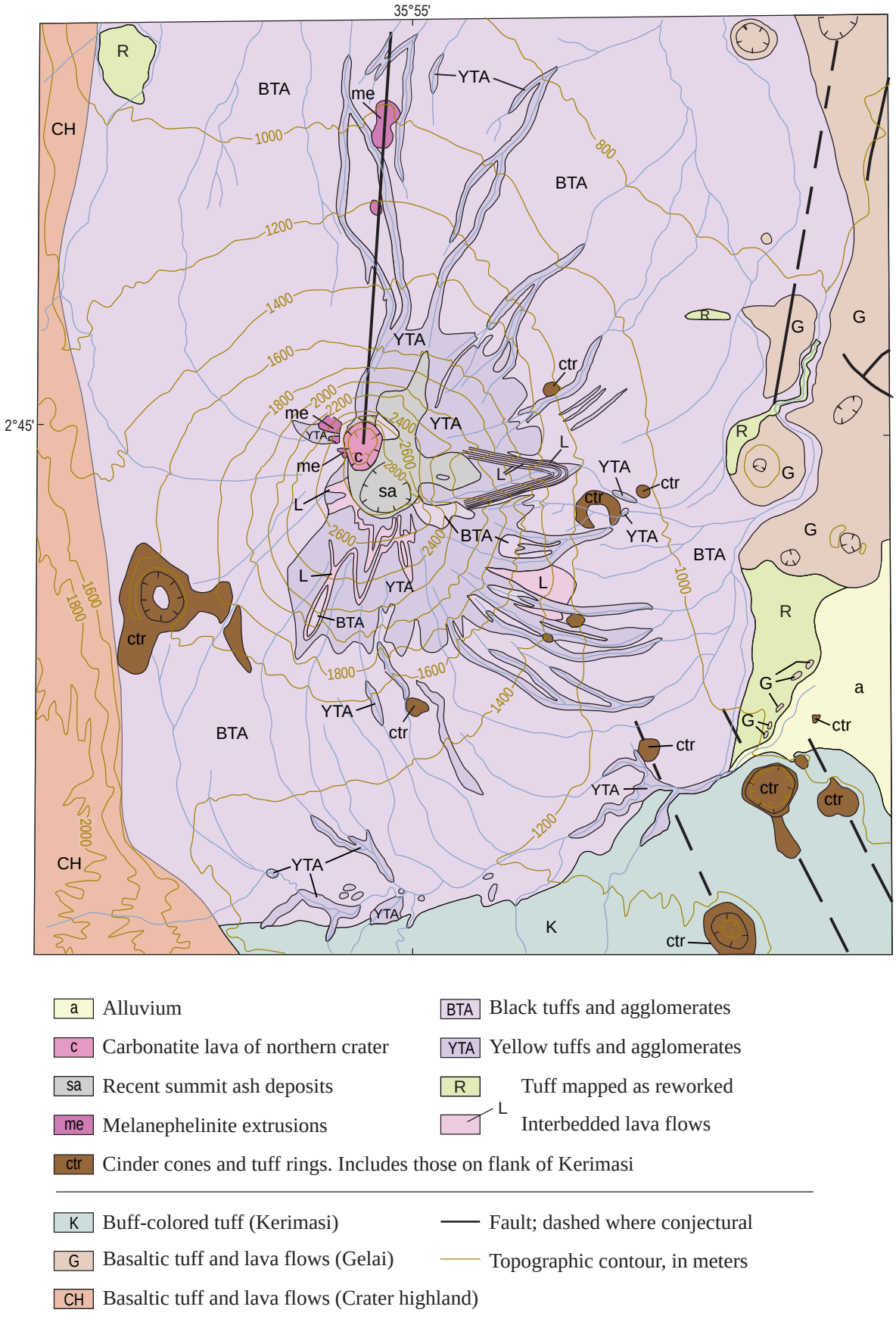

Figure 11. Dawson's (1962) geologic map of Oldonyo Lengai. Map was compiled by Dawson from nonrectified aerial photographs, without geodetic control. Scale therefore varies greatly across area of map, but image area is about 14 km wide and 16 km high when estimated from topographic map. Topographic contours added here to convey topographic relief; they have been rubber sheeted (distorted) to fit the recognizable geographic features.

sorted beds at Oldonyo Lengai are classified as tuff breccia or lapilli tuff. Each of these terms describes size and sorting characteristics of volcaniclastic deposits (fig. 13) (Schmid, 1981; Fisher and Schmincke, 1984; Le Maitre, 2002). For example, tuff is indurated ash (grain size less than 2 mm); hence, a tuff contains >75 percent fine particles in a moderately sorted or well sorted rock. Agglomerate (or breccia) describes a coarse-grained rock (>75 percent of material larger than 64 mm). Between these end members lies the range of poorly sorted volcaniclastic rocks in which the abundance of ash-size material forms 25–75 percent of the rock. If the balance of material (aside from the ash-size component) is larger than 64 mm (blocks and bombs), then the rock is a tuff breccia or tuff agglomerate; if the balance of material is small (size 2–64 mm, lapilli), then the rock is a lapilli tuff. The poorly sorted rocks such as lapilli tuff and tuff breccia commonly form by flowage phenomena—pyroclastic flows (glowing avalanches), lahars (volcanic mudflows or debris flows), and debris avalanches. All three processes are important at Oldonyo Lengai.

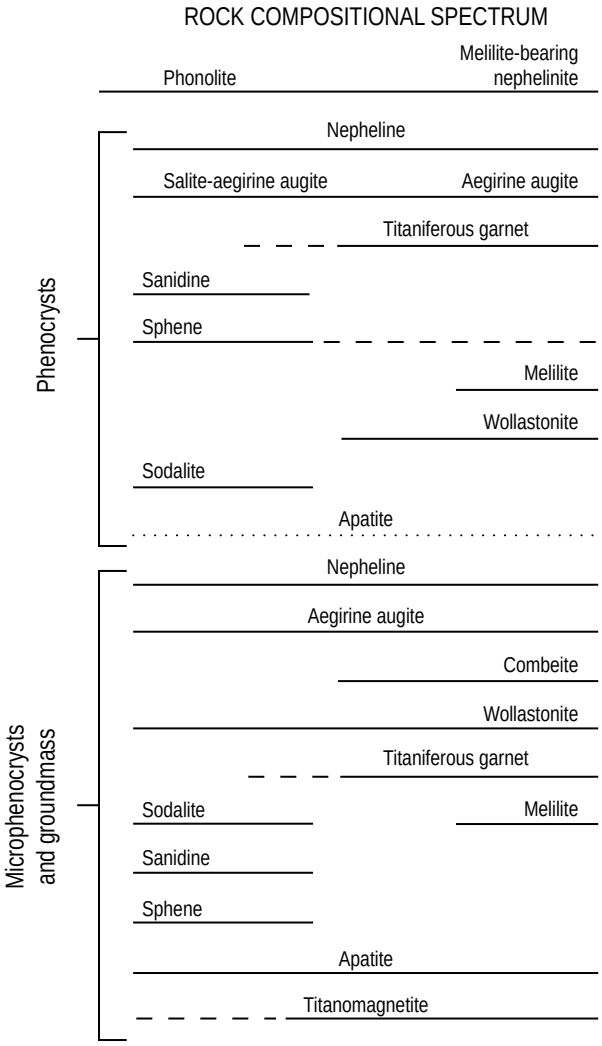

Figure 12. Mineral associations across the rock-compositional spread of Oldonyo Lengai lava. Dashed line, mineral is less abundant; dotted line, mineral is sparse. Vertical sequence among phenocrysts roughly approximates the paragenetic sequence (early formed minerals at top of grouping). Illustration composited from Donaldson and others (1997, fig. 2) and Klaudius and Keller (2006, fig. 3).

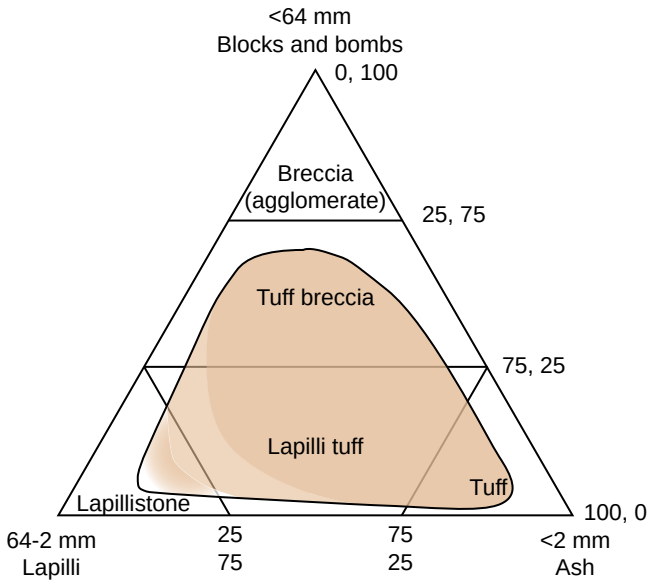

Figure 13. Volcaniclastic rock classification based on size and proportion of fragments (fig. 5-1 of Fisher and Schmincke, 1984). Shown shaded is approximate range of volcaniclastic rock types in Dawson's (1962) units of yellow tuff and agglomerate (YTA) and black tuff and agglomerate (BTA) as found in the Oldonyo Lengai stratovolcano (our unit Qom, main-cone deposits).

Figure 14. Tuff and lapilli tuff in midcone exposures of the Eastern Chasm. View north to north chasm wall at 1540-m altitude. Photo encompasses about 30 m of stratigraphic section, entirely volcaniclastic. Photo 7374, February 23, 2010.

Table 7. Whole-rock major and trace element chemical analyses from lava flows of Oldonyo Lengai.

[Major-element analyses normalized to 100 percent, volatile free. Also shown are original oxide totals and values for loss on ignition. Data compiled and available in a spreadsheet that accompanies this publication. For analytical methods see appendix 3]

Table No.	1	2	3	4	5	6	7	8
Sample No.	S10-L110	S10-L276	S10-L274	S10-L303	S10-L305	S10-L307	S10-L279	S10-L103
Rock type	Foidite	Foidite	Foidite	Phonolite	Phonolite	Phonolite	Phonolite	Phonolite
Major-element analyses, normalized water-free (weight percent)								
SiO_2	46.39	47.15	47.32	49.67	50.05	51.18	52.32	53.77
TiO_2	0.98	1.28	1.08	1.19	1.15	1.13	1.15	1.08
Al_2O_3	19.09	16.01	13.88	18.17	20.15	19.26	18.99	19.03
FeO*	6.71	8.06	9.51	7.19	7.09	7.01	5.77	5.72
MnO	0.25	0.32	0.41	0.26	0.22	0.22	0.19	0.19
MgO	0.78	1.36	0.73	0.87	0.67	0.62	0.97	0.76
CaO	6.69	9.54	8.94	6.01	3.84	4.25	4.85	3.80
Na_2O	13.77	10.36	12.14	11.19	10.40	10.63	10.52	10.60
K_2O	5.09	5.29	5.57	5.16	6.29	5.57	4.89	4.76
P_2O_5	0.25	0.63	0.43	0.29	0.14	0.12	0.37	0.28
Loss on ignition	3.57	5.05	5.76	4.87	4.01	3.57	1.93	1.53
Original oxide total	95.73	93.45	91.54	93.60	94.93	95.12	96.29	96.90
Trace-element analyses (parts per million)								
Ni	5	9	8	5	3	5	5	4
Cr	2	5	3	2	2	2	3	2
Sc	2	2	2	2	1	1	3	2
V	133	183	125	117	83	125	92	69
Ba	1467	1714	2628	1555	1584	1533	1628	1454
Rb	101	148	127	83	120	96	119	100
Sr	2325	2444	3341	2575	1384	2387	2102	1820
Zr	550	933	898	551	516	526	575	599
Y	42	50	36	40	33	36	33	36
Nb	154	205	325	159	152	159	172	170
Ga	29	33	35	30	32	30	27	29
Cu	10	28	35	13	12	14	11	11
Zn	186	218	307	193	166	180	147	154
Pb	31	32	48	40	27	31	29	34
La	120	108	200	143	110	113	148	155
Ce	180	151	288	212	181	184	249	247
Th	14	10	22	20	23	24	27	29
Nd	54	51	82	60	59	58	81	77
U	6	9	11	11	3	7	7	7

Table 8. Whole-rock major and trace element chemical analyses from scoria bombs on flanks of Oldonyo Lengai.

[Major-element analyses normalized to 100 percent, volatile free. Also shown are original oxide totals and values for loss on ignition. Data compiled and available in a spreadsheet that accompanies this publication. For analytical methods see appendix 3]

Table No.	1	2	3	4	5
Sample No.	S10-L275B	S10-L271	S10-L79	S10-L46	S10-L47
Rock type	Foidite (nephelinite)	Foidite (nephelinite)	Phonolite	Foidite (melilitite)	Foidite (nephelinite)
Geographic location	Pre-collapse, crater-filling bed	Inactive south wall of northern crater	South flank, thin debris flow	East of Kirurum	East of Kirurum
Major-element analyses, normalized water-free (weight percent)					
SiO_2	41.70	46.58	51.49	38.24	43.21
TiO_2	1.80	1.08	1.16	1.70	0.87
Al_2O_3	13.67	14.47	18.70	11.41	21.41
FeO*	10.76	8.63	6.05	9.52	5.19
MnO	0.38	0.37	0.23	0.45	0.14
MgO	1.05	1.42	0.88	3.13	3.45
CaO	19.30	14.15	4.34	25.18	9.94
Na_2O	7.02	7.79	12.03	8.34	10.92
K_2O	4.20	4.53	4.83	1.31	3.83
P_2O_5	0.13	0.99	0.29	0.73	1.04
Loss on ignition	7.11	9.34	0.81	7.38	1.33
Original oxide total	90.76	88.57	97.74	88.46	98.70
Trace-element analyses (parts per million)					
Ni	8	9	5	16	7
Cr	2	5	2	17	3
Sc	2	1	1	4	4
V	400	161	101	288	78
Ba	561	2012	1698	918	367
Rb	96	128	97	23	60
Sr	1828	3282	2277	3192	887
Zr	588	798	665	545	427
Y	52	45	38	109	21
Nb	212	285	205	306	67
Ga	26	30	30	23	22
Cu	12	33	4	54	9
Zn	138	240	177	500	62
Pb	11	44	31	7	7
La	99	170	163	167	69
Ce	261	256	267	382	124
Th	17	19	32	35	5
Nd	126	82	85	202	50
U	8	10	9	8	3

Table 9. Whole-rock major and trace element chemical analyses for lapilli from tephra falls and tephra cones.

[Major-element analyses normalized to 100 percent, volatile free. Also shown are original oxide totals and values for loss on ignition. Data compiled and available in a spreadsheet that accompanies this publication. For analytical methods see appendix 3. The two samples with melilitite composition (L97, L236) are from vents assigned to Natron-Engaruka volcanic field. All others erupted from Oldonyo Lengai]

Sample No.	S10-L299	S10-L106	S10-L259	S10-L300	S10-L97	S10-L236	S10-L154
Rock type	Foidite (nephelinite)	Foidite (nephelinite)	Foidite (nephelinite)	Foidite (nephelinite)	Foidite (melilitite)	Foidite (melilitite)	Foidite (nephelinite)
Geographic location	Tephra on escarpment	Bomb in xtl-lithic tuff	Lapilli fall NW flank	YTA lapilli fall	Lapilli from Dorobo cone	Lapilli from Embalulu Oltatwa	Scoria cone near Embalulu Oltatwa
Major-element analyses, normalized water-free (weight percent)							
SiO_2	44.49	45.61	46.18	46.42	31.55	38.76	45.66
TiO_2	1.18	1.62	1.37	1.77	2.77	4.41	1.68
Al_2O_3	15.86	15.49	15.55	14.04	6.69	9.30	16.92
FeO*	6.68	9.26	8.97	9.01	11.40	13.18	8.48
MnO	0.25	0.33	0.34	0.28	0.45	0.24	0.31
MgO	1.85	1.94	1.59	2.63	6.25	13.51	1.71
CaO	11.96	10.89	11.31	13.07	31.97	11.71	9.95
Na_2O	11.07	8.94	9.22	7.44	3.57	4.39	10.34
K_2O	5.95	5.02	4.65	4.27	2.80	3.30	4.43
P_2O_5	0.70	0.88	0.83	1.08	2.53	1.19	0.52
Loss on ignition	14.58	7.61	7.38	8.71	18.73	6.69	4.76
Original oxide total	83.52	91.29	90.25	89.67	77.90	91.78	93.72
Trace-element analyses (parts per million)							
Ni	18	10	11	18	62	144	7
Cr	17	5	8	24	151	298	4
Sc	3	3	2	6	12	25	2
V	208	154	167	164	269	194	165
Ba	1250	1634	1343	1706	2877	590	1607
Rb	160	125	127	144	132	100	84
Sr	5380	2650	2135	2740	6467	1595	2320
Zr	360	560	821	479	472	484	530
Y	38	49	47	40	64	35	53
Nb	174	186	222	160	146	164	197
Ga	24	25	29	21	13	17	24
Cu	30	25	42	36	120	152	14
Zn	141	208	210	152	195	129	192
Pb	29	30	28	20	54	11	34
La	122	150	102	107	211	131	174
Ce	207	235	164	179	294	262	275
Th	29	12	10	8	17	17	18
Nd	72	77	55	65	95	111	95
U	8	7	3	5	9	4	9

Table 10. Whole-rock major and trace element analyses from blocks in tuff breccia on Oldonyo Lengai and within debris avalanche deposits.

[Major-element analyses normalized to 100 percent, volatile free. Also shown are original oxide totals and values for loss on ignition. Data compiled and available in a spreadsheet that accompanies this publication. For analytical methods see appendix 3]

Table No.	1	2	3	4	5	6	7	8
Sample No.	S10-L304	S10-L82	S10-L306	S10-L156	S10-L26A	S10-L149	S10-L26B	S10-L49
Rock type	Foidite (nephelinite)	Foidite (nephelinite)	Foidite (nephelinite)	Foidite (nephelinite)	Foidite (nephelinite)	Foidite (nephelinite)	Foidite (nephelinite)	Foidite (nephelinite)
Lithologic unit	Tuff breccia	Tuff breccia	Tuff breccia	Tuff breccia	Debris av.	Debris av.	Debris av.	Debris av.
Major-element analyses, normalized water-free (weight percent)								
SiO_2	47.52	47.68	49.76	49.82	46.76	46.91	49.04	44.77
TiO_2	1.44	0.97	1.11	1.16	1.92	1.37	2.13	1.67
Al_2O_3	17.26	17.45	19.18	18.04	16.11	15.37	17.43	15.88
FeO*	7.87	7.54	6.69	6.59	9.07	8.15	8.65	8.74
MnO	0.25	0.28	0.21	0.23	0.26	0.27	0.23	0.28
MgO	1.19	0.57	0.63	1.07	1.83	1.53	1.85	2.16
CaO	6.80	6.01	4.51	5.79	10.01	9.06	7.83	13.38
Na_2O	12.49	13.74	12.38	12.16	9.64	12.39	7.97	7.80
K_2O	4.72	5.46	5.30	4.68	3.70	4.41	4.41	4.49
P_2O_5	0.45	0.29	0.23	0.47	0.69	0.55	0.46	0.83
Loss on ignition	3.10	3.79	4.31	3.04	6.21	1.93	4.47	6.32
Original oxide total	95.00	94.32	94.10	96.24	92.98	95.90	94.18	92.73
Trace-element analyses (parts per million)								
Ni	7	4	4	5	6	17	7	9
Cr	2	1	2	0	5	21	3	7
Sc	1	1	2	2	3	3	5	4
V	159	144	111	97	192	191	172	185
Ba	1449	1796	1350	1515	1627	1716	1527	1174
Rb	105	106	101	84	73	79	89	79
Sr	2407	2406	1822	1894	2819	2491	2660	2751
Zr	512	576	493	577	504	510	559	525
Y	39	32	34	36	37	37	37	45
Nb	161	203	150	183	171	180	190	157
Ga	27	30	31	27	20	29	26	24
Cu	18	12	14	9	24	18	33	18
Zn	178	221	170	163	156	190	154	174
Pb	28	34	31	25	15	27	25	17
La	126	142	114	137	145	151	148	109
Ce	189	224	181	245	247	251	263	177
Th	19	22	22	25	18	22	26	9
Nd	60	71	58	84	86	84	86	62
U	7	7	6	7	5	6	2	5

The main-cone lapilli tuff and tuff breccia at Oldonyo Lengai are characterized by dense lava fragments in a fine-grained matrix. Most such deposits on the middle and upper slopes are nearly monolithologic in their clast population (fig. 14). Many are poorly sorted mixtures of fallout ash, blocks, and bombs, both in primary deposits and in the somewhat better sorted beds where the debris has rolled downslope before coming to rest. The blocks and lapilli commonly have distinct rims that, because of alteration, are darker than the core of the fragments. The rims doubtless were once glassier than the cores, a textural distinction now mimicked by the color contrast. Dense or slightly vesicular fragments are the mainstay of the volcaniclastic beds; neither breadcrusted bombs nor pumiceous fragments were seen.

On the lower flanks, debris-flow deposits increase in abundance. They form thicker beds, are more poorly sorted, have scattered large blocks, and are more heterogeneous in their component clasts (fig. 15).

Shown separately on Dawson's (1962) map are a few lava flows, tephra cones, and tuff rings on the lower flanks (fig. 11). Their boundaries are readily traced in the field, so many of these same units appear on our geologic map. Lava flows within the main-cone sequence, exposed in the south wall of the Eastern Chasm, are difficult to show at common map scales. As pictured in figure 16, the four lava sequences mapped in the Eastern Chasm by Dawson (1962) comprise several 'a'ā lava flows 2–6 m thick. These lava sequences, each about 10–20 m thick, extend only about 2.2 km from the present-day summit (approximate volcanic center). They thin abruptly downslope as the number of flows within them decreases. The lava sequences form about 20–30 percent of the Eastern Chasm stratigraphic section, which is relatively near the vent. Conceivably the bulk of the cone contains that proportion of lava flows, even if the current surface exposures show far less. Lava flow compositions are listed in table 7.

The interlayered sequences of lava flows leave open the question of whether some of the lapilli tuff and tuff breccia of the main cone may have originated by collapse of the leading edges of the lava flows. Such a process is likely on a steep volcano, producing what is known as Merapi-type glowing avalanches. But we saw little evidence among the volcanic deposits, such as radially jointed blocks, for flow-front-collapse processes.

Summit Craters and Summit Structure

The summit of Oldonyo Lengai is crowned by its northern eruptive crater. The northern crater is active today and has been the center of eruptions during the past several thousand years. The extent and size of the northern crater have changed frequently during the past 50 years. Current descriptions can be found on the Smithsonian Institution's website for the Global Volcanism Program (http://www.volcano.si.edu/world/) or on a site long maintained by Frederick Belton (http://oldoinyolengai.pbworks.com/). Conditions as we found them in March 2010 are described in appendix 6.

The volcano's southern crater, in contrast, is a shallow, 7-m-deep, elongate trough, a vestige of what was once a much larger central crater for the volcano. Its south rim is the south wall of that ancestral crater. The trough is pinched in on its north side by the volcanic buildup that rims the northern crater, including the highest point on the volcano today.

The ancestral large central crater, now obscured, was infilled with bomb-laden lapilli tuff and tuff breccia. These deposits are exposed as flat-lying strata at the head of the Eastern Chasm (fig. 17). The crater-filling beds are buttressed against steeply dipping volcaniclastic beds and lava flows exposed on the south side of the Eastern Chasm, a contact we have viewed from lower on the northeast slope but have not approached. The outcrops of flat-lying beds at the head of the Eastern Chasm span a north-south distance of 600 m. Farther north, outcrops of the flat-lying beds terminate abruptly where buried by eruptive deposits of the past

Figure 15. Debris-flow deposits (lahars) in gulch east of lower Nasira cone. Boulders near center of photo are 0.8–1.0 m across. Photo 6865, February 6, 2010.

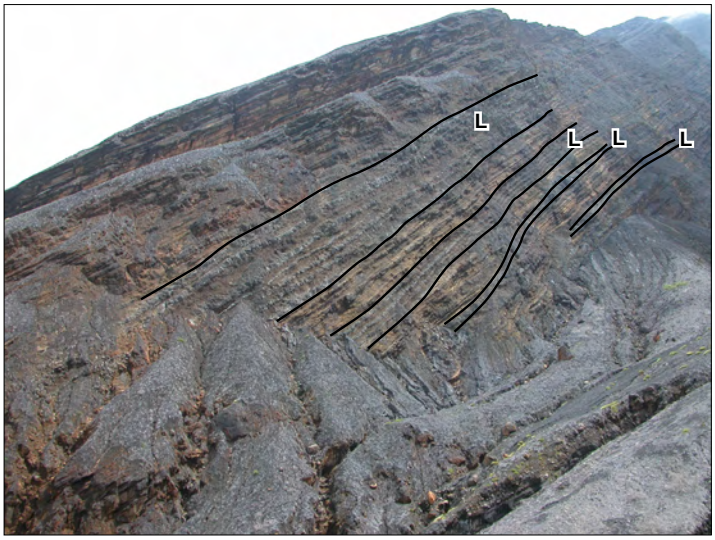

Figure 16. Interbedded sequences of lava flows and lapilli tuff exposed in Eastern Chasm of Oldonyo Lengai. View south 400 m to cliffs of Eastern Chasm; cliff height about 200 m. Lines on photo demarcate boundaries between beds of chiefly lava flows (**L**) and those of lapilli tuff. Photo 7384, February 23, 2010.

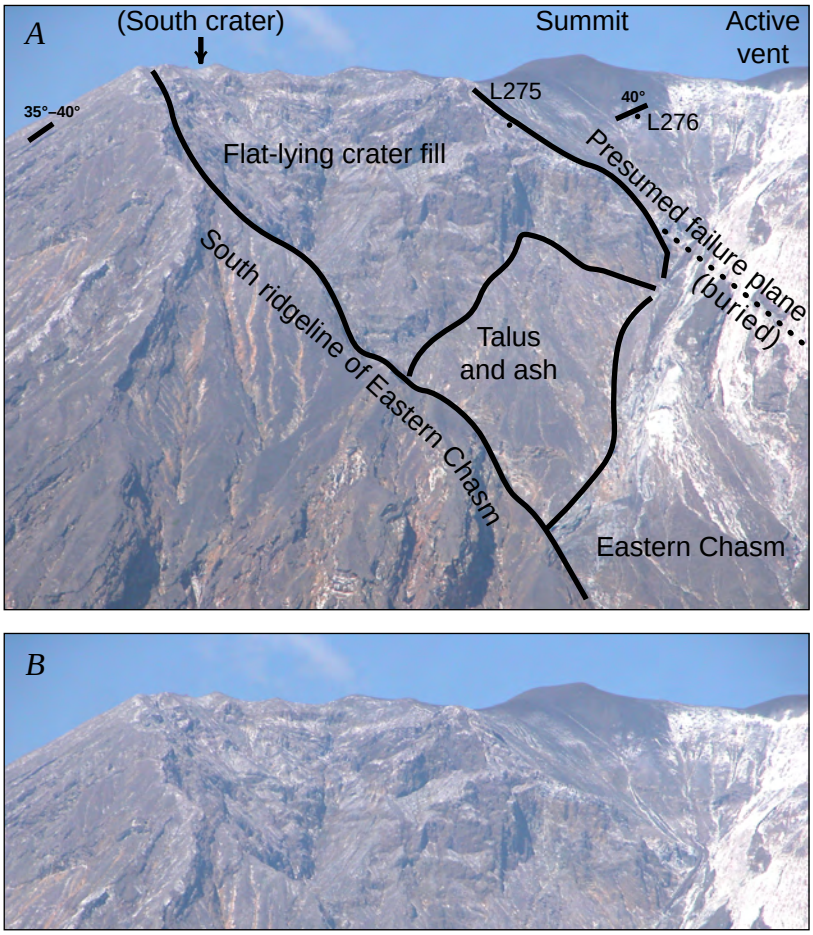

Figure 17. View west into Eastern Chasm and summit area. *A*, Annotated photo to show features discussed in text. The south wall of Eastern Chasm curves in behind the ridgeline, so that left third of photo shows volcano flank. Flat-lying strata at head of Eastern Chasm are interpreted as the infill of an ancestral main crater whose south edge, where traced across the summit, forms the southern edge of shallow modern trough known as southern crater. Shown dotted is the failure plane that we consider the headwall for at least one of the debris avalanches whose deposits, as first interpreted by Keller (2002), litter the area north of Oldonyo Lengai. Other labeled features include dip of south flank beds, apparent dip (line) and actual dip of lava layer at sample site L276, and approximate location of sample L275, the other of two analyzed samples collected within field of view. *B*, Unadorned photo 6766, February 3, 2010.

few centuries. The old central crater would have been 600–1,000 m in diameter.

The northern termination of the flat-lying beds begs a structural question that was first posed by Keller (2002): have the beds been truncated by slope collapses from the north side of the volcano? In the interpretation of Klaudius and Keller (2006), the south-wall corresponds to the headwall of the slope failure, which gutted the northern flank of early Oldonyo Lengai (the cone they called "Lengai I"). The resulting debris avalanches spread northward across the southernmost Lake Natron basin; thus, the main sheet of debris-avalanche deposits (unit $Qoda_5$; the zebra unit of Klaudius and Keller, 2006) is the splayed guts of Lengai I. Subsequent volcanic eruptions rebuilt the cone to its modern height (their volcanic phase Lengai II), and the flat-lying beds are part of Lengai II.

Although concurring that Oldonyo Lengai is the source of the debris-avalanche deposits, we consider it likely that the main sheet of debris-avalanche deposits originated from an ancestral cone, the stump of which is entirely buried by today's main cone (south and north flanks). The flat-lying central-crater beds likely are truncated at their northern limit, but the cause may be relatively small slope failures and not the major event that formed the main-sheet debris-avalanche deposits. It is difficult to explain the substantial thickness of flat-lying strata near the volcano's summit unless those beds formed while the central crater was nearly intact, with a bounding northern rim. If slope failure had already chiseled its way back to the south flank before the flat strata were deposited, the vent of today's northern crater would have been shedding fragmental debris and lava flows into beds that slope against an old south flank. Although it may seem petty to argue about the positioning of a fundamental truncation—1,000 m north or south—the conclusion may be important for future scientists who bring new tools to bear on near-vent evidence for the age of the collapse event.

Summit Carbonatite Lava Flows

As far as is known, carbonatite lava at Oldonyo Lengai erupts only from the summit. In the past century the vent for these lava flows has been the northern crater, which has filled passively and been excavated explosively several times. When full or nearly so, the crater and its carbonatite lava flows have been approachable for close study. Interest in these flows has remained high because Oldonyo Lengai is the only volcano in the world currently displaying such activity. The research on carbonatite fills books and scientific journals (for example, Bell and Keller, 1995).

A few carbonatite lava flows from the summit vent flowed onto the middle flanks of Oldonyo Lengai. Since about 2005, these have been mapped successfully by remote sensing techniques (for example, Kervyn and others, 2008b; Vaughan and others, 2008). One of the most extensive of these lava flows spilled down the west flank of the volcano in 2006, forming pāhoehoe and ʻaʻā (fig. 18).

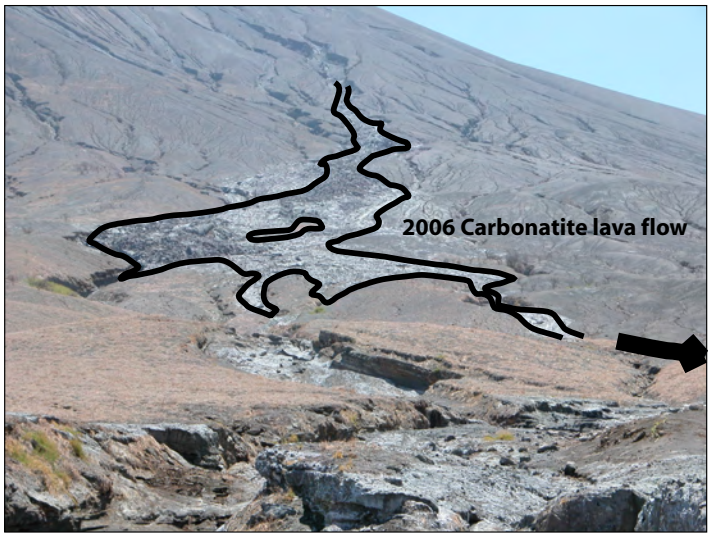

Figure 18. View southwest across lower reach of carbonatite lava flow of 2006. Erupted from the volcano's summit, this lava filled a small canyon on the steep west slope and then spread out on the gentler lower slope. Photo 6267, January 19, 2009.

Lava Flows and Vents on the Lower Flanks

Phonolite Lava on the East Flank

The stubby snout of a 100-m-thick phonolite lava (unit Qomlp; table 7, No. 8; fig. 19) is exposed prominently at the 1,200-m altitude on the volcano's east flank. A climbers' trail surmounts the south edge of the flow en route to the summit. The base of the lava is not exposed.

Alkali feldspar from the phonolite yielded a $^{40}Ar/^{39}Ar$ plateau age of 338±23 ka (table 11, No. 1). The lava forms part of the gently sloping apron upon which the modern cone of Oldonyo Lengai is built, and its age suggests the phonolite is among the oldest of the rocks exposed on the volcano's modern flanks. Little else is known about the stratigraphic position of this lava in the main-cone sequence, except that it is overtopped by south-flank tephra and debris-flow deposits. Its outcrops cannot be traced far upslope. As an alternate hypothesis, the phonolite lava could have erupted locally from a vent centered in the semicircular area defined by its eastern outcrop limit, thereby forming a flat-topped dome about 800 m in diameter; we think this hypothesis unlikely.

Because of its phonolitic composition, this lava's age is of more than passing interest. One petrologic model of Oldonyo Lengai's magmatic history suggests that phonolite magma has not erupted since the demise of Lengai I, an early stage of Oldonyo Lengai's growth that preceded emplacement of the main sheet of debris-avalanche deposits (Klaudius and Keller, 2006)—an event that occurred more than 10,000 years ago, as discussed below in a section entitled Debris-Avalanche Deposits. The radiometric age of the phonolite permits that petrologic model.

A small tephra cone lies about 300 m southeast of the phonolite lava. Its lapilli are highly porphyritic and mineralogically similar to the lava. A sample analyzed by Klaudius and Keller (2006, their sample OL442) gave a phonolitic composition, whereas our analysis of a porphyritic bomb (table 9, sample S10-L106) is somewhat lower in silica and total alkalis.

Embalulu Oltatwa (Oltatwa Crater)

Oltatwa is a 650-m-diameter tuff ring on the lower east flank of Oldonyo Lengai. The ring is incomplete in map view because its south side has been overtopped by debris from Oldonyo Lengai. Consequently, it is largely infilled by fluvial sand, debris flows, and fallout tephra. During rainy periods, streams cascade down the west crater wall, pour across the crater floor, and escape through notches in the east wall. Debris-flow deposits flank all sides, burying the contact between tuff ring and underlying strata.

Primary magmatic material comprises lapilli and ash of olivine+phlogopite melilitite(?) (table 9, sample S10-L236). Bombs are lacking; the largest lapilli found are rarely 3 cm across. Phlogopite and olivine also occur as free crystals in the ashy matrix of the tuff beds. Lithic lapilli 0.2–1 cm across crowd most layers. Bedrock lava fragments as large as 1.5 m are scattered throughout the deposit, which ranks Oltatwa among the coarser-grained tuff rings in the area.

The age of the tuff ring is 353±65 ka ($^{40}Ar/^{39}Ar$ from phlogopite, table 11, No. 2), on the basis of a sample collected about two-thirds up the west wall. The Oltatwa tuff ring lies 750 m north of, and only slightly lower (altitude 1,100–1,200 m) than, the phonolite lava flow (unit Qomlp; fig. 19). The tuff ring and phonolite lava are some of the oldest rocks exposed in Oldonyo Lengai's cone, jutting out from the lower apron of the cone and slowly being buried by its growth.

A small debris-avalanche deposit (or thick coarse debris flow) banks against the upslope, west flank of the Oltatwa tuff ring. The debris-avalanche deposit (unit $Qoda_1$) may have formed during the debris-avalanche event that gutted the Eastern Chasm and shed deposits east-northeast (unit $Qoda_2$) to bank against Lalarasi cone. Alternatively, it may have formed later, during some smaller flank failure. Oltatwa lies south of the run-out path for the unit-2 debris-avalanche deposits ($Qoda_2$), so the absence of those deposits on Oltatwa has no bearing on relative stratigraphic ages of these various units.

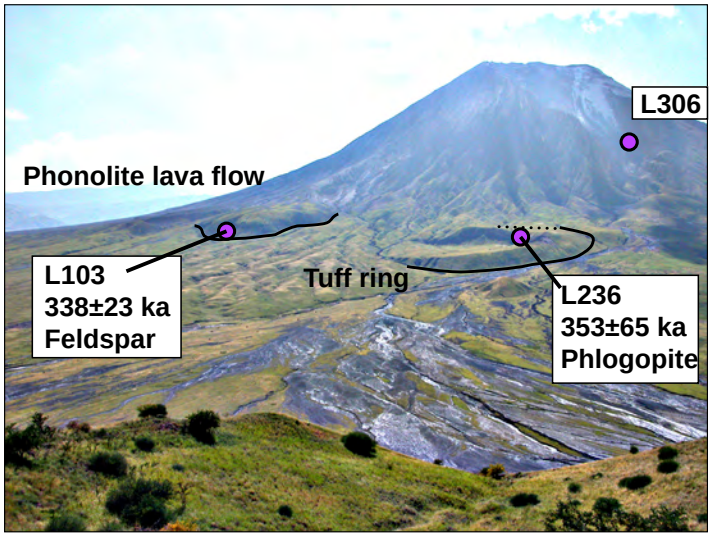

Figure 19. Photo of east flank of Oldonyo Lengai to show geography of Oltatwa tuff ring and phonolite lava flow. Photo 6773, February 3, 2010, retouched here to remove haze.

Table 11. New $^{40}Ar/^{39}Ar$ radiometric ages from Oldonyo Lengai.

[Preferred ages are plateau ages, shown in bold. Errors are estimates of analytical precision at the 95-percent confidence level. MSWD, mean square of weighted deviates (York, 1969). $^{40}/_{36}$ i, $^{40}Ar/^{36}Ar$ isochron intercept. See appendix 5 for argon plateau and isochron diagrams]

			Plateau age					Isochron age			
	Sample	Material	%^{39}Ar (steps)		Age (ka)	Error (2σ)	Total-gas age (ka)	Age (ka)	Error (2σ)	MSWD	$^{40}/_{36}$i
Oldonyo Lengai cone											
1.	S10-L103	Alkali feldspar	94.6	(8 of 10)	**338**	**23**	377±25	330	44	0.21	296.6±5.0
2.	S10-L236B	Phlogopite	94.3	(7 of 8)	**353**	**65**	336±71	342	523	0.04	296.1±30.6
Blocks within debris-avalanche deposits shed from Oldonyo Lengai											
3.	S10-L136	Phlogopite	99.4	(6 of 8)	**460**	**75**	511±100	455	548	0.08	295.9±46.9
4.	S10-L65	Phlogopite	99.2	(6 of 9)	**793**	**63**	862±94	721	494	0.21	300.4±33.5

[1] Locations (WGS84):

S10-L103	lat -2.7718	long 35.9497	S10-L136	lat -2.5507	long 35.8875
S10-L236B	lat -2.7579	long 35.9501	S10-L65	lat -2.6373	long 35.9837

Nasira Cones

Three tephra cones, four spatter mounds, and two ‘a‘ā lava flows were erupted from a fissure on the north flank of Oldonyo Lengai (fig. 20). The cones are among the few in the map area built chiefly of scoria—vesicular to dense primary lapilli and bombs. In contrast, most other cones visited are either tuff (virtually no lapilli) or fine-grained lapilli cones in which most material is smaller than 2 cm grain size. The lava and tephra are nephelinite (table 12) that lie within the field defined by other Oldonyo Lengai compositions (black squares on fig. 4).

The tephra cones are aligned on a trend N. 7° E. The northern two cones (lowest on slope, 1 and 2 on fig. 20) form an overlapping pair, each possessing a circular spatter rim that defines a shallow crater (fig. 21*A*). A stubby ‘a‘ā lava flow fringes the southeast side of cone 2 (site of sample S10-L28 in fig. 21*A*).

South of them is the third, and largest, cone. It, too, has a summit crater. ‘A‘ā lava issued from low on the flank of this cone and flowed downslope 1 km. Cone 3 is notable for its dense spherical lapilli and bombs 2–10 cm across. A scalloped exposure on the southeast side shows 12 m of beds, many of them rich in these cannonball lapilli. A gulch exposure on the east side has cannonball lapilli packed tightly in a bed 1 m thick. As noted by Keller and others (2006), the cannonball lapilli commonly are cored bombs, containing small inclusions of ijolite, a plutonic rock composed mainly of nepheline and pyroxene.

Continuing south and upslope, the Nasira vent alignment is defined by four small spatter mounds, 1–4 m high (fig. 21*B*), that are aligned on trend N. 18° E., slightly askew from the alignment defined by the tephra cones (fig. 20). The farthest mound upslope, at 1,170 m altitude, is 650 m from the crater of the large cone. The Nasira vents span a total distance of 1.2 km.

Also annotated in figure 21*B* (label DF) is a semicircular lobe even farther upslope, beyond the highest spatter mound. We investigated it to see if it might be the half-buried (downslope) edge of another tephra cone in the alignment, but no evidence

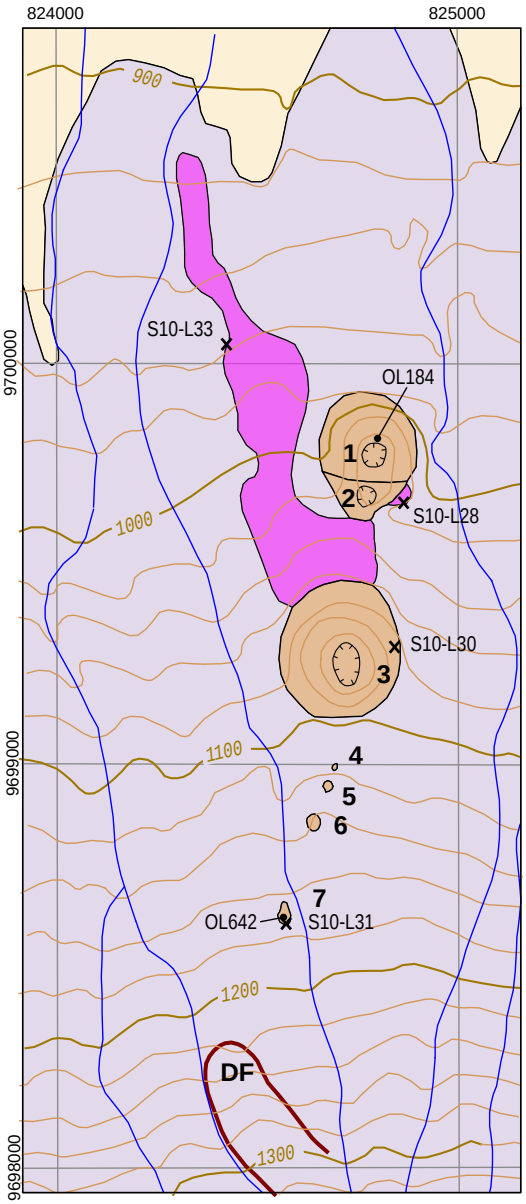

Figure 20. Geologic map of Nasira tephra cones (1–3), spatter mounds (4–7) and lava flows, north flank Oldonyo Lengai. Bold line and label DF show lobate snout of debris flow. Sample numbers indicate whole-rock geochemical analyses (OL numbers from Keller and others, 2006; S10 numbers from this publication, table 12). UTM grid, with 1-km spacing for scale, is in datum Arc 1960, to match geologic map. Vertical grid members (eastings) run essentially north-south (grid divergence is nil). Contour interval 20 m.

Table 12. Whole-rock major and trace element chemical analyses from Nasira cones and lava flows.

[Dashes, no data; b.d., below detection level. Major-element analyses normalized to 100 percent, volatile free. Also shown are original oxide totals and values for loss on ignition, for completeness. Data compiled and available in a spreadsheet that accompanies this publication. References: 1, Keller and others, 2006; 2, this report. For analytical methods see source references or, for this report, appendix 3]

Table No.	1	2	3	4	5	6
Sample No.	S10-L33	S10-L28	OL184	S10-L30	S10-L31	OL624
Feature	Lava flow	Northern cone	Northern cone	Southern cone	Spatter mound	Spatter mound
Rock type	Nephelinite	Nephelinite	Nephelinite	Nephelinite	Nephelinite	Nephelinite
Reference	2	2	1	2	2	1
Major-element analyses, normalized water-free (weight percent)						
SiO_2	44.73	42.60	41.19	42.07	44.82	45.13
TiO_2	1.59	1.80	1.64	1.51	1.44	1.40
Al_2O_3	13.08	13.33	12.58	11.43	12.56	12.78
FeO*	10.87	11.41	14.93	10.26	10.49	10.37
MnO	0.43	0.42	0.40	0.42	0.43	0.43
MgO	1.59	2.08	1.96	1.55	1.31	1.33
CaO	11.16	14.40	13.19	12.00	9.36	9.18
Na_2O	10.35	8.38	8.50	14.50	13.25	12.88
K_2O	5.43	4.41	4.65	5.35	5.69	5.86
P_2O_5	0.76	1.16	0.96	0.91	0.65	0.63
Loss on ignition	4.50	7.36	3.94	4.10	0.56	0.56
Original oxide total	97.53	98.05	98.14	97.34	97.46	97.84
Trace-element analyses (parts per million)						
Ni	10	10	b.d.	9	9	b.d.
Cr	5	5	--	6	4	20
Sc	2	3	--	3	2	--
V	250	269	225	374	266	216
Ba	1809	1913	1779	2002	1822	1564
Rb	121	94	85	125	132	107
Sr	2409	2920	2436	2812	2326	1947
Zr	979	886	794	901	1002	842
Y	41	48	56	43	38	42
Nb	312	291	238	294	336	264
Ga	38	33	23	32	41	36
Cu	66	80	75	70	60	52
Zn	293	258	248	277	318	283
Pb	38	32	33	35	40	35
La	130	149	--	137	133	--
Ce	192	231	--	196	193	--
Th	9	10	8	9	11	8
Nd	59	77	--	62	60	--
U	8	9	6	9	10	6

of vent deposits was found. Admittedly, the lobe is thickly mantled with ash from summit eruptions, but the sparse float is lithologically diverse. The semicircular geomorphic expression is likely the snout of a debris flow that fortuitously terminated at about the point where the Nasira alignment crosses the slope.

The Nasira deposits are undated but assigned a Holocene age on the basis of their youthful landforms. Tephra fallout from eruptions at Oldonyo Lengai's summit have cloaked the Nasira area, but these tephra beds are themselves quite youthful. The large cone 3 has its base exposed in a gully on the east flank. No charcoal was found in the thin paleosol that caps an underlying debris-flow deposit, but the area warrants future searches for radiocarbon dating samples.

Downwind Fallout Tephra

Fallout deposits (in unit Qot) are mapped separately wherever they thoroughly mask underlying rock units. Their distribution, in map view, creeps up the west flank of the volcano where slopes are relatively gentle. In some of these areas the youngest part of the fallout results from the 2007–08 eruptions. This ash quickly "set up" (became cemented), so that some steep slopes are now perilous to tread across. For example, the debris fan that descends into Embalulu Kirurum (76 m deep; southwest flank of the volcano, see geologic map) may once have provided a convenient angle-of-repose ramp to the crater floor, but its recent ash coating now requires the cutting of footholds. A misstep there (and the unlikely chance of self arresting upon such durable substrate) would lead to a calamitous slide.

On the escarpment west of Oldonyo Lengai, fallout tephra has been accumulating since the volcano first began erupting. At the escarpment site of sample L300, 6.2 km west-northwest of the summit (geologic map), bedded tephra deposits 40 m thick may be entirely from Oldonyo Lengai's outpourings (fig. 22). The upper half of that sequence is fresh and likely equivalent to the

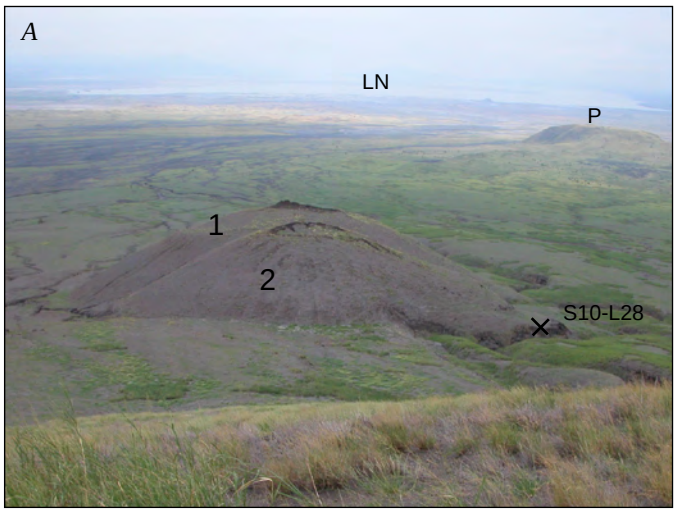

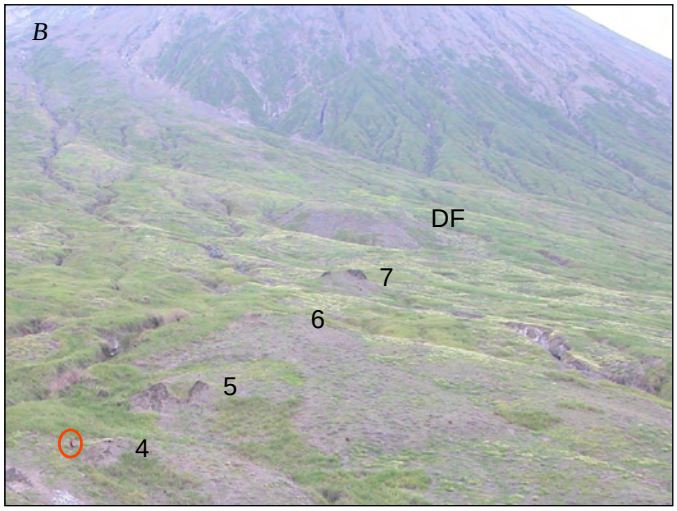

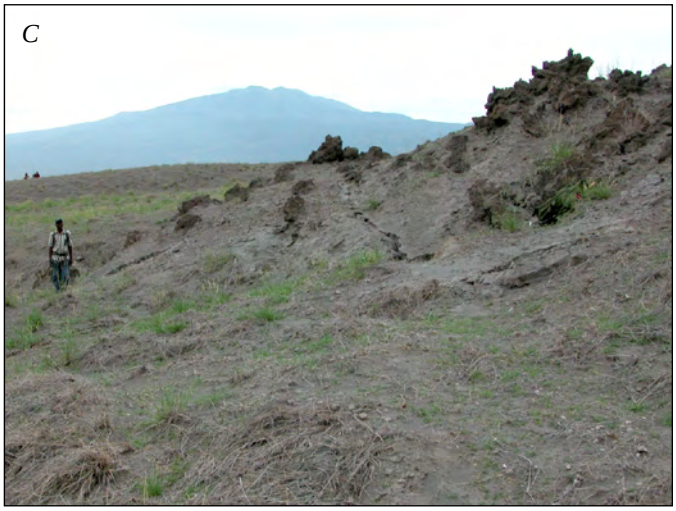

Figure 21. Eruptive features of Nasira cone alignment. Labeling scheme matches that on geologic map (fig. 20). Photos from February 6, 2010.
A, View north from summit of largest tephra cone to the northerly cones (1, 2), 400 m distant. Also visible in photo is phonolite dome (P) 10 km northeast of Oldonyo Lengai's summit and Lake Natron (LN) in distance. Photo 6869.
B, View south across spatter-mound alignment. DF, debris-flow snout that forms semicircular lobe coincidentally where the fissure crosses slope. Red-garbed Olemelok Nantatwa is visible at lower left, 20 m left of spatter mound 4. Photo 6870.
C, Edge of 'a'ā lava flow that issued from largest tephra cone (3), at sample site S10-L33 on map. Shimba Kwelwa for scale. Photo 6893.

black tuff-and-agglomerate unit that Dawson (1962) mapped on the volcanic edifice. Chemical analyses from some fallout tephra lapilli are compiled in table 9.

A tantalizing outcrop (site 8 on geologic map) was photographed from the bluff of the L300 traverse, looking south across the thick ash deposits that blanket the top of the escarpment (fig. 23). It shows a color contrast that may mark the boundary between Dawson's (1962) yellow and black tuff-agglomerate units, beneath which is an east-dipping angular unconformity that separates the escarpment lava flows (QTel) from the draping tuff beds. The well-indurated layers just above the unconformity probably predate Oldonyo Lengai. We include the photo as a temptation and guide for future Earth scientists, because a substantial understanding of the volcano's geochemical evolution may someday come from a detailed study of the downwind sites, unless alteration in the older deposits proves too great an analytical problem. A serious shortcoming of our study is the lack of forays into the area west of the volcano.

Figure 22. Tephra sequence atop escarpment west-northwest of Oldonyo Lengai. Photo 0097, March 17, 2010.

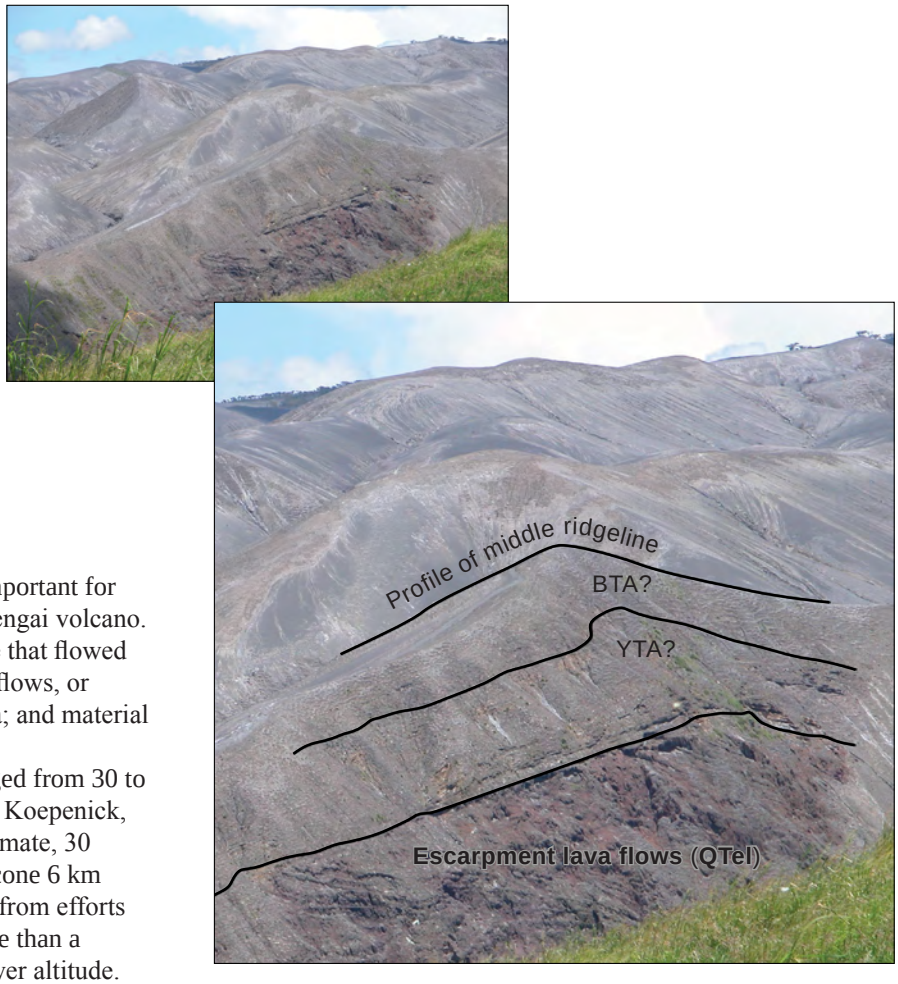

Figure 23. View south across fallout that blankets the block west of the Natron escarpment. In the outcrop, lava flows of the Natron escarpment (QTel) are beveled by an angular unconformity, above which is an east-dipping sequence of tuffaceous strata. The color change from dark gray to yellowish gray may mark the boundary between black and yellow tuff-and-agglomerate units mapped by Dawson (1962) at Oldonyo Lengai (labeled BTA and YTA on photo). The lowest, well-indurated tuffaceous layers may predate Oldonyo Lengai. Site not visited by us. Photo 0109, March 17, 2010.

Volume of Oldonyo Lengai's Cone

The volume and age of erupted products are important for estimating long-term eruption rates for Oldonyo Lengai volcano. Deposits include those preserved in the cone; those that flowed beyond the cone's limit, either as lava, pyroclastic flows, or debris avalanches and landslides; downwind tephra; and material eroded into adjacent basins.

For the cone itself, volume estimates have ranged from 30 to 60 km^3 (Donaldson and others, 1987; Brantley and Koepenick, 1995; Kervyn and others, 2008a). The smallest estimate, 30 km^3, is roughly the volume of a simple geometric cone 6 km in diameter and 2 km high. Larger estimates result from efforts to model the base of the volcano as something more than a horizontal plane or when the base is placed at a lower altitude.

We derived a cone volume of 46±9 km^3 (error corresponds to 20 percent of the estimate). GIS software was used to grid the volcano's modern surface and an idealized pre-volcano planar surface that slopes northward toward Lake Natron from Kerimasi volcano (fig. 24). On the west, this ancestral slope steepens abruptly along the Natron escarpment. Cone volume is contained between the two surfaces, reported here with no correction to dense-rock equivalent. A similar volume, 41 km^3,was reported by Kervyn and others (2008a) using similar methods. The two estimates differ because of assumptions about the topography of the basal surface and the outline (extent) of the volcanic edifice. Even so, they are roughly equivalent at any but the most conservative estimates of analytical uncertainty.

Age of Oldonyo Lengai

New Radiometric Ages

Using $^{40}Ar/^{39}Ar$ incremental-heating techniques, groundmass or phenocrysts were analyzed for four samples (table 11 and appendix 5), two from the Oldonyo Lengai edifice and two from debris-avalanche deposits downslope of it. Plateau ages are favored here (table 11) because the samples meet the commonly accepted criteria for meaningful incremental-heating ages (McDougall and Harrison, 1999, p. 32), namely (1) a well-defined plateau comprising more than 50 percent of ^{39}Ar released, (2) a well-defined isochron for plateau gas fractions, (3) concordant plateau and isochron ages, and (4) a $^{40}Ar/^{36}Ar$ isochron intercept not significantly different from 295.5.

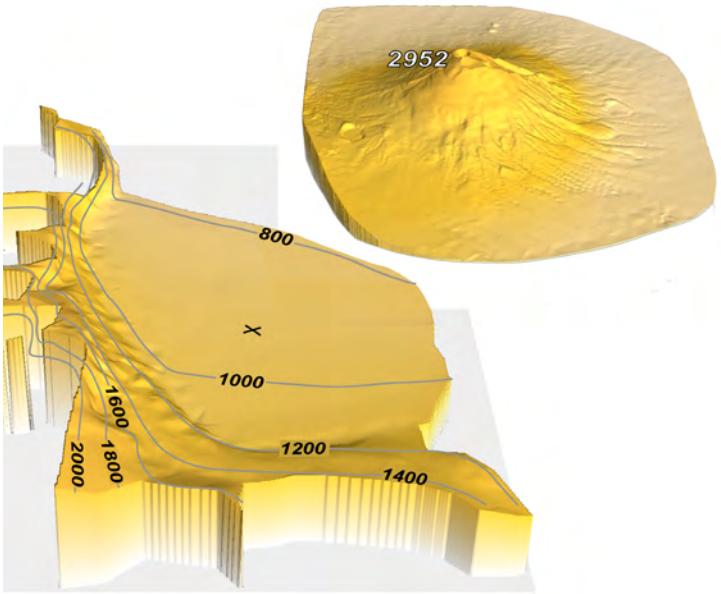

Figure 24. Hillshade relief images depicting the modern Oldonyo Lengai cone and the topographic surface that would have predated it, to convey the basis for assigning volume estimate to Oldonyo Lengai. View to north; slope of Kerimasi in foreground, alluvial plain beyond it, and Natron escarpment on left (west). Contours in meters; X marks location where future summit of Oldonyo Lengai will tower (here set off in midair).

The aforementioned new radiometric ages from the phonolite lava flow (338±23 ka) and tuff ring (353±65 ka) on the volcano's east flank indicate that Oldonyo Lengai had already begun its growth by about 350 ka, when the broad lower slopes of the volcano were well established. The imposing, steep main cone has continued to grow during subsequent millennia, with eruptions continuing into the 21st century.

Two older ages have been obtained from material in the debris-avalanche deposits north of the volcano. We interpret them to date an ancestral Oldonyo Lengai, the stump of which is now entirely buried beneath the modern cone. Oldest of these ages, 793±63 ka (table 11, No. 5), came from phlogopite in a mica-rich tuff layer exposed in a megablock of debris-avalanche deposit (unit $Qoda_6$). The relation of the tuff-bearing block (and hence the age) to an early Oldonyo Lengai cannot be established unequivocally, since the megablock could be from older bedrock caught up in the slope-failure event and transported northward with the rest of the debris.

The other age, 460±75 ka (table 11, No. 4), is also from a phlogopite-rich tuff, this one in debris-avalanche deposits emplaced at some later time (unit $Qoda_5$). These two ages span about as much time (200,000–400,000 yr) as that preserved by strata in today's cone from the summit to the lower east flank phonolite and tuff ring—an indication that a similar-size ancestral volcano grew and collapsed, perhaps more than once, during episodes of slope failure and erosion. If the dated megablocks really are from early Oldonyo Lengai, the ages from debris-avalanche deposits are the best available evidence that Oldonyo Lengai has been active throughout much of the past 600,000–800,000 years. In that case, this new finding pushes back the onset of Oldonyo Lengai volcanism by 300,000 years or more, and it warrants a search for corroborative evidence.

Previously Published Ages from Oldonyo Lengai

A whole-rock K-Ar age of 0.15±0.02 Ma (Bagdasaryan and others, 1973) has been cited as an Oldonyo Lengai age (for example, Foster and others, 1997). The sample was described as phonolite collected "near Oldonyo Lengai" and no other details provided (Bagdasaryan and others, 1973). A GIS rendering of the sample location (using the small-scale map of Bagdasaryan and others, 1973) places it near the lava flow of Ildonyo Loolmurwak, a tephra cone of the Natron-Engaruka volcanic field in the southeast corner of the geologic map. Alternatively, the sample may have been collected from a block in a debris-avalanche deposit (unit $Qoda_4$) traversed by the Engaruka-Loliondo road southeast of Oldonyo Lengai, which would prove interesting because it would establish a maximum age for the avalanching event there (avalanche must be younger than rocks contained in it). Unfortunately, the sample-location information is too vague to be used reliably.

Radiocarbon ages of 3,000 and 2,500 ^{14}C yr B.P. have been reported from organic matter at the base of fallout deposits erupted from a tephra cone at the 1,200-m altitude on the east flank of Oldonyo Lengai (Keller and others, 2006, their "Dorobo cone"). Two other radiocarbon ages, 2,050 and 1,300 ^{14}C yr B.P., were obtained from calcium carbonate-bearing soil layers associated with reworked sequences of ash deposits at shallow depth 15 km northeast of the volcano (3–5 km south of Lake Natron) (Hay, 1976, p. 192; Hay, 1989). Eight kilometers southeast of the volcano, a radiocarbon age of 3,500±100 ^{14}C yr B.P. was obtained from calcareous soil deposits that overlie ash, collected in the walls of a gaping crack that crosses the floor of Loolmurwak crater (Hay, 1976). The ages of 1,300 and 3,500 ^{14}C yr B.P. were transcribed as 130,000 yr and 350,000 yr in Dawson's (2008) appendix 1 (bottom of col. 1, p. 93).

Evidence from Dating at Olduvai Gorge

Previous estimates for the inception and duration of Oldonyo Lengai's volcanic activity came not from rocks on or adjacent to the volcano but from ages and stratigraphic relations of primary and reworked tephra at Olduvai Gorge, 70–80 km downwind of the southernmost Lake Natron basin. The Olduvai Gorge work originated in the investigation of early man, and the accumulated ash from Oldonyo Lengai is an important part of the stratigraphic setting for hominid cultural relicts.

At Olduvai Gorge, a sequence of sandstone and tuff known as the Masek Beds was thought to be derived from Kerimasi volcano (Dawson, 1964; Hay, 1976, p. 152–154), the next volcano south of Oldonyo Lengai. Above the Masek lies the Ndutu Beds, presumably derived from Oldonyo Lengai (Hay, 1976). These relations are depicted in figure 25. The Masek Beds stratigraphic unit was assigned a maximum age of about 700 ka on the basis of its normal-polarity magnetization and some estimates of sedimentation rates. A minimum age of about 370 ka for the Masek (Hay, 1976) relied on two mica-rich tuff rings that overlie Kerimasi strata on the volcano's northeast flank (table 2, Nos. 3 and 4; Macintyre and others, 1974). That is, if the tuff rings overlie Kerimasi volcano, and if the downwind Masek Beds (or at least the primary fallout tephra in them) are all from Kerimasi, then the Masek would be older than the tuff rings. And because, in that line of reasoning, Oldonyo Lengai's activity entirely postdates deposition of the Masek Beds, then a roughly 400-ka age (end of Masek time) marks the beginning of Oldonyo Lengai.

Also from Hay's (1976) work, the overlying Ndutu Beds (at Olduvai Gorge), which contain tephra from Oldonyo Lengai volcanism, have amino acid racemization ages of 56 and 32 ka (fig. 25). Deposition of the Ndutu and compositionally similar younger beds culminated by about 15,000 years ago, on the basis of radiocarbon ages from pedogenic calcium carbonate ("calcrete") sampled at the gorge (Hay, 1976).

More recently, $^{40}Ar/^{39}Ar$ dating of crystals in fallout tuff at Olduvai Gorge has redefined the age of the Ndutu Beds, whose lower part is older than 400 ka and upper part in the range 220–450 ka (fig. 25; Manega, 1993, his table 3.6). An estimated age of the underlying Masek, 600–860 ka, comes from sedimentation rates (Manega, 1993). This new information leaves Hay's (1976) initial estimation essentially unchanged, although it probably indicates an earlier onset (perhaps as early as 500 ka) for deposition of the Ndutu Beds. But more critical is the question raised by our new radiometric ages from blocks in debris-avalanche deposits at Oldonyo Lengai: "Does the Masek Beds stratigraphic unit include, at least in its upper part, fallout from Oldonyo Lengai eruptions?" We suggest the answer is yes; and if correct, then the growth of Oldonyo Lengai may have begun before 600 ka.

To finish the story of evidence from Olduvai Gorge, younger tuff and alluvial sandstone continued to accumulate

into more recent time. Atop the Ndutu (at Olduvai Gorge) lies a compositionally similar sequence of beds, the Naisiusiu (fig. 25). Radiocarbon ages of 22 and 15 ka were obtained from pedogenic calcium carbonate in the Naisiusiu (Hay, 1976). Dating of single crystals in tuff produced $^{40}Ar/^{39}Ar$ ages in the range 13–42 ka (Manega, 1993). An electron-spin resonance age of 62 ka from equid teeth in the Naisiusiu has also been reported (Skinner and others, 2003).

Eruptions at Oldonyo Lengai continued after 15,000 years ago to form capping deposits at Olduvai Gorge. One of the younger beds, the Namorod Ash, has an estimated age of 1,250 ^{14}C yr B.P. The estimate relies on a radiocarbon age from a snail fossil found in waterlaid silt 2 m below the Namorod Ash at Olduvai Gorge and presumptions about sediment accumulation rates preceding Namorod time (Hay, 1976).

Geochemistry and Stratigraphic Relations at Oldonyo Lengai

It is difficult to test hypotheses about changes in chemical composition through time for a volcano as little incised as Oldonyo Lengai, because full stratigraphic sequences are lacking. A start, however, is to use published analyses that include assignments to one or the other of Dawson's (1962) main-cone stratigraphic units: yellow tuff and agglomerate and the younger black tuff and agglomerate (for example, Donaldson and others, 1987; Bell and Simonetti, 1996). These samples were collected mostly during Dawson's (1962) mapping of Oldonyo Lengai. Our sampling (this map) also includes assignments to Dawson's two main-cone stratigraphic units.

On the basis of published analyses, phonolite forms about 80 percent of the samples from the older unit (yellow tuff and agglomerate; fig. 26). Nephelinite forms the remainder, using a boundary proposed by Klaudius and Keller (2006). The sampling suite for the yellow tuff and agglomerate favors lava flows over volcaniclastic rocks (80 and 20 percent of samples, respectively).

Greater variation is seen among samples of younger deposits—those assigned to the black tuff and agglomerate. Many of these samples are nephelinite, but a few are phonolite.

Missing from this discussion is the geographic setting of the samples and whether phonolite-bearing pyroclastic rocks are lacking on the volcano's north slope. Many of our phonolite samples (from the yellow tuff and agglomerate) were collected elsewhere: from the lower east flank, the mid-slope reach of the Eastern Chasm, and the upper south flank. The single phonolite we assigned to the black tuff and agglomerate is a dense fresh block collected from a coarse lapilli tuff on the lower south flank, a deposit that probably originated as a debris slurry and therefore contains reworked (albeit fresh) material. In that case, the possibility remains that the analyzed block was first deposited in strata destined to become yellow tuff and agglomerate, although the freshness of all the material in the sampled bed makes that unlikely. No geographic information accompanies the several phonolite analyses from the Dawson sample suite.

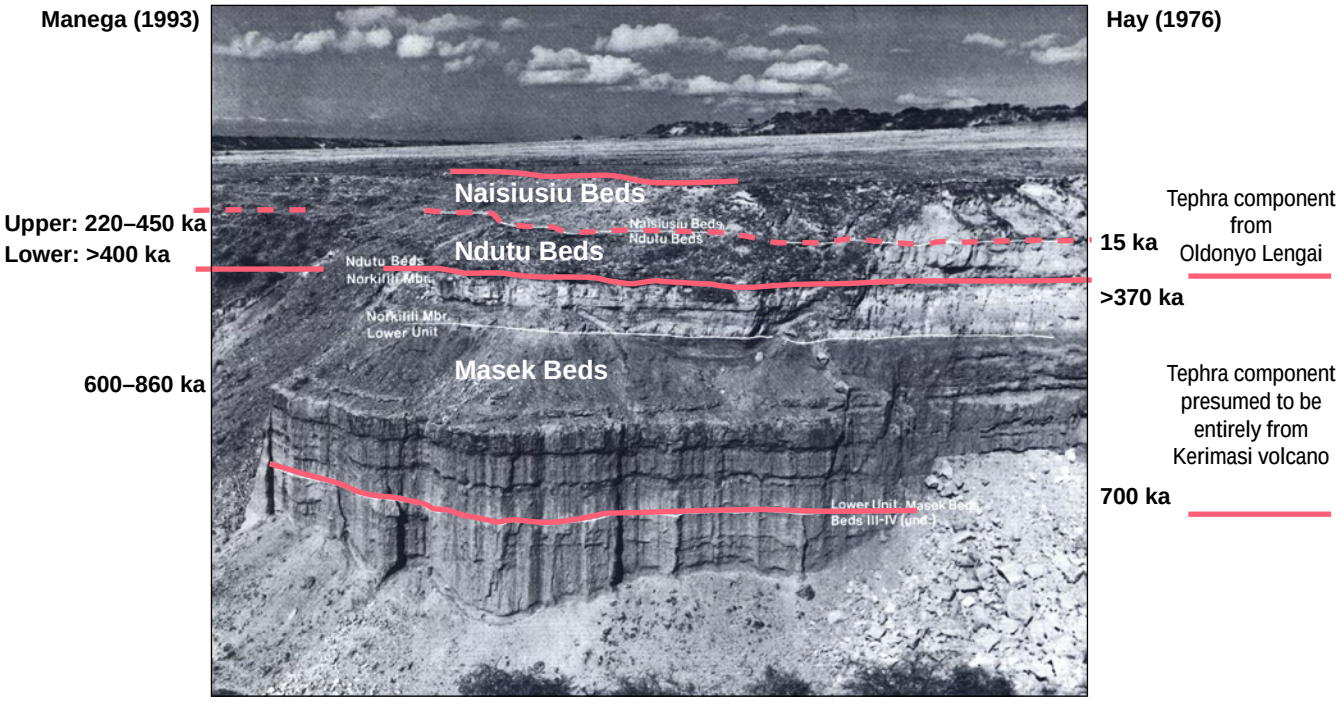

Figure 25. Radiometric dating from Olduvai Gorge and its interpretation for timing of volcanism at Oldonyo Lengai. Photograph and delineation of stratigraphic units from Hay (1976, his plate 6), whose interpretations are shown on right side. For sense of scale, Masek Beds (lower unit and Norkili Member) in this photo total about 15 m thick. Age range for Masek Beds was based on assumption that Kerimasi was source, Kerimasi was older than 400 ka on basis of age of an overlying tuff ring on north flank of volcano, and normal-polarity magnetization of Masek beds (hence younger than 780 ka). Ages from Ndutu Beds were by amino acid racemization (Hay, 1976). On left side of illustration are ages from Manega (1993, his table 3.6), who used $^{40}Ar/^{39}Ar$ dating of crystals in fallout tuff at Olduvai Gorge for Ndutu Beds. Age of Masek Beds estimated from sedimentation rates (Manega, 1993). Our oldest age from Oldonyo Lengai debris-avalanche deposits, 793 ka, raises the possibility that tuff in Masek Beds is derived entirely from Oldonyo Lengai volcano. Photograph by R.I.M. Campbell, copyright © 2013, PHOTOSHOT.

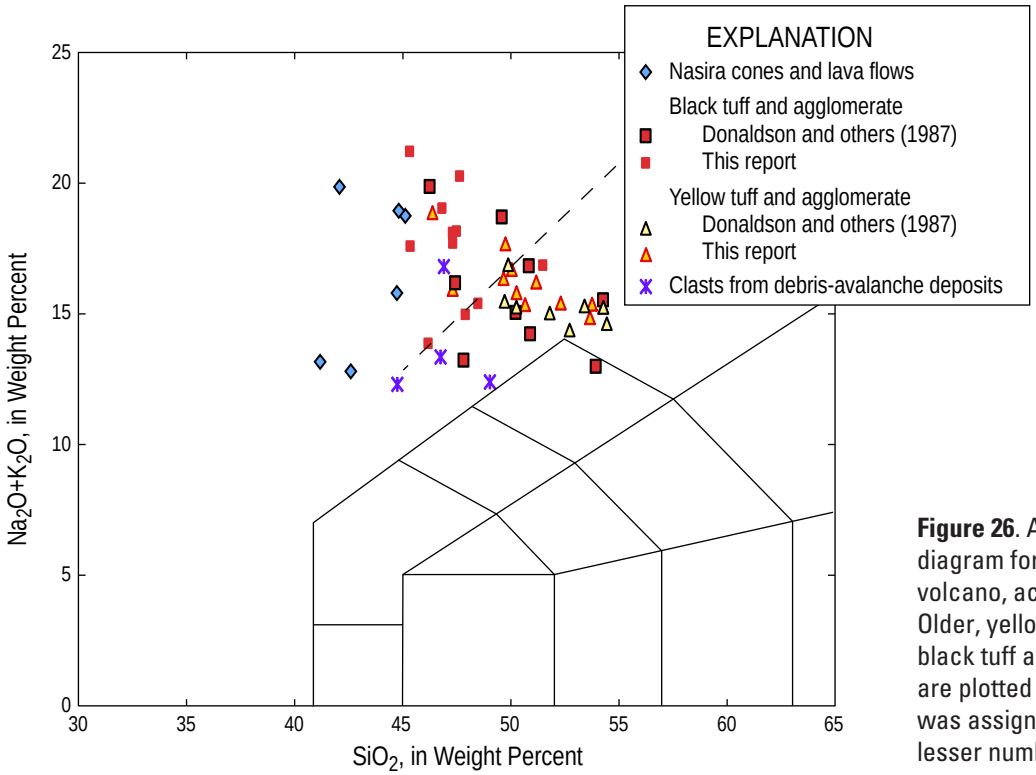

Figure 26. Alkali-silica (Na_2O+K_2O vs. SiO_2) diagram for volcanic rocks of Oldonyo Lengai volcano, according to generalized age criteria. Older, yellow tuff and agglomerate; younger, black tuff and agglomerate. Only those samples are plotted for which stratigraphic position was assigned during mapping; this explains the lesser number shown here than on figure 4.

We remain open to the proposal by Klaudius and Keller (2006) that Oldonyo Lengai changed from a phonolite+nephelinite volcano (Lengai I) to a nephelinite-only volcano (Lengai II), but it seems at odds with the geochemical data just presented. Lengai I, in the Klaudius-Keller model, is preserved today as the south half of the volcano; its northern part failed in a large sector collapse that shed debris-avalanche deposits northward to Lake Natron (Kervyn and others, 2008a). By this interpretation, eruptive activity at the vent of the northern crater rebuilt the volcano to its current form, with the younger cone stepping north above the older cone. The Lengai II cone lacks phonolite, according to Klaudius and Keller (2006). In contrast is the mapping by Dawson (1962), which shows most of the volcano built by the strata of yellow tuff and agglomerate (found on all flanks) and then capped by black tuff and agglomerate (fig. 11). Both these stratigraphic units are phonolite bearing.

The volcano is inadequately sampled geographically, especially on its north flank between 1,400 and 2,400 m altitude. Analyses from volcaniclastic strata there could support or refute the Lengai I-II model of petrochemical evolution (the interpretation of debris-avalanche failure is not questioned). Most of the volcano's midslope reaches are difficult areas in which to work, because of numerous precipitous gullies that impede cross-slope traverses.

Strontium isotopic ratios ($^{87}Sr/^{86}Sr$) also fail to distinguish the yellow tuff and agglomerate from black tuff and agglomerate. Ratios range from 0.70428 to 0.70522 (fig. 27), and samples from each of the two major stratigraphic units are scattered throughout the span of values (Keller and Krafft, 1990; Bell and Dawson, 1995; Bell and Simonetti, 1996). A greater range was once thought to exist (Bell and others, 1973), but most of those samples have been reanalyzed (Bell and Dawson, 1995), leading to the more restricted range cited here.

Rocks from other volcanic centers in the map area, including the Natron-Engaruka volcanic field, have generally lower $^{87}Sr/^{86}Sr$, 0.7036–0.7043 (fig. 27; Paslick and others, 1995, 1996; Keller and others, 2006). A tephra cone on the lower northeast flank, possibly part of the Oldonyo Lengai magmatic system, has $^{87}Sr/^{86}Sr$ of 0.70379 (Keller and others, 2006). Alternatively, this tephra cone could be part of the Natron-Engaruka volcanic field that lies coincidentally within the geographic limit of Oldonyo Lengai's main cone.

Origin of Oldonyo Lengai Magma

Magma genesis in the East African rift of northern Tanzania occurs where an asthenospheric mantle plume brings melts into, or induces melting in, the lithospheric mantle. Sections drawn across the rift about 100 km south of the southern Lake Natron basin (Ebinger and others, 1997; Last and others, 1997) show crust and lithosphere thicknesses estimated from seismic, gravity, xenolith, and geochemical data (fig. 28).

The eastern branch of the East African rift system may be deflected along structural controls imposed by the boundary between the Tanzanian Archean craton and adjacent Proterozoic Mozambique fold belt (fig. 29; Nyblade and Brazier, 2002). (See Dawson [2008, chap. 3] for a concise summary of the regional geology.) Lithospheric thickness is in the range 80–120 km beneath the craton but thinner beneath the Mozambique belt (evidence summarized in Ebinger and others, 1997). Crustal thickness is roughly 36–42 km across the lines, with no significant difference in thickness between crust of the Tanzanian craton and Mozambique belt (Last and others, 1997). Neogene and Quaternary volcanic rocks of the eastern branch in Tanzania are emplaced chiefly atop rocks of the Mozambique belt (Pinna and others, 2004), but the eastward dip of the structural boundary between cratonic and fold-belt rocks suggests that Tanzanian volcanoes of the eastern branch have erupted through Archean

cratonic lithosphere, with implications for the composition and isotopic systematics of the volcanic rocks (Dawson, 2008, chap. 3).

Petrologic models have converged on a magmatic evolutionary scheme in which carbonated olivine nephelinite or melilitite forms the parental magma (Peterson, 1989; Dawson, 1998; Keller and others, 2006; Dawson, 2012). Some melts migrate upward rapidly to erupt as melilitite and olivine nephelinite; their rapid ascent explains xenolith content and isotopic signatures that indicate little or no interaction with the lithospheric mantle. Lava and tephra of these compositions are characteristics of the Natron-Engaruka volcanic field.

Other melts pond in, and react with, the lithospheric upper mantle, where they undergo olivine-pyroxene-spinel fractionation (for example, Dawson, 1998; 2012). Compositional variation among resulting magma batches arises as a consequence of variable residence time and character of lithosphere with which they react. The focused eruptions of these more evolved magma batches have built the Oldonyo Lengai edifice.

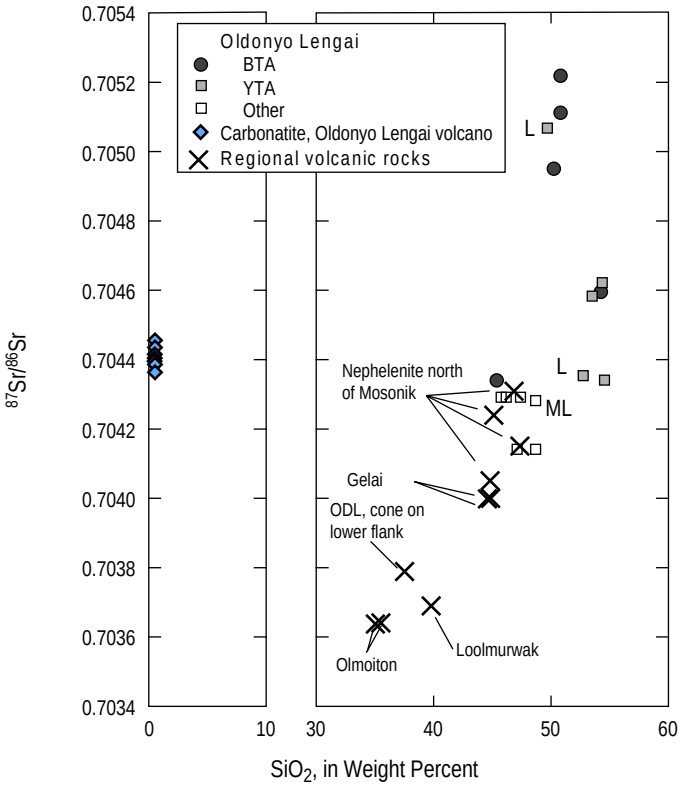

Figure 27. Strontium isotopic ratios ($^{87}Sr/^{86}Sr$) for volcanic rocks in map area. BTA, YTA, black and yellow tuff and agglomerate, respectively, of Dawson (1962). All samples from these two units are blocks in volcaniclastic deposits except those labeled L, lava flow. ML, melanephelinite lava flow. Data for regional volcanic rocks and carbonatite from Paslick and others (1995, 1996) and Keller and others (2006). Data for Oldonyo Lengai silicate rocks from Donaldson and others (1987), Keller and Krafft (1990), and Keller and others (2006). Data for Oldonyo Lengai carbonatite from Bell and Blenkinsop (1987), Keller and Krafft (1990), and Bell and Simonetti (1996). ODL, Oldonyo Lengai.

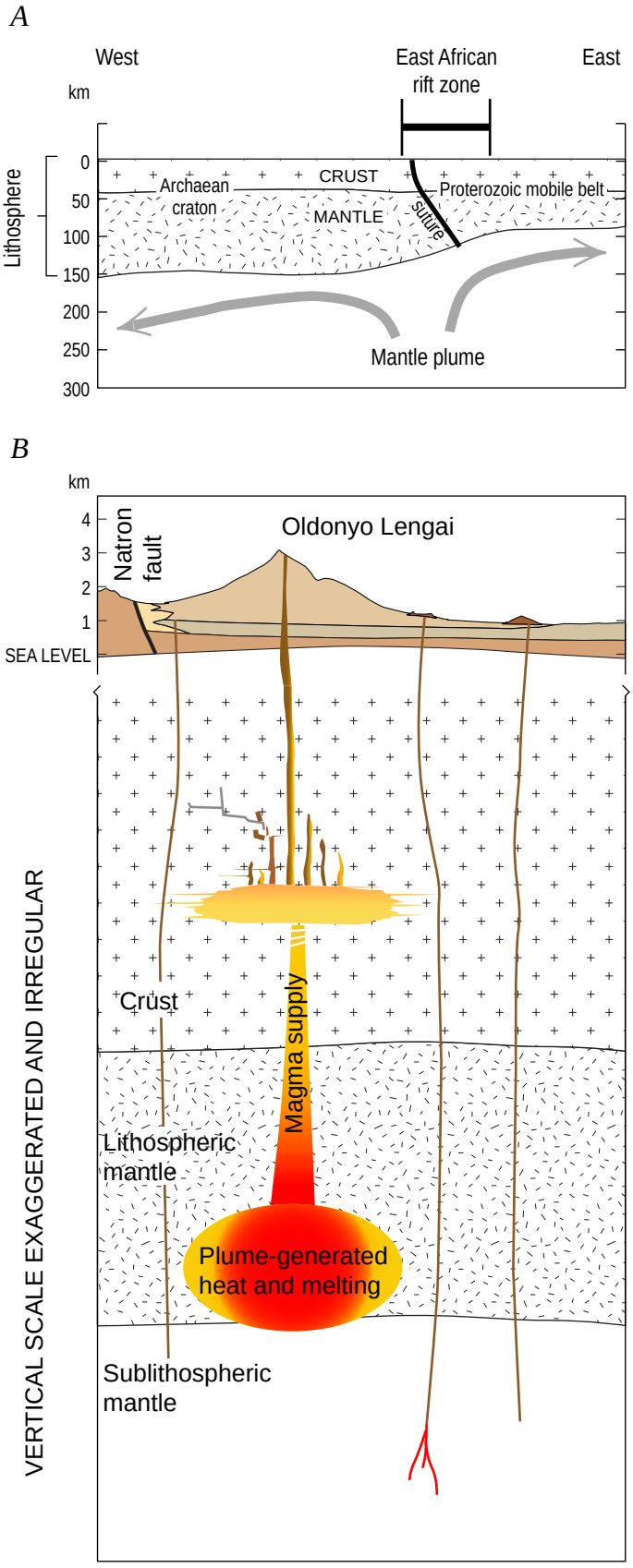

Figure 28. Crustal section (*A*) and simplified sketch (*B*) showing magmatic pathways through lithosphere beneath Oldonyo Lengai. Panel A, from Ebinger and others (1997), corresponds to line labeled "geophysical cross section" on figure 29.

The origin of Oldonyo Lengai's natrocarbonatite lies in the manner in which CO_2 is released from an initially carbonated melt (Peterson, 1989; Dawson, 1998). As a melt ascends and cools along some pressure-temperature path, CO_2 saturation increases. If a melt is suitably CO_2 saturated, then CO_2 may exsolve, sweeping alkalis and halogens with it to produce carbonatite liquids.

Debris-Avalanche Deposits

It was only after the catastrophic eruption of Mount St. Helens (USA) that Earth scientists came to understand debris-avalanche deposits. In 1980, the northern slope of Mount St. Helens slid away and moved with startling speed down an adjacent river valley. Since then, the deposits of debris avalanches have become a widely recognized phenomenon at volcanoes worldwide.

Even if not well understood before 1980, the deposits had been recognized at Oldonyo Lengai as early as the 1960s. Hummocky terrain characterizes much of the basin between Oldonyo Lengai and Lake Natron, and those areas on Dawson's (1962) map were identified by him as reworked yellow agglomerate, thus acknowledging the source (Oldonyo Lengai) and remobilization by some mechanism. A suggestion that the hummocky terrain originated by failure of Oldonyo Lengai was offered by Isaac (1967), "A mudflow from the Lengai area ran northward along the foot of the escarpment and forms a striking feature around the southern end of Lake Natron. (Isaac, 1967, p. 243)." What else could he have meant by "a striking feature" except the many hills (megablocks) that are clustered near the lake? Regardless, it is only in the past decade that the deposits at Oldonyo Lengai have been recognized as formed by debris avalanches (for example, Keller, 2002; Klaudius and Keller, 2004), and a detailed study of them has been published recently (Kervyn and others, 2008a).

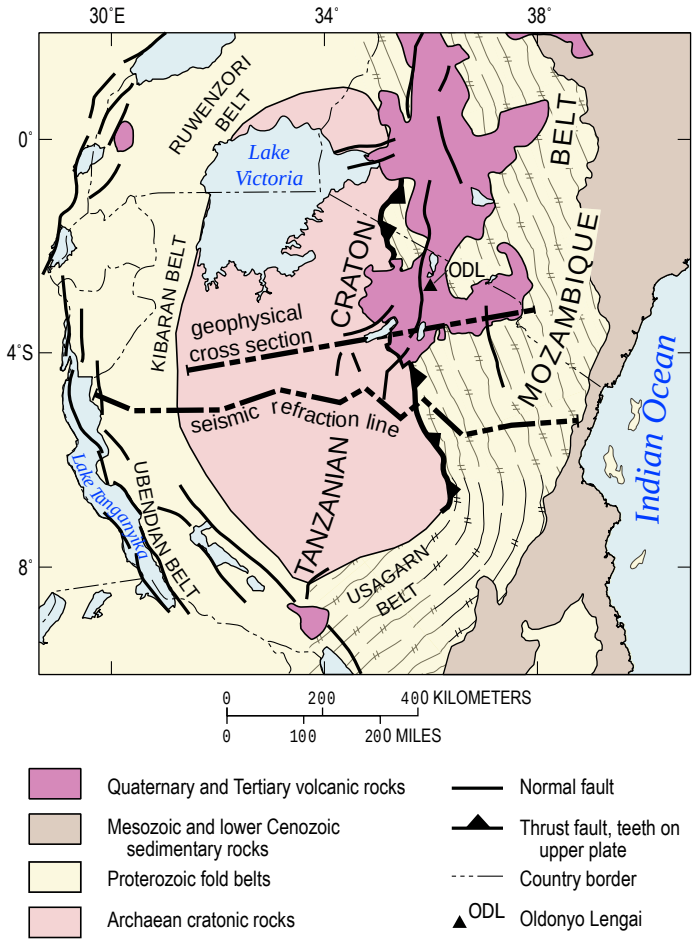

Figure 29. Regional tectonic map, after Nyblade and Brazier (2002). Geologic contacts in Tanzania from Pinna and others (2004); those in Kenya from Smith and Mosley (1993) and Ebinger and others (1997). Line of geophysical cross section corresponds to line T-T′ of Ebinger and others (1997). Seismic refraction line is that described by Last and others (1997).

Earliest Known Avalanche Events Probably Those Exposed Northeast of Oldonyo Lengai

In the northeast corner of map area, near Gelai school, are scattered small blocks of debris-avalanche deposits (unit $Qoda_6$). Their association with highly deformed lacustrine sedimentary beds (unit Ql_3) suggests emplacement in the time between 240 and 135 ka (Hillaire-Marcel and others, 1986) or earlier, if the lacustrine deposits date to an even older (higher) shoreline.

A $^{40}Ar/^{39}Ar$ plateau age of 793±63 ka came from a mica-rich tuff bed in one of the debris-avalanche blocks (table 11, No. 4). The age is a maximum age for the debris avalanche, which must be younger than the debris it contains. Thus unit $Qoda_6$ is known only to have been emplaced sometime between about 850–750 ka and 240–135 ka.

Widespread Deposits North of the Volcano

Distribution

Three debris-avalanche sequences cover much of the basin floor north and northeast of Oldonyo Lengai. They have been delineated mainly on the basis of their distribution (Klaudius and Keller, 2004; Kervyn and others, 2008a). From oldest to youngest, they are, in the terminology of Kervyn and others (2008a), the zebra (our unit $Qoda_5$), oryx ($Qoda_3$), and cheetah ($Qoda_2$) debris-avalanche deposits. We adopt this previously established grouping on our map, although it is unclear that much, if any, time separated two of them (units $Qoda_5$ and $Qoda_3$). The critical evidence, such as intervening soil or weathering horizons, is nearly impossible to find in the absence of good exposures across their contacts. The numerals in the map-unit labels are an informal assignment that roughly approximates relative stratigraphic age.

The most extensive of these units is our main-sheet debris-avalanche deposit, unit $Qoda_5$. It reaches north to the shore of Lake Natron, and some large hummocks are preserved as islands in the lake (Kervyn and others, 2008a)[4]. The main-sheet deposits can be found northward to the limit of our mapping, or about 24 km from the volcano's summit. Chemical analyses from characteristic blocks in unit $Qoda_5$ are compiled in table 10.

[4]Volcanologists interested in how debris avalanches interact with lakes might be curious about the bathymetry of Lake Natron. Because the lake today is notably shallow, it seems unlikely that much avalanche sedimentology could be gleaned. Water depth reportedly varies from a few centimeters in the north to 1–2 m in the south, where the permanent part of the lake persists (Vicens and Casanova, 1987).

Included with the main sheet are debris-avalanche deposits along the Natron fault escarpment. Those near Engare Sero stand as much as 170 m above the adjacent basin floor, owing to quirks of the fault-block topography. The escarpment south of Engare Sero stream is a single major cliff that presented a uniform barrier to the avalanche's westward advance. As the debris avalanche approached, it plastered the east-facing escarpments to form buttressing contacts commonly steeper than 45°. But northward from Engare Sero stream, the escarpment's structural setting is more complex. Its narrow fault blocks, which drop down successively to the east, are also tilted slightly southward, so that the blocks' flattish upper surfaces slope gently back toward the volcano. In these areas, the debris avalanche could move directly up the ramps, leaving a stair-stepping depositional sequence. Subsequent faulting has been minor.

The debris-avalanche deposits along the escarpment north of Engare Sero stream are bedded, 4–8 m thick (overall unit thickness 30 m), and somewhat better sorted than deposits along the axis of the southern Lake Natron basin. Good exposures can be found in a canyon near Engare Sero village (feature 10 in "Index to Notable Features" on geologic map). The bedding and sorting characteristics suggest the deposits in this area may be transitional to debris flows. Matrix material is similar to that found elsewhere: a crystal-lithic lapilli tuff studded with subangular to subrounded fragments 1–10 cm across. The number and sizes of large blocks are diminished compared to deposits closer to the volcano. As a consequence, the deposit's surface is less littered with bouldery float. Engare Sero village is built upon such debris-avalanche deposits.

Age

The main-sheet debris-avalanche deposits (unit $Qoda_5$) are older than 11,500 years (cal B.P.) and probably older than 50,000 years, because they are mantled by traces of dated lake beds from earlier high stands of Lake Natron (Hillaire-Marcel and others, 1987). Some of these shoreline gravels are exposed at about the 620-m altitude 5.5 km northwest of Gelai school (sites 1 and 2 on geologic map). We discount an event age of 11,000 years suggested by Kervyn and others (2008a; reported here as calibrated age), who recognized the occurrence of lacustrine stromatolites atop the debris-avalanche deposits but presumed the stratigraphic relation meant contemporaneous emplacement (avalanche emplaced into 11,000–14,000-yr-old lake). Instead, the stromatolites are evidence for a minimum emplacement age (avalanche must be older than 11,000 yr).

A $^{40}Ar/^{39}Ar$ plateau age of 460±75 ka was obtained from phlogopite in a tuff remnant within a debris-avalanche block near the northern outcrop limit of the deposits (table 11, No. 3). The age is a maximum limiting age for unit $Qoda_5$—admittedly not much help in restricting the age of emplacement.

Engare Sero Fan

Large debris avalanches can dam streams they encounter, at least temporarily. Engare Sero stream met such a fate when the main-sheet debris avalanche roared northward along the Natron escarpment. The evidence of the blockade is preserved today in the landforms and deposits at the foot of the Natron escarpment (fig. 30).

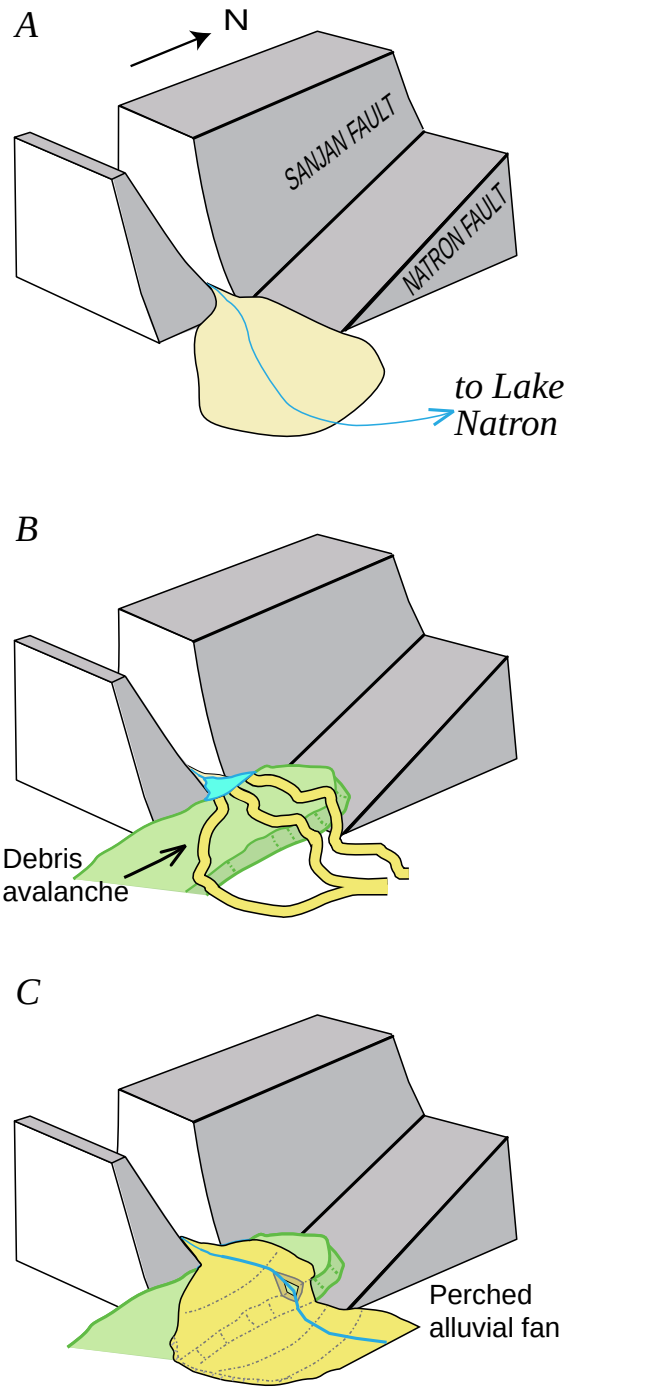

Figure 30. Block diagram showing the geologic evolution of the alluvial fan at mouth of Engare Sero stream. *A*, Before debris-avalanche deposits. Stream exits its narrow canyon at the Natron escarpment and deposits sand across the alluvial plain that slopes northeast toward Lake Natron. *B*, Debris avalanche from Oldonyo Lengai encroaches from south to north, ascends the ramplike surface of an adjacent fault block and abruptly dams Engare Sero stream. The stream tries to reestablish itself across the flattish upper surface of the debris-avalanche deposits, building a sandy fan. *C*, Thick sheet of thin-bedded sand atop debris-avalanche deposits. In panel C the stream is shown having nicked downward through its own deposits into the debris-avalanche deposits, where it becomes entrenched. The result will be the narrow shallow gorge that ultimately developed along this part of the stream.

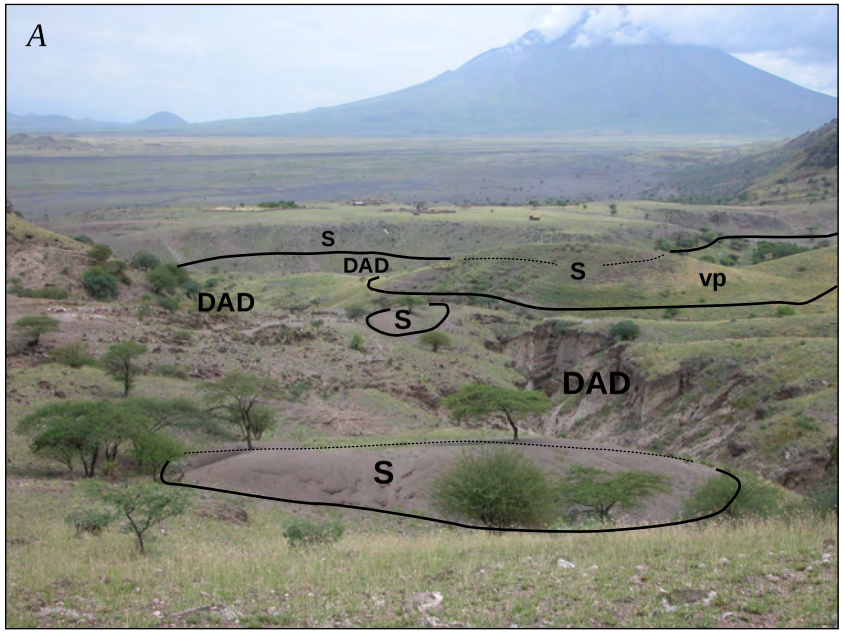

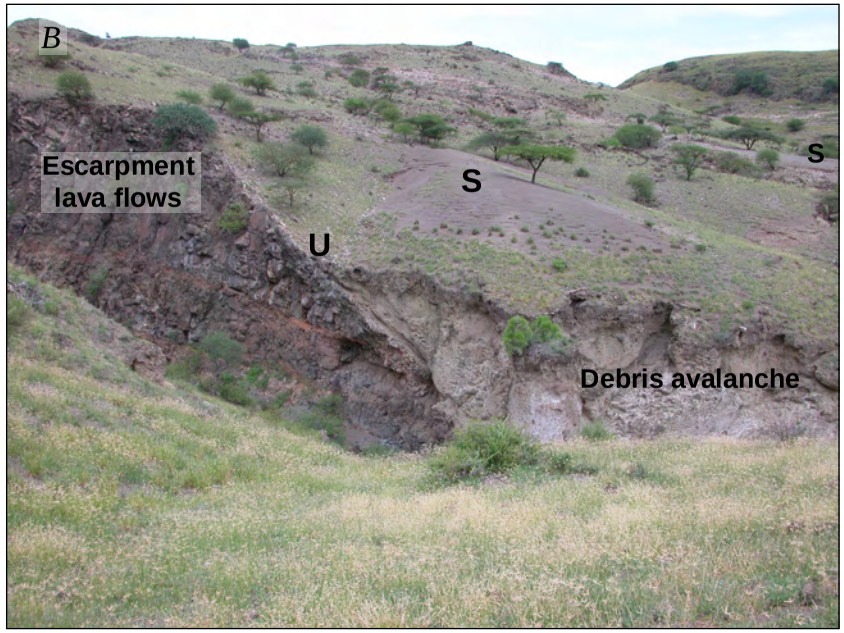

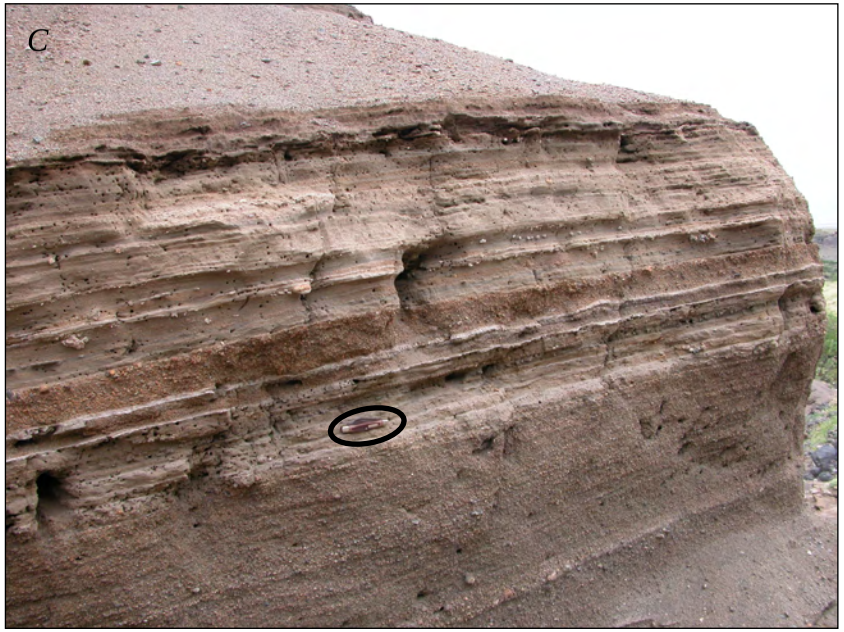

Figure 31. Debris avalanche and overlying sedimentary deposits at mouth of Engare Sero stream. Photo date February 22, 2010.
A, View south-southeast toward Oldonyo Lengai, the source of debris avalanches, 15 km distant. Flattish surface of perched Engare Sero alluvial fan is underlain by sandy deposits (S) in middle ground, and remnants of similar deposits seen closer to camera. These lie atop debris-avalanche deposits (DAD) well exposed along a south-draining tributary. vp, vantage point for panel-B photograph. Photo 7333.
B, View back to the north across the same area from vantage point vp. A more westerly tributary has carved a spectacular exposure of the buttress unconformity where debris-avalanche deposits slammed onto Pleistocene lava flows of the escarpment. U, unconformity; S, sandy deposits above debris-avalanche deposits. Photo 7320.
C, Character of the coarse to fine sand deposits. Scale provided by 8-cm-long pocket knife (in center of photo). Slope of bedding is depositional, not tectonic. Photo 7317.

Complete damming of Engare Sero stream surely resulted in the deposition of lacustrine deposits upstream, but the narrow canyon is a poor site to preserve them. Upon exiting the canyon, the stream must have sought paths across the flattish top of the debris-avalanche deposits (fig. 30*B*). Aggradation of sand and gravel (in unit Qa_3) occurred because the abruptly flattened stream gradient caused the stream to lose water and drop its entrained load (fig. 31). At some point the stream became entrapped along a specific path after it nicked into the edge of the debris-avalanche deposits. Downcutting thereafter excavated the slot through the perched alluvial sand and underlying debris-avalanche deposits.

As an aside, the limited time available in reconnaissance mapping forces decisions of where to go and what to see. The mapping of the Engare Sero fan arises from the scientific need to account for features that are beyond the ordinary. The outer, steep prow of the fan demanded an explanation, and we first suspected that a fault escarpment was the explanation. Indeed, tectonically offset fans are common in rift basins. But in this case, the presence of the debris-avalanche deposit and its thick mantling sand led instead to an interpretation of the nontectonic sequence of events just described.

Leshuta Canyon

Another substantial canyon farther north, Leshuta, also saw the debris avalanche build a short-lived dam. Debris-avalanche material entered the mouth of Leshuta canyon, blocking off the lower 600 m of stream length. The canyon likely had a configuration and depth similar to that found today, judging from erosional exposures of the base of the debris-avalanche deposits at or only slightly above the modern alluvial floor. As at Engare Sero stream, the blockage modified Leshuta stream's base level, as indicated by two features. Fine-grained sediment backfilled a shallow graben that extends north 400 m from the main canyon (in unit Ql_3). And at the canyon mouth, sediment built an alluvial fan that now stands as high as 40 m above the active stream floor (unit Qa_3). The modern Leshuta stream exits the canyon along the north side of this fan.

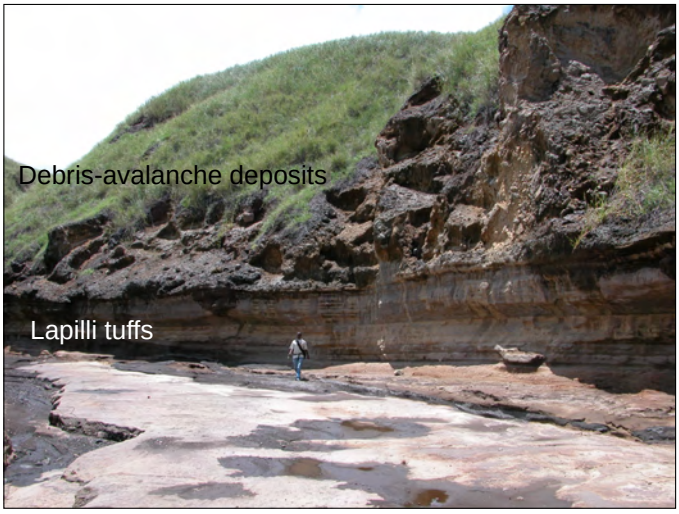

Figure 32. Kisana Mollel approaches the lapilli tuff and sandstone that separate two debris-avalanche deposits on lower south flank of Oldonyo Lengai. Traverse to this point along stream floor ascended through an older debris-avalanche deposit, just below stream floor at this altitude. Photo 7558, March 3, 2010.

Deposits South and Southeast of the Volcano

Debris-avalanche deposits on the south and southeast sides of Oldonyo Lengai were recognized previously by Dawson (1962), who included them in his unit of reworked yellow agglomerate. The southerly deposits (in unit $Qoda_4$) lap onto the flank of Kerimasi volcano, 6 km south of Oldonyo Lengai's summit. They are unusual for an exposure of interbedded lapilli tuff and sandstone 4–6 m thick in the upper reach of Sidan Indare stream, which provides solid evidence that the two south-flank avalanche events were separated in time (fig. 32; site 5 on geologic map).

Deposits southeast of the volcano (also in unit $Qoda_4$) form a gently rolling grassland dotted with small mounds, none showing more than 3 m relief. The crowns of these mounds expose blocks of phonolite and tuff breccia similar to that seen in deep exposures of debris-avalanche deposits elsewhere around the volcano. In places, phonolite- and nephelinite-rich debris is banked like a berm against preexisting tephra cones; for example, the Engaruka-Loliondo road is cut into such a berm as it descends onto the Sidan Indare floodplain. The debris avalanche swamped the gap between two tephra cones 700 m west of there, then oozed out, leaving flow levees recognizable in air photos, albeit obscure on the ground. (Flow levee symbol shown on geologic map, 1 km south of Lalarasi cone, east side of map area.) We suspect the phonolite sample dated by Bagdasaryan and others (1973) (0.15 Ma; table 2, No. 1) came from a block in this unit of debris avalanche deposits, but published descriptions are too vague to reliably place the location. (See appendix 4 for further discussion of sample location.)

Young Debris-Avalanche Deposits at Foot of Eastern Chasm and the Small Lake That Formed above Them

Young debris-avalanche deposits extend 9 km east-northeast of Oldonyo Lengai (unit $Qoda_2$; the cheetah unit of Kervyn and others, 2008a). Their youthfulness is demonstrated by sharp margins against adjacent bedrock. (With increasing age, the work of mass wasting and slope wash redistributes material off the flanks of older debris-avalanche deposits and blurs what were once sharp boundaries.) These east-northeast deposits are littered with large blocks of lava, more so than other units of debris-avalanche deposits around the volcano. The abundant blocks probably indicate a source area rich with interlayered, thick lava flows. Block-laden surfaces are lacking in debris-avalanche deposits at similar distance from the volcano's summit on the south, southeast, and north sides.

As explained by Kervyn and others (2008a), the Eastern Chasm is the likely source area of the east-northeast deposits, which lie downslope from the Eastern Chasm. Also the concave-upslope end loop (marginal levee) that defines the termination of these deposits points directly to the discharge point of the Eastern Chasm (fig. 33). As supporting evidence, the volume of the east-northeast debris avalanche is a close match to the volume of material missing from the Eastern Chasm (Kervyn and others, 2008a).

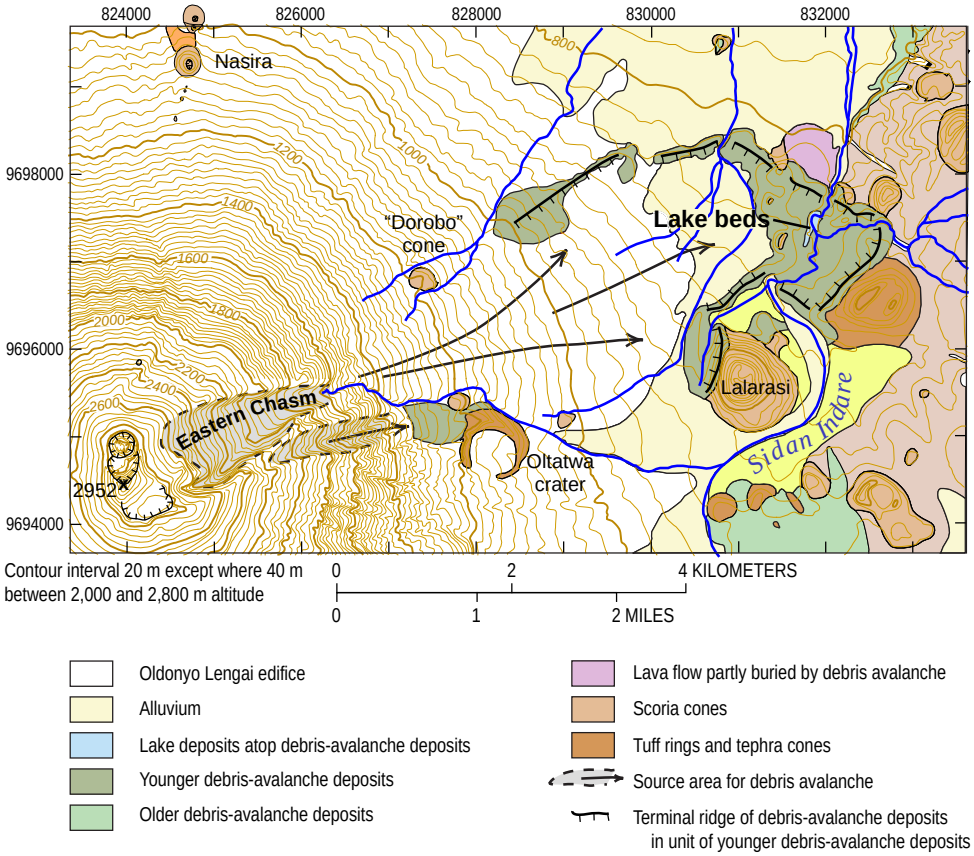

Figure 33. Map showing details of youthful debris-avalanche deposits on east-northeast flank of Oldonyo Lengai. UTM grid and datum Arc 1960, zone 36.

Figure 34. Lake deposits atop debris-avalanche deposits, now exposed by downcutting of Sidan Indare stream. Masota Magigita and Shimba Kwelwa, each about 1.5 m tall, provide scale. Photo 6761, February 3, 2010.

The east-northeast-directed debris avalanche overran several tephra cones and much of an adjacent lava flow in the Natron-Engaruka volcanic field. The northernmost cone is best exposed because it lies at about the termination of the debris-avalanche deposits. Exposures of the middle cone were found only on its eastern face (leeward of avalanche source area); whereas its other flanks are littered with avalanche debris. The south cone was not visited but likely is also poorly exposed, given its position closer to the chasm.

The east-northeast debris-avalanche deposits are unusual for hosting some thin-bedded siltstone and claystone of lacustrine origin (unit Ql_2; fig. 34). The lacustrine deposits occupy a hollow in the hummocky terrain of the debris-avalanche deposits. Subsequent downcutting by Sidan Indare stream has exposed these beds in cross section. Individual layers are 1–5 cm thick, but the entire sequence is 20–25 m thick.

An obvious interpretation is that these lacustrine deposits comprise sediment deposited by Sidan Indare stream as it was reestablishing itself across the debris-avalanche deposits. Three features, however, suggest a different source. First, the deposits are notably fine grained. Although sandy and pebbly beds were searched for, only one sandy layer was found, a discontinuous bed 1 cm thick that lies about midway up the stratigraphic section. The fine grain size is difficult to explain if a stream with the carrying capacity of Sidan Indare (during its seasonal flash floods) were the source of the waters. Second, tephra deposits (ash beds) are lacking. Although the absence of fallout tephra can be explained by the westerly flow of prevailing winds in the area of Oldonyo Lengai, reworked ash should abound in downstream deposits fed by Sidan Indare, whose upslope tributaries would have been flushing ash from the volcano. Third, the deposits are of limited extent. Lack of exposures might excuse this problem, but the flat upper surface of the lakebed unit should be a high-water mark traced handily across the irregular terrain of debris-avalanche deposits and forming a path toward a Sidan Indare source. We have some confidence that the lake beds are no more extensive than mapped.

Proposed instead is that the material in these lake beds was carried onto the debris-avalanche deposits by a stream feeding from the east. Today, such a stream has its confluence with Sidan Indare at the location of the lake beds. Its headwater basin is mantled with extensive tuff deposits (unit Qnet) of the Natron-Engaruka volcanic field. This small-basin source (7 km^2) explains the limited extent of the lake beds, the fine grain size of the deposits, and the lack of abundant Oldonyo Lengai ash as a reworked component in the lake beds.

The age of the lake beds, if known, would be a useful minimum-age constraint on the emplacement of the underlying debris-avalanche deposit. We searched for but did not find organic material suitable for dating, nor do we know of applicable ages. Kervyn and others (2008a, p. 6,583) mention "^{14}C dating of these ~10-m-thick, fine-grained lake sediments and the pyroclastics underlying the debris-avalanche deposits near Dorobo [tephra] cone." The ages, 3,000 and 2,500 ^{14}C yr B.P., are "from plants incorporated into the base of that cone's pyroclastics," not from the lake beds (Keller and others, 2006, p. 155). The cone lies 4 km west of the lake beds and 320 m upslope; and to the best of our knowledge, no evidence establishes a relative stratigraphic age between the tephra and the lake beds themselves. Dorobo cone has none of the debris-avalanche deposits slapped against its flank, but the cone is at or beyond the margin where deposition might be expected (fig. 33), so even the relative ages of cone and debris avalanche are not established.

Late Pleistocene and Holocene Faults in the Southern Basin

Escarpments, faulted surfaces, gaping cracks, sags, and subsidence pits are found in late Pleistocene and Holocene volcanic and alluvial deposits that floor the Lake Natron basin—an unsurprising abundance of tectonic features given the basin's setting in an active rift. Some escarpments are well preserved laterally along the fault traces, especially where streams have yet to erode the thick debris-avalanche deposits that host them. Others would go unnoticed except that the fault planes are exposed in the walls of incised streams. The most youthful features may have formed or expanded in breadth or offset following a M_w 5.9 and smaller earthquakes and an ensuing eruption in 2007 (for example, Baer and others, 2008; Calais and others, 2008), although field-based investigations for that event were focused 6 km east of the map area, in the area of the 2007 faulting and dike intrusion (Baer and others, 2008).

Holocene Faults Recently Active

Enarok Kohoke Fault

Abundant evidence of recent activity marks the fault whose curvilinear trace passes through Enarok Kohoke, a Pleistocene tephra cone of the Natron-Engaruka volcanic field (fig. 35). An escarpment as high as 3 m characterizes part of this fault where it displaces the tephra cone (fig. 35*B*). Eastward a few tens of meters are smaller escarpments with less offset and gaping cracks. Some of these have the roots of adjacent shrubbery stretched across them, proof that some of the displacement occurred within the past two decades, which is probably the maximum duration that such tightly strung roots might persist in midair.

Southeastward from Enarok Kohoke, the main strand of this fault projects across the alluvial floor of the southern Lake Natron basin. There, displaced sandy alluvial beds are exposed wherever the fault trace crosses active gullies (fig. 35*C*). Farther southeast, the surface expression of the fault is limited to a few gaping cracks and oblong topographic sags where the fault crosses into debris-avalanche deposits.

The fault lacks expression north of Enarok Kohoke, but a large circular subsidence pit 350 m northeast is likely related to the faulting. The pit is 190 m in diameter and 15 m deep (fig. 35*D*). Within it are three smaller-diameter pits nestled against the circumferential fracture of the main pit. The subsidence pit is not seen in air photos flown in 1959. According to our local guide, Olemelok Nantatwa of Engare Sero village, the pit formed and deepened within his lifetime (within the past 30 years).

The crescentic map pattern of Enarok Kohoke owes itself to a truncation of the tephra cone's east flank, presumably by a buried fault on its east side. As seen in figure 35*A*, the regional topographic slope pitches down to the 640-m contour and then flattens northeastward, a feature obvious in the field when

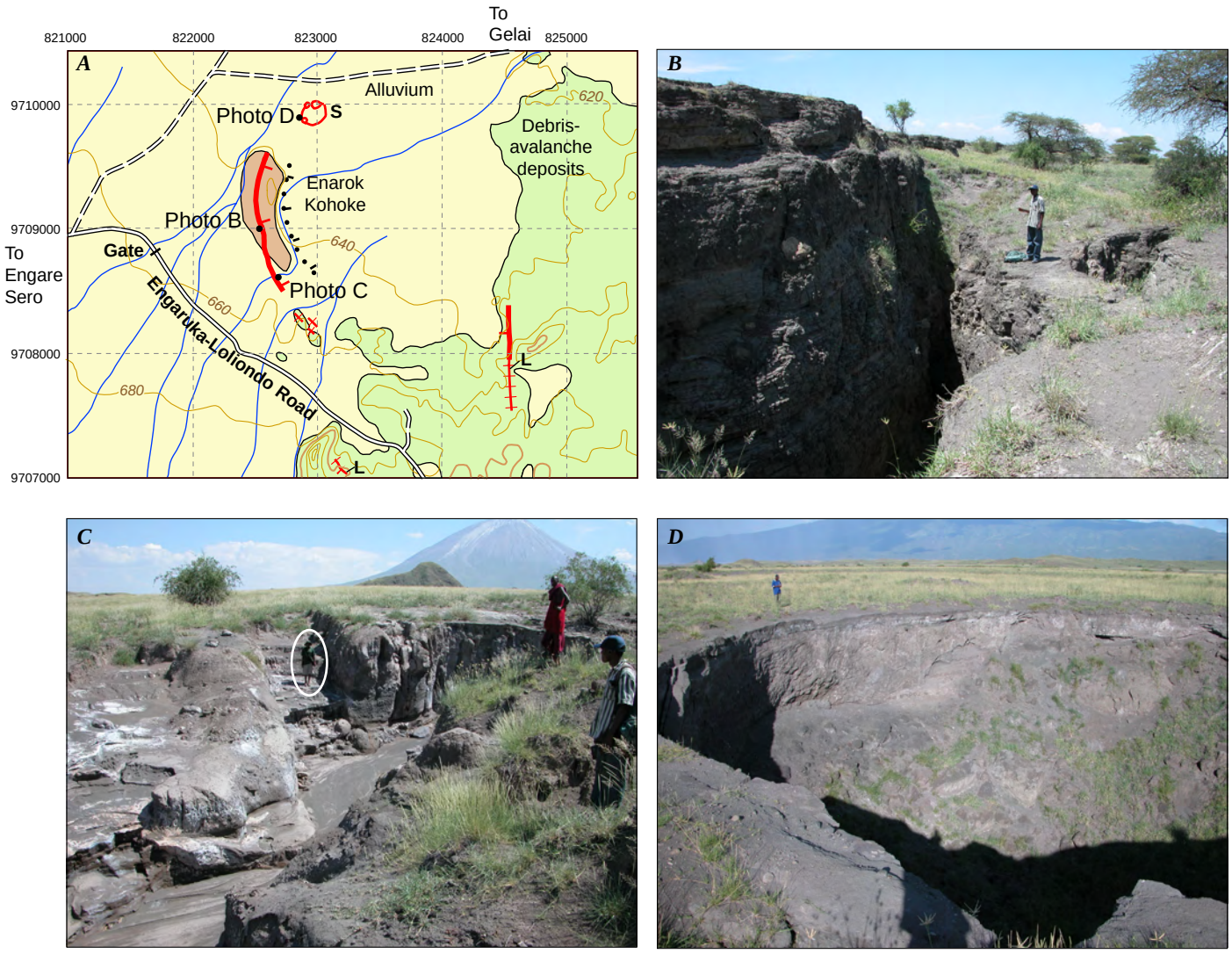

Figure 35. The Enarok Kohoke fault and related subsidence. Photos from February 1, 2010, except panel D. *A*, Geologic setting (from plate 1). Holocene faults shown as bold red line, tickmarks on downthrown side. Speculative buried Pleistocene fault shown by dotted black line; tick marks on downthrown side. Hachured thin red lines are gaping cracks. L, Liquefaction sand boils; S, sag pit, with pit rims shown by thin red lines. Topographic base from Mosonik quadrangle; altitude in meters. UTM grid provides scale and approximate north orientation; datum Arc 1960. *B*, Shimba Kwelwa provides scale on east side of escarpment where fault cuts fine-grained tephra beds of the Enarok Kohoke tephra cone. Photo 6711. *C*, Kisana Mollel (in oval) stands in a small graben exposed by gully incision along the fault 185 m southeast of Enarok Kohoke. Photo 6715. *D*, subsidence (sag) pit 370 m northeast of Enarok Kohoke, view east-northeast. Photo 7650, March 6, 2010.

looking northeast from the area of figure 35*C*. Likely the Enarok Kohoke fault and the buried fault northeast of it mark a zone of differential basin subsidence (less to the southwest, more to the northeast), and the basin may favor this zone as a focus for future earthquakes in years ahead, as subsidence continues.

Sag Troughs in Alluvium near Sidan Indare Stream

Shallow, north-trending linear troughs as long as 170 m and a few meters wide are found in some alluvial deposits (unit Qa_2) adjacent to the downstream reach of Sidan Indare stream, in the eastern part of the map area (for example, fig. 36; feature 11 in Index to Notable Features on geologic map). Wall exposures are poor, owing to sloughing of the poorly consolidated sediment. The troughs likely mark small graben sags (surface expression of the kind of feature seen in section along the Enarok Kohoke fault on fig. 35*C*).

Liquefaction Features along Gaping Cracks, Holocene or Late Pleistocene in Age

Thin sandy deposits locally rich in pebbles were found atop the main-sheet debris-avalanche deposits at three sites within 6.5 km of Lake Natron's modern shoreline. The pebbles, entirely volcanic in provenance, are similar in hand-sample mineralogy and texture to rocks at Oldonyo Lengai. Neither pebbles of sedimentary rocks (sandstone or siltstone) nor fragments of intrusive rocks were found. The rounded character of the pebbles

Figure 36. View north along trough developed above Holocene fault(?) east of Sidan Indare stream. Hillocks in middle distance are blocks in debris-avalanche deposits. Oldonyo Sambu on skyline, 53 km distant. Photo 7590, March 5, 2010.

and their whitish weathering aspect, which results from thin carbonate films, distinguish them from angular and subangular fragments that weather from the debris-avalanche deposits. The sand-and-pebble deposits are discontinuous, covering at most a few square meters or tens of meters. Site altitudes range from 660 to 700 m (lake level is about 600 m), and each site stands far above the modern stream system, which rules out alluviation as a mechanism to emplace the sand-and-pebble beds.

Gaping cracks characterize two of the sites, along either side of the Engaruka-Loliondo road. North of the road (map, site 6), subrounded to well-rounded pebbles as large as 8 cm in diameter surround pits and troughs along about 170 m of the crack (fig. 37*A*–*C*), which itself is about 500 m long. Farther north the crack grades into a normal fault with 2–6 m of vertical displacement (fig. 37*D*).

South of the road (geologic map, site 4), a crack 20 m deep strikes northwest (fig. 38*A*). At its southeastern end are pebbles and weakly indurated sandy layers that blanket only a few square meters (fig. 38*B*, *C*).

The third site is adjacent to a 1–2-m-high escarpment (geologic map, site 3). It strikes northwest for 40 m before losing relief. Open ground cracks are lacking here. Round pebbles as large as 10 cm across lie on the downthrown side of the escarpment.

We interpret these sand-and-pebble deposits to have formed by expulsion of water in response to seismically induced liquefaction of alluvium or lake deposits that underlie the debris-avalanche deposits. Conditions would have been ideal: a water table nearly at the surface, a thick debris-avalanche deposit that quickly became impermeable as its matrix altered to clay, and a tectonic rift setting where earthquakes are capable of generating sufficient horizontal ground accelerations to alter fluid pore pressure in the water-laden sediment. The coincidence of extensive gaping cracks and sand-and-pebble deposits is analogous to sand blows that form along fractures during large earthquakes. Rounded pebbles and sand derived from Oldonyo Lengai form the shallow subsurface alluvial plain beneath the debris-avalanche deposits and could have been the source of the pebbles on the surface.

The site just mentioned is even more unusual owing to an adjacent shallow crater 40 m in diameter and only a few meters deep. The crater is visible in 50,000-scale air photos (vintage 1959), which guided us to it. Its rim lacks constructional buildup. Slumping above a subsidence pit in the underlying alluvium is a likely explanation for this crater.

Figure 37. Liquefaction features along crack-fault trace in debris-avalanche deposits north of Engaruka-Loliondo road. Photos from February 18, 2010. *A*, View south along crack-fault trace, with Oldonyo Lengai shrouded by distant clouds. Light-colored bank near middle of photo is sandy rim deposit rich in subrounded pebbles. Photo 7208. *B*, Shimba Kwelwa examines crack-rimming deposit. Contact between debris-avalanche deposits and rim deposit is at waist height. Beyond him to the southwest is the rolling topographic surface of the debris-avalanche deposit and Natron escarpment along the skyline. Photo 7211. *C*, Kisana Mollel points to pebble-rich layer near top of rim deposit. Photo 7207. *D*, View north from same vantage. Arrow points to where Shimba leans against the escarpment, showing magnitude of offset (about 4 m), down on west. Photo 7215.

Volcano Hazards

[By Gari Mayberry, Thomas Casadevall, and David Sherrod. Modified from a U.S. Geological Survey volcano-hazards report issued to the United Republic of Tanzania following eruptive activity at Oldonyo Lengai in 2007–08.]

Oldonyo Lengai volcano possesses a complex history, including (1) periods of explosive activity that produced accumulations of ash; (2) periods when parts of the volcano failed and produced large debris-avalanche deposits; and (3) periods when rainfall washed over the surface of the volcano and produced mudflows and floods of volcanic material (fig. 39). The deposits can be mapped to identify zones or areas on the volcano with elevated hazard for people, livestock, and structures such as houses and roads.

Tephra Fallout

The recent explosive eruptions of Oldonyo Lengai began in September 2007 and persisted until about March 2008. Four similar-size eruptions occurred in the 20th century. The most disruptive aspect of the September 2007 eruption was the ash that fell thickly on the flanks of the volcano (fig. 40) and dusted areas as far west as Ngorongoro Crater National Park. Grasslands were still barren over an area of 60 to 100 km^2 west of the volcano four years after the end of the 2007–08 eruption.

The villages of Naiyobi and Kapenjiro, each with populations between 5,000 and 6,000, took the brunt of damage from ash fallout of the September 2007 eruption (fig. 41). Ash thicknesses of 5–6 cm were measured in January 2009 near Naiyobi. These villages, 12 and 15 km from the volcano, respectively, were evacuated over the short term because of the ill health effects

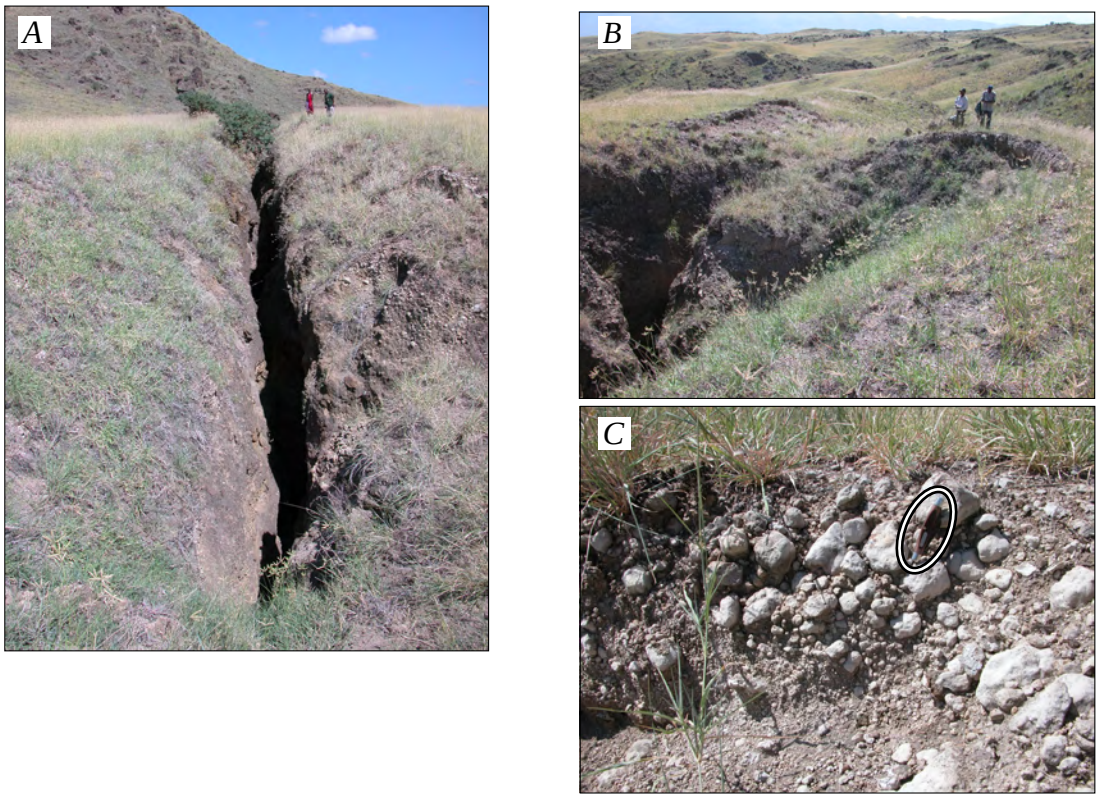

Figure 38. Liquefaction features along gaping cracks in debris-avalanche deposits south of Engaruka-Loliondo road. Photo date February 12, 2010. *A*, View N. 45° W. (315) along gaping crack. Crack is deeper than 20 m as measured with laser rangefinder; curved face of fracture prevents a view (and measurement) to maximum depth. Photo 7073. *B*, At southeast end of crack, a circular rim deposit comprises sand and pebbles. Photo 7074. *C*, Subrounded, carbonate coated pebbles in deposit. Ellipse encloses 8-cm pocket knife, for scale. Photo 7075.

of volcanic ash on people and livestock. The ash had a caustic nature owing to its high alkalinity. In addition to respiratory ills that commonly arise under conditions of fallout, this ash also led to burning of the skin on infants and the burning of hides or loss of hair on stock, primarily cattle and goats.

Pyroclastic Flows

The vertical part of an eruption column may be heavily laden with ash. In some eruptive conditions, this ash falls back to earth to descend the volcano flanks in dense clouds known as pyroclastic flows. Many particles in the clouds produced by Oldonyo Lengai are hot (300–500°C) and may burn everything in their path. The ash coats the lungs and throats of people and animals overwhelmed by the pyroclastic flows, usually leading to death.

Small pyroclastic flows have been a part of Oldonyo Lengai's past eruptive activity. The September 2007 ash fallout deposits include, at their base, a fine grayish brown ash that resulted from pyroclastic flows (fig. 40). These 2007 pyroclastic-flow deposits were found at altitude of 1,220 m on the northwest and west flanks of the volcano. Photos from later in the eruptive sequence show that pyroclastic flows accompanied explosive eruptions until at least March 2008 (fig. 42).

The hazard zone for pyroclastic flows encompasses all flanks of the volcano outward to distances of about 6 km from the summit (fig. 43). The south crater has largely shielded the volcano's south flank from pyroclastic flows of small eruptions, but a slight increase in the size of an ash eruption would be sufficient to overwhelm this minor topographic barrier. Deposits would be more extensive as the explosive power and duration of an eruption increase.

Summit Explosions

Of particular hazard to those who climb the flanks and summit area of the volcano is the risk of being struck by fist-size or larger blocks of volcanic material ejected during small explosions from the north crater area. These blocks move at high velocity and almost surely will cause severe injury or death if they strike a person (fig. 44). The hazard zone for ballistics is included with the proximal hazard zone (fig. 43) and demarcated by a circle of radius 5 km centered on the north crater. The 5-km radius is characteristic of ballistics fallout from vulcanian explosions (Morrissey and Mastin, 2000). It encompasses the entire summit and the steep upper and middle flanks.

Carbon Dioxide Gas

Carbon dioxide (CO_2) is a common volcanic gas, second in abundance only to water. The gas is heavier than air and, consequently, in calm (nonwindy) conditions CO_2 may accumulate in closed depressions such as volcanic craters, ground cracks, and small pits, where it displaces oxygen. People and animals that enter these areas will die of suffocation. Because CO_2 is odorless, it kills without warning. Previous gas measurements at Oldonyo Lengai show that CO_2 discharge is confined to the volcano's summit crater; apparently the gas does not leak diffusely through the volcano's flanks (Koepenick and

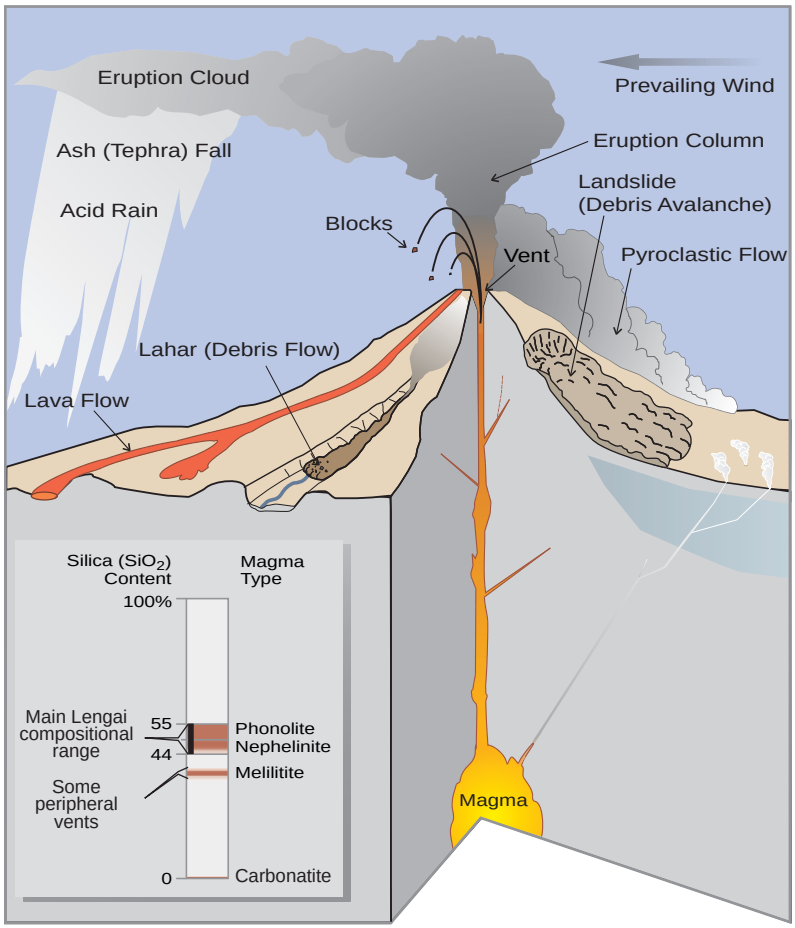

Figure 39. The variety of hazardous events associated with a volcano like Oldonyo Lengai. Some events, such as lahars and landslides (debris avalanches), can occur even when the volcano is not erupting. Sketch from Myers and others (2002).

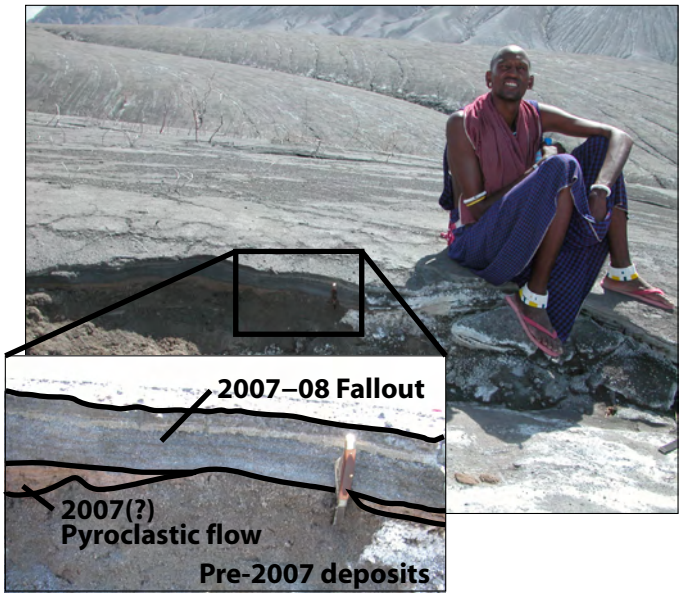

Figure 40. Olemelok Nantatwa sits atop ash fallout from eruptions of Oldonyo Lengai in 2007. The photograph was taken January 19, 2009, on the west side of the volcano, in an area where vegetation is completely buried by the fallout.

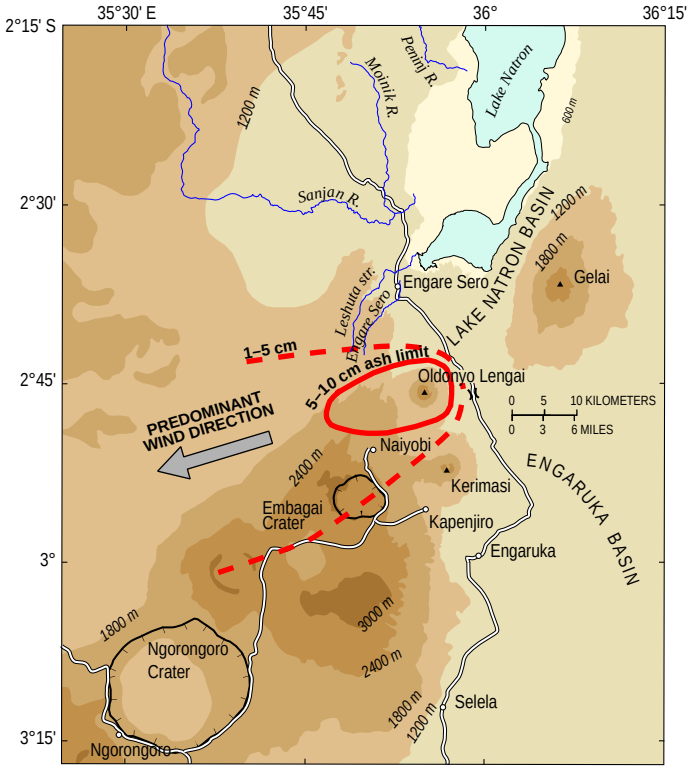

Figure 41. Map showing distribution of ash from 2007–08 eruptions of Oldonyo Lengai.

others, 1996). These surveys were conducted during times of volcanic repose.

The hazard zone for CO_2 is limited to the summit region, a 200-ha area encompassed by the 2,600-m topographic contour line, which includes the north and south summit craters (fig. 43). The hazard zone includes areas entered by climbers, their guides, and porters on trekking expeditions to the summit craters. Neither grazing nor home sites occur in the hazard region. The active north crater is the obvious hazard within this zone. The south crater has substantially smaller hazard, in part because it is not an active volcanic crater but also because it is so broad and shallow that it remains well ventilated under most conditions. The south crater is the most common summit camping area, so the standard precaution is to sleep higher than the south-crater rim, thereby avoiding low ground. Little is known about the diffusive spread of CO_2 through the main cone when the volcano is active.

Lava Flows

Lava flows present a hazard because of their tremendous heat and their inexorable downslope advance, overwhelming and covering all in their path. Lava may flow so rapidly on steep volcanoes or during voluminous eruptions that it overtakes people or animals fleeing from it. The hazard at Oldonyo Lengai is heightened by a peculiar type of magma, carbonatite, that erupts periodically. Crystal-poor carbonatite lava has low yield strength (viscosity), so it flows readily.

The hazard zone for carbonatite and silicate lava encompasses the area within 6 km of the volcano's summit (fig. 43). The area includes the reach of most lava flows that have issued from the volcano. For example, in 2006 a carbonatite lava flow traveled west downslope to 1,200-m altitude, extending a distance of 4.2 km from the central vent. Active lava flows on the lower flanks present similar hazard but advance more slowly, which diminishes their impact on people, livestock, and wildlife.

Lahars

Volcanic debris flows, also known as lahars or mudflows, are watery slurries of rock fragments that range in size from blocks to sand and silt. A volcano's eruptive activity provides an abundant source of rock fragments. Interstitial water is present within the main-cone rocks of Oldonyo Lengai, despite the dry surface conditions. Water further saturates the slopes during periods of high rainfall. Lahars have the consistency of wet concrete and may flow rapidly, overwhelming any structures in their path.

Lahars can form at any time during or after an eruption, especially during the rainy season. They originate on the volcano's upper and middle flanks and flow by the influence of gravity. Small lahars will fill existing drainages, whereas medium or large-volume lahars will bury existing drainages and spread over adjacent terrain.

The hazard zone for lahars, which reaches about 9 km from summit, is drawn with a consideration of likely run-out limits

Figure 42. Oldonyo Lengai in eruption on March 3, 2008, with pyroclastic flows descending northwest flank. Photograph by Tony Drummond-Murray, used with permission.

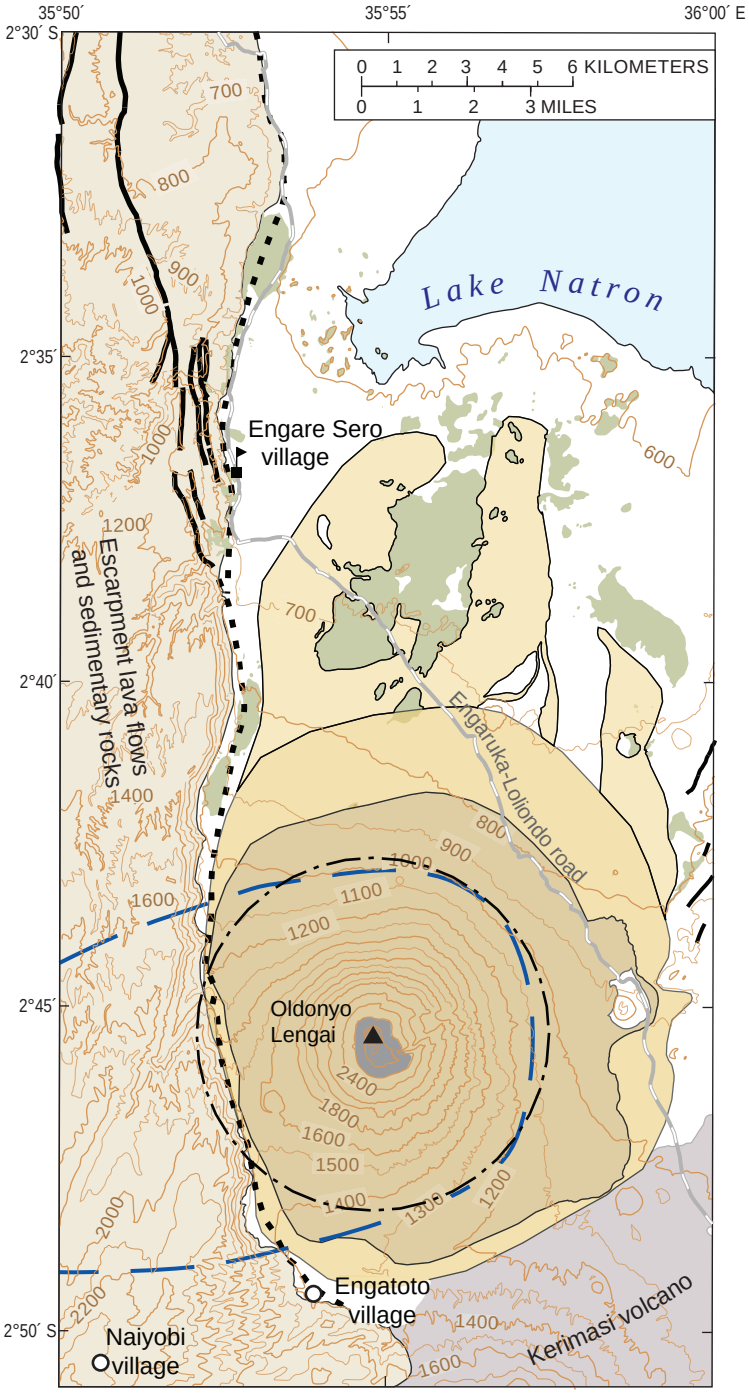

EXPLANATION

Hazard zones

- Near-vent: CO_2
- Proximal: Lava flows, ballistics, pyroclastic flows, and close-in lahars. Dot-dash line shows 5-km radius for ballistics
- Medial: Limit of most lahars and small to medium debris avalanches
- Distal: Dilute lahars and flood deposits
- Widespread debris-avalanche deposits. Shows preserved distribution from largest known event
- 5–10-cm thickness line, 2007–2008 ash fallout deposits
- Foot of major topographic escarpment. Dotted where buried by Kerimasi volcano
- Topographic contour. Contour interval 100 m

Figure 43. Volcano hazards map.

controlled by the diminishing topographic slope away from the volcano and the effect of topographic barriers (fig. 43). High escarpments block the advance of lahars on the west and southwest sides, and a low topographic divide prevents their advance to the south.

Not attempted in this report is sophisticated numerical modeling to simulate lahar distribution. The models work well where a volcano is drained by moderate to large valleys. Confining effects of canyons restrict the lateral spread of lahars and focus them downslope. Because Oldonyo Lengai and its adjacent plains are, for the most part, only slightly incised, these models are of limited usefulness except for small-volume eruptions.

Debris Avalanches

Debris avalanches begin as landslides from the flanks of volcanoes. Although once poorly understood, the deposits of debris avalanches have become a widely recognized phenomenon at volcanoes worldwide, owing to the lessons learned from the catastrophic eruption of Mount St. Helens (USA) in 1980. During that event, the northern slope of Mount St. Helens slid away and moved with startling speed down an adjacent river valley.

Figure 44. View south-southwest across South Crater, 0.7 km from North Crater vent. Arrows point to four of the more than 200 ballistic craters visible in the field of view. Photo 8068, March 12, 2010.

Debris avalanches have occurred repeatedly in the past at Oldonyo Lengai. The resulting deposits form the irregular hilly terrain crossed by the Engaruka-Loliondo road northeast of the volcano. Debris-avalanche deposits extend northward at least 24 km along the west side of Lake Natron. Six or more debris-avalanche events have occurred in Oldonyo Lengai's history, judging from the composition and geometry of the deposits (Kervyn and others, 2008a; this map). The timing of these events is poorly constrained, though the most extensive of the deposits were emplaced more than 10,000 years ago, on the basis of past lake shoreline positions. The youngest of the deposits, likely less than 10,000 years in age, extends only 8–10 km from the summit.

Debris avalanches may occur in the absence of volcanic activity. Magnitude 6 and 7 earthquakes, likely events in the East African rift, can initiate shallow-seated debris avalanches. Debris avalanches commonly transition to lahars at their downslope limit.

Debris avalanches are events that have the potential for great devastation across large areas. Fortunately, large avalanches are rare events. Their infrequent occurrence makes it impractical to define useful or beneficial hazard zones for their far-traveled deposits. Small debris avalanches would be encompassed by the same zones that mark the hazard for lahars, pyroclastic surges, and lava flows; that is, an area within 5–10 km of the volcano's summit (fig. 38). The largest debris avalanches are probably associated with volcanic activity and have reached the shore of Lake Natron.

Summary

Essential geologic features of Oldonyo Lengai and the southern Lake Natron basin have been pieced together by many previous researchers, to which we add a substantive geologic map. The Lake Natron area has been a depocenter for much of the past 2–3 million years. The basin as seen today, with west-side escarpment and an eastern boundary at Gelai volcano, has existed for most of the past million years. It is here that the stratovolcano Oldonyo Lengai has erupted for several hundred thousand years, a history that includes periodic collapse of the volcano's flanks and deposition of volcanic debris-avalanche deposits across the southern basin floor. During this time Lake Natron receded to its modern shoreline, about 597 m above sea level.

Significant new findings include the ~350-ka radiometric ages for rocks on the lower slopes of Oldonyo Lengai. An important finding from the mapping is the previously unrecognized debris-avalanche deposits along the east side of the basin near Lake Natron. These, perhaps the oldest of the debris-avalanche deposits, show evidence of having ploughed into an ancestral Lake Natron whose shore would have lapped higher than the 640-m topographic contour. New radiometric ages from phlogopite-bearing blocks within the oldest and next younger of the debris-avalanche units suggest that Oldonyo Lengai has been active since at least 500,000 years ago. This interpretation hinges on the presumption that the debris-avalanche blocks themselves were derived from an ancestral Oldonyo Lengai, but the ages are in keeping with revised stratigraphic ages of fallout deposits determined independently at Olduvai Gorge.

Volcano hazards associated with Oldonyo Lengai are similar to those of any stratovolcano: near-vent CO_2 and, out to about 5-km radius, the proximal-zone hazards of ballistics, tephra fallout, pyroclastic flows, and lahars. Beyond that lie the hazard zones encompassing the full extent of lahars and debris-avalanche runout. Downwind tephra-fall hazards extend far beyond the volcano mainly to the southwest and west owing to prevailing wind.

Acknowledgments

Our work at Oldonyo Lengai was made possible by funding from the USAID Office of Foreign Disaster Assistance. The work was facilitated by Abdul Mruma (Director, Tanzania Geological Survey) and Crispin Kinabo (University of Dar es Salaam). Kinabo deserves special mention for assistance with tactical matters in Dar es Salaam and his camaraderie in the field. The section of this report describing volcano hazards relies heavily on an earlier version by Gari Mayberry and Tom Casadevall (both USGS), who were part of a posteruption team that visited Oldonyo Lengai in 2009; each of them have contributed in many ways to the completion of this map. We would be remiss in overlooking Charles Wenger and Jon DeBord of the USGS library, who somehow uncovered the path to every obscure piece of scientific literature we requested. Florian Neukirchen (University of Freiburg) provided a copy of his unpublished master's thesis.

Kisana Mollel and Olemelok Nantatwa are mentioned several times in this pamphlet, and with good reason: they contributed materially in the field work for the geologic map. Kisana, our driver (Arusha town, Dorobo Safaris Inc.) is a patient, indomitable teacher in the matters of culture and field biology of northern Tanzania. Olemelok, our guide (Engare Sero village), has the innate knowledge of terrain that comes to those who spend their days afield. If his formal training and opportunity were in the Earth sciences he might have already published a geologic map much like ours.

Access to the southern Lake Natron basin has improved over the years, as have the technical advances in the Earth sciences. Each of these leads to an improved understanding of the basin's geology along the frontier with Kenya. Even so, the landscape of the southern Lake Natron basin is little changed by the hand of man. For field geologists, it is easy to think back to the mid-1950s, when a young Barry Dawson would have begun his mapping and study of Oldonyo Lengai in what was then Tanganyika. The road from Engaruka stopped south of the volcano. All work was done from spike camps several miles from road's end, to which both food and water were carried. Then, as now, gullies on the volcano prevented much across-slope traversing; nothing came easy. A grasp of these conditions makes the subsequent report (Dawson, 1962) even more stunning. Dawson continued to publish on the topic of Oldonyo Lengai throughout a long career. Many volcanoes deserve such a dedicated biographer, but few of them are so fortunate. Barry passed away in January 2013, as this map was nearing completion.

Technical reviews were provided by J.B. Dawson, J. Muirhead, D.A. Swanson, K.A. Howard, and C. Landowski.

References Cited

Anderson, H., 2005, Young Explorers survey Tanzanian volcano–Ol Doinyo Lengai: The Reporter [Heerbrug, Switzerland, Leica Geosystems AG], no. 52, p. 4–7. http://www.leica-geosystems.com/en/9134.htm, accessed January 2011.

Baer, G., Hamiel, Y., Shamir, G., and Nof, R., 2008, Evolution of a magma-driven earthquake swarm and triggering of the nearby Oldoinyo Lengai eruption, as resolved by InSAR, ground observations, and elastic modeling, East African rift, 2007: Earth and Planetary Science Letters, v. 272, p. 339–352, doi:10.1016/j.epsl.2008.04.052.

Bagdasaryan, G.P., Gerasimovskiy, V.I., Polyakov, A.I., Gukasyan, R.K., and Vernadskiy, V.I., 1973, Age of volcanic rocks in the rift zones of East Africa: Geochemistry International, v. 10, p. 66–71.

Bell, K., and Blenkinsop, J., 1987, Nd and Sr isotopic compositions of East African carbonatites: Implications for mantle heterogeneity: Geology, v. 15, no. 2, p. 99–102.

Bell, K., and Dawson, J.B., 1995, Nd and Sr isotope systematics of the active carbonatite volcano, Oldoinyo Lengai, *in* Bell, K., and Keller, J., eds., Carbonatite volcanism—Oldoinyo Lengai and the petrogenesis of natrocarbonatites: Berlin, Springer, IAVCEI Proceedings in Volcanology 4, p. 100–112.

Bell, K., and Keller, J., eds., 1995, Carbonatite volcanism—Oldoinyo Lengai and the petrogenesis of natrocarbonatites: Berlin, Springer, IAVCEI Proceedings in Volcanology 4, 210 p.

Bell, K., and Simonetti, A., 1996, Carbonatite magmatism and plume activity: implications from the Nd, Pb and Sr isotope systematics of Oldoinyo Lengai: Journal of Petrology, v. 37, no. 6, p. 1321–1339.

Bell, K., Dawson, J.B., and Farquhar, R.M., 1973, Strontium isotope studies of alkalic rocks: the active carbonatite volcano Oldoinyo Lengai, Tanzania: Geological Society of America Bulletin, v. 84, no. 3, p. 1019–1029.

Brantley, S.L., and Koepenick, K.W., 1995, Measured carbon dioxide emissions from Oldoinyo Lengai and the skewed distribution of passive volcanic fluxes: Geology, v. 23, no. 10, p. 933–936.

Calais, E., d'Oreye, N., Albaric, J., Deschamps, A., Delvaux, D., Déverchère, J., Ebinger, C., Ferdinand, R.W., Kervyn, F., Macheyeki, A.S., Oyen, A., Perrot, J., Saria, E., Smets, B., Stamps, D.S., and Wauthier, C., 2008, Strain accommodation by slow slip and dyking in a youthful continental rift, East Africa: Nature, v. 456, p. 783–788, doi:10.1038/nature07478.

Chorowicz, J., and Sorlien, C., 1992, Oblique extensional tectonics in the Malawi Rift, Africa: Geological Society of America Bulletin, v. 104, no. 8, p. 1015–1023.

Cox, K.G., Bell, J.D., and Pankhurst, R.J., 1979, The interpretation of igneous rocks: London, George Allen and Unwin, 450 p.

Dalrymple, G.B., 1979, Critical tables for conversion of K-Ar ages from old to new constants: Geology, v. 7, no. 11, p. 558–560.

Dawson, J.B., 1962, The geology of Oldoinyo Lengai: Bulletin of Volcanology, v. 24, p. 349–387.

Dawson, J.B., 1964, Carbonatitic volcanic ashes in northern Tanganyika: Bulletin of Volcanology, v. 27, p. 81–91.

Dawson, J.B., 1992, Neogene tectonics and volcanicity in the North Tanzania sector of the Gregory rift valley: contrasts with the Kenya sector: Tectonophysics, v. 204, nos. 1–2, p. 81–92.

Dawson, J.B., 1998, Peralkaline nephelinite-natrocarbonatite relationships at Oldoinyo Lengai, Tanzania: Journal of Petrology, v. 39, nos. 11–12, p. 2077–2094.

Dawson, J.B., 2008, The Gregory rift valley and Neogene-Recent volcanoes of northern Tanzania: Geological Society of London Memoir 33, 112 p.

Dawson, J.B., 2012, Nephelinite-melilitite-carbonatite relationships: evidence from Pleistocene-recent volcanism

in northern Tanzania: Lithos, v. 152, p. 3–10, doi:10.1016/j.lithos.2012.01.008
Dawson, J.B., and Powell, D.G., 1969, The Natron-Engaruka explosion crater area, northern Tanzania: Bulletin Volcanologique, v. 33, no. 3, p. 791–817.
Dawson, J.B., Smith, J.V., and Jones, A.P., 1985, A comparative study of bulk rock and mineral chemistry of olivine melilitites and associated rocks from East and South Africa: Neues Jahrbuch für Mineralogie (Abhandlungen), v. 152, p. 143–175.
Donaldson, C.H., Dawson, J.B., Kanaris-Sotiriou, R., Batchelor, R.A., and Walsh, J.N., 1987, The silicate lavas of Oldoinyo Lengai, Tanzania: Neues Jahrbuch für Mineralogie (Abhandlungen), v. 156, no. 3, p. 247–279.
Dundas, D.L., and Adwalla, G.W., 1999, Geologic map of the Loliondo quarter-degree sheet (16 & 27): Dodoma, Tanzania, Geological Survey of Tanzania, scale 1:125,000.
Ebinger, C., Poudjom Djomani, Y., Mbede, E., Foster, A., and Dawson, J.B., 1997, Rifting Archaean lithosphere: the Eyasi-Manyara-Natron rifts, East Africa: Journal of the Geological Society of London, v. 154, p. 947–960, doi:10.1144/gsjgs.154.6.0947.
Evans, A.L., Fairhead, J.D., and Mitchell, J.G., 1971, Potassium-argon ages from the volcanic province of northern Tanzania: Nature, v. 229. no. 1, p. 19–20.
Fisher, R.V., and Schmincke, H.-U., 1984, Pyroclastic rocks: Berlin, Springer-Verlag, 472 p.
Foster, A., Ebinger, C., Mbede, E., and Rex, D., 1997, Tectonic development of the northern Tanzanian sector of the East African rift system: Journal of the Geological Society, London, v. 154, p. 689–700.
Gradstein, F.M., Ogg, J.G., and Smith, A.G., 2004, Construction and summary of the geologic time scale, chap. 23 *of* Gradstein, F.M., Ogg, J.G., and Smith, A.G., eds., A geologic time scale 2004 (reprinted with corrections 2006): Cambridge, Cambridge University Press, p. 455–464.
Guest, N.J., 1953, The geology and petrology of the Engaruka-Oldonyo L'engai-Lake Natron area of northern Tanganyika Territory: Sheffield, U.K., University of Sheffield, Ph.D. dissertation, 199 p.
Guest, N.J., and Pickering, R., 1966a, Geologic map of the Kibangaini quarter-degree sheet (28): Dodoma, Tanzania, Geological Survey of Tanzania, scale 1:125,000.
Guest, N.J., and Pickering, R., 1966b, Geologic map of the Gelai and Kitumbeine quarter-degree sheet (40): Dodoma, Tanzania, Geological Survey of Tanzania, scale 1:125,000.
Guest, N.J., James, T.C., Pickering, R., and Dawson, J.B., 1961, Geologic map of the Angata Salei quarter-degree sheet (39): Dodoma, Tanzania, Geological Survey of Tanzania, scale 1:125,000.
Hay, R.L., 1976, Geology of the Olduvai Gorge: Berkeley, University of California Press, 203 p.
Hay, R.L., 1983, Natrocarbonatite tephra of Kerimasi volcano, Tanzania: Geology, v. 11, no. 10, p. 599–602.
Hay, R.L., 1989. Holocene carbonatite-nephelinite tephra deposits of Oldoinyo Lengai, Tanzania: Journal of Volcanology and Geothermal Research, v. 37, p. 77–91.
Hillaire-Marcel, C., Carro, O., and Casanova, J., 1986, ^{14}C and Th/U dating of Pleistocene and Holocene stromatolites from East African paleolakes: Quaternary Research, v. 25, p. 312–329.
Hillaire-Marcel, C., Casanova, J., and Taieb, M., 1987, Isotopic age and lacustrine environments during Late Quaternary in the Tanzanian rift (Lake Natron), p. 117–123 *in* Rampino, M.R., Sanders, J.E., Newman, W.S., and Koningsson, L.K., eds., Climate: history, periodicity, and predictability: New York, Van Nostrand Reinhold Co., 588 p.
[Title page misspells Hillaire-Marcel's name.]
Isaac, G.L., 1965, The stratigraphy of the Peninj beds and the provenance of the Natron Australopithecine mandible: Quaternaria, v. 7, p. 101–130.
Isaac, G.L., 1967, The stratigraphy of the Peninj Group—early middle Pleistocene formations west of Lake Natron, Tanzania, *in* Bishop, W.W., and Clark, J.D., eds., Background to evolution in Africa: Chicago, University of Chicago Press, p. 229–257.
Isaacs [sic], G.L., and Curtis, G.H., 1974, Age of early Acheulian industries from the Peninj Group, Tanzania: Nature, v. 249, p. 624–627, doi:10.1038/249624a0.
Johnson, L.H., Jones, A.P., Church, A.A., and Taylor, W.R., 1997, Ultramafic xenoliths and megacrysts from a melilitite tuff cone, Deeti, northern Tanzania: Journal of African Earth Sciences, v. 25, no. 1, p. 29–42.
Keller, J., 2002, Cone collapses, flank stability and hazard at Oldoinyo Lengai, Tanzania [abs.]: IAVCEI International Congress, 1902 Mount Pelée Centennial Workshop, Martinique, Abstracts, p. 68.
Keller, J., and Krafft, M., 1990, Effusive natrocarbonatite activity of Oldoinyo Lengai, June 1988: Bulletin of Volcanology, v. 52, p. 629–645.
Keller, J., Zaitsev, A.N., and Wiedenmann, D., 2006, Primary magmas at Oldoinyo Lengai: The role of olivine melilitites: Lithos, v. 91, p. 150–172.
Kervyn, M., Ernst, G.G.J., Klaudius, J., Keller, J., Mbede, E., and Jacobs, P., 2008a, Remote sensing study of sector collapses and debris avalanche deposits at Oldoinyo Lengai and Kerimasi volcanoes, Tanzania: International Journal of Remote Sensing, v. 29, no. 22, p. 6565–6595, doi:10.1080/01431160802168137.
Kervyn, M., Ernst, G.G.J., Klaudius, K., Keller, J., Kervyn, F., Mattsson, H.B., Belton, F., Mbede, E., and Jacobs, P., 2008b, Voluminous lava flows at Oldoinyo Lengai in 2006: chronology of events and insights into the shallow magmatic system: Bulletin of Volcanology, v. 70, p. 1069–1086, doi:10.1007/s00445-007-0190-x.
Klaudius, J., and Keller, J., 2004. Quaternary debris avalanche deposits at Oldoinyo Lengai (Tanzania) [abs.]: Volcanism and its impact on Society, IAVCEI General Assembly, Pucón, Chile, 2004, Symposium 02-B, Abstract s02b_pth_048, available at http://www.iavcei.org/documents/pucon04/pucon04abs.html, accessed Nov. 14, 2013.
Klaudius, J., and Keller, J., 2006, Peralkaline silicate lavas at Oldoinyo Lengai, Tanzania: Lithos, v. 91, p. 173–190.
Koepenick, K.W., Brantley, S.L., Thompson, J.M., Rowe, G.L., Nyblade, A.A., and Moshy, C., 1996, Volatile emissions from the crater and flank of Oldoinyo Lengai volcano, Tanzania: Journal of Geophysical Research, v. 101, no. B6, p. 13819–13830.
Last, R.J., Nyblade, A.A., Langston, C.A., and Owens, T.J., 1997, Crustal structure of the East African Plateau from receiver functions and Rayleigh wave phase velocities: Journal of Geophysical Research, v. 102, no. B11, p. 24469–24483.

Le Maitre, R.W., ed., 2002, Igneous rocks: a classification and glossary of terms: recommendations of the IUGS Subcommission on the Systematics of Igneous Rocks (2d ed.): Cambridge, Cambridge University Press, 236 p.

Macintyre, R.M., Mitchell, J.G., and Dawson, J.B., 1974, Age of fault movements in Tanzanian sector of East African rift system: Nature, v. 247, p. 354–356.

Manega, P.C., 1993, Geochronology, geochemistry, and isotopic study of the Plio-Pleistocene hominid sites and the Ngorongoro volcanic highland in northern Tanzania: Boulder, University of Colorado, Ph.D. dissertation, 328 p.

Mattsson, H.B., and Tripoli, B.A., 2011, Depositional characteristics and volcanic landforms in the Lake Natron–Engaruka monogenetic field, northern Tanzania: Journal of Volcanology and Geothermal Research, v. 203, p. 23–34, doi:10.1016/j.jvolgeores.2011.04.010.

McDougall, I., and Harrison, T.M., 1999, Geochronology and thermochronology by the $^{40}Ar/^{39}Ar$ method: New York, Oxford University Press, 269 p.

Morrissey, M.M., and Mastin, L.G., 2000, Vulcanian eruptions, *in* Sigurdsson, HR., Houghton, B.F., McNutt, S.R., Rymer, H., and Stix, J., eds., Encyclopedia of Volcanoes: San Diego, Calif., Academic Press, p. 463–475.

Myers, B., Brantley, S.R., Stauffer, P., and Hendley, J.W., III, 2002, What are volcano hazards?: U.S. Geological Survey Fact Sheet 002-97, revised 2004, 2 p., available at http://pubs.usgs.gov/fs/fs002-97/, accessed Nov. 14, 2013.

Neukirchen, F., Finkenbein, T., and Keller, J., 2010, The lava sequence of the East African Rift escarpment in the Oldoinyo Lengai–Lake Natron sector, Tanzania: Journal of African Earth Sciences, v. 58, no. 5, p. 734–751, doi:10.1016/j.jafrearsci.2010.06.002.

Nyblade, A.A., and Brazier, R.A., 2002, Precambrian lithospheric controls on the development of the East African rift system: Geology, v. 30, no. 8, p. 755–758.

Paslick, C., Halliday, A., James, D., and Dawson, J.B., 1995, Enrichment of the continental lithosphere by OIB melts: Isotopic evidence from the volcanic province of northern Tanzania: Earth and Planetary Science Letters, v. 130, p. 109–126.

Paslick, C., Halliday, A.N., Lange, R.A., James, D., and Dawson, J.B., 1996, Indirect crustal contamination: evidence from isotopic and chemical disequilibria in minerals from alkali basalts and nephelinites from northern Tanzania: Contributions to Mineralogy and Petrology, v. 125, p. 277–292.

Peterson, T.D., 1989, Peralkaline nephelinites, I.—Comparative petrology of Shombole and Oldoinyo L'engai, East Africa: Contributions to Mineralogy and Petrology, v. 101, p. 458–478.

Pinna, P., Muhongo, S., Mcharo, B.A., Le Goff, E., Deschamps, Y., Ralay, F., and Milesi, J.P., 2004, Geology and mineral map of Tanzania: Orléans, France, Bureau de Recherches Géologiques et Minières, scale 1:2,000,000.

Renne, P.R., Deino, A.L., Walter, R.C., Turrin, B.D., Swisher, C.C., Becker, T.A., Curtis, G.H., Sharp, W.D., and Jaouni, A.-R., 1994, Intercalibration of astronomical and radioisotopic time: Geology, v. 22, no. 9, p. 783–786.

Schmid, R., 1981, Descriptive nomenclature and classification of pyroclastic deposits and fragments: recommendations of the IUGS Subcommission on the Systematics of Igneous Rocks: Geology, v. 9, p. 41–43.

Skinner, A.R., Hay, R.L., Masao, F., and Blackwell, B.A.B., 2003, Dating the Naisiusiu Beds, Olduvai Gorge, by electron spin resonance: Quaternary Science Reviews, v. 22, p. 1361–1366.

Smith, M., and Mosley, P., 1993, Crustal heterogeneity and basement influence on the development of the Kenya rift, East Africa: Tectonics, v. 12, no. 2, p. 591–606.

Stamps, D.S., Calais, E., Saria, E., Hartnady, C., Nocquet, J-M., Ebinger, C.J., and Fernandes, R.M., 2008, A kinematic model for the East African Rift: Geophysical Research Letters, v. 35, L05304, 6 p., doi:10.1029/2007GL032781, 2008.

Steiger, R.H., and Jäger, E., 1977, Convention on the use of decay constants in geo- and cosmochronology: Earth and Planetary Science Letters, v. 36, p. 359–362.

Taylor, J.R., 1982, An introduction to error analysis: Mill Valley, Calif., University Science Books, 270 p.

Vaughan, R.G., Kervyn, M., Realmuto, V., Abrams, M., and Hook, S.J., 2008, Satellite measurements of recent volcanic activity at Oldoinyo Lengai, Tanzania: Journal of Volcanology and Geothermal Research, v. 173, p. 196–206.

Vicens, A., and Casanova, J., 1987. Modern background of Natron-Magadi basin (Tanzania-Kenya): physiography, climate, hydrology and vegetation: Bulletin Sciences Geologiques (Strasbourg, Institut de Geologie, Universite Louis Pasteur de Strasbourg), v. 40, nos. 1–2, p. 9–21.

York, D., 1969, Least squares fitting of a straight line with correlated errors: Earth and Planetary Science Letters, v. 5, p. 320–324.

Appendix 1. About the Geologic Map

Geologic maps are tools of exploration. They show the distribution of rocks and unconsolidated deposits exposed at the Earth's surface. Geologic maps include information about the age of deposits (known or estimated) and the processes that formed them. Thus, in volcanic provinces they provide insight to a volcano's history and an aid to forecast future eruptive behavior. Additional mapped features include faults and other tectonic structures, the relative age of which may be assessed by determining the age of deposits deformed by them. Finally, geologic maps provide a useful format to compile and discuss already published data, thereby creating a guide to the places where unanswered scientific questions can be addressed successfully.

This geologic map is the result of $1^1/_2$ months of field work in February–March 2010. It covers a large area, 480 km^2, in varying detail. The map was produced in two phases: prefield and field work. A preliminary photogeologic map was compiled in December 2009. Using stereophoto coverage (photos of 1959), contacts were interpreted and rectified to topographic base maps using a Kern PG-2 photogrammetric plotter. Then, during the field phase of the mapping, the photo map was checked and additional data added to it. Traverses are shown on a small-scale map (fig. 45).

Field-based contacts and faults are locally as accurate as ±10 m where traced with handheld GPS receivers. Overall, however, accuracy is in the range ±50 m (±1 mm measured on the map) owing to the reconnaissance nature of the mapping and the 50,000-scale of the topographic map. A few inferred or highly

approximated contacts and faults doubtless have accuracy that is twice as poor.

All map data were digitized using GIS software. The digital map databases and metadata may be downloaded online from Geological Survey of Tanzania (http://www.gst.go.tz) or the U.S. Geological Survey's publication website that hosts this map (http://pubs.usgs.gov/ofr/2013/1306).

Appendix 2. Geographic Names

Names used here are those from published topographic quadrangle maps, where possible (table 13). Few geographic features are labeled on maps of the region, so names have been added after consultation with Maasai elders from Engare Sero village. The consultation included a day-long field trip to visit many of the sites, during which the names were written, their origins and meanings discussed, and it was determined whether a name is unique to the area or might apply to similar features throughout the adjacent region. In rare cases we show both names—the preferred local name and, parenthetically, the name on a published map; for example, Olmoiton (Armykon hill). Additional names, such as Eastern Chasm, have crept in through geologic publications. Spelling of some words can be problematic owing to variants among Swahili, Maa, and English; indeed, some spellings differ even among successive editions of the same topographic map. The names and spellings used here are our best effort to match local usage while conforming with previously published names, for sake of consistency. Our usage does not represent official approval for geographic names appearing on this map, a task we leave to Tanzanian geographers.

Many readers will be familiar with the word for mountain, oldonyo (Swahili spelling), and Oldonyo Lengai, literally mountain of the gods. Its most common spelling in the Earth sciences literature is Oldoinyo Lengai or, if two words, Ol Doinyo Lengai. We use the spelling as found on the published topographic quadrangle maps of the area (Mosonik, 1990; Oldonyo Lengai, 1990). A hill is ildonyo. The word for a large crater is embalulu (em-ba-LU-lu), and several of them are labeled by their place names added to the map.

Disagreement surrounds the name Lalarasi (la-la-RA-si), which on the topographic maps is applied to a prominent tephra cone east of Oldonyo Lengai. Maasai living in the area apply "Lalarasi" to a large hill (unnamed on topographic maps) lying 9 km north-northwest of the tephra cone. For them, the tephra cone is Olorok Kimojik (o-lo-ROK ki-MO-jik), words that describe the dark downslope ridges that have developed by extensive gullying (erosion). We steer clear of this particular controversy by using the name as found on the topographic base map but hope for a final solution that honors local Maasai traditions.

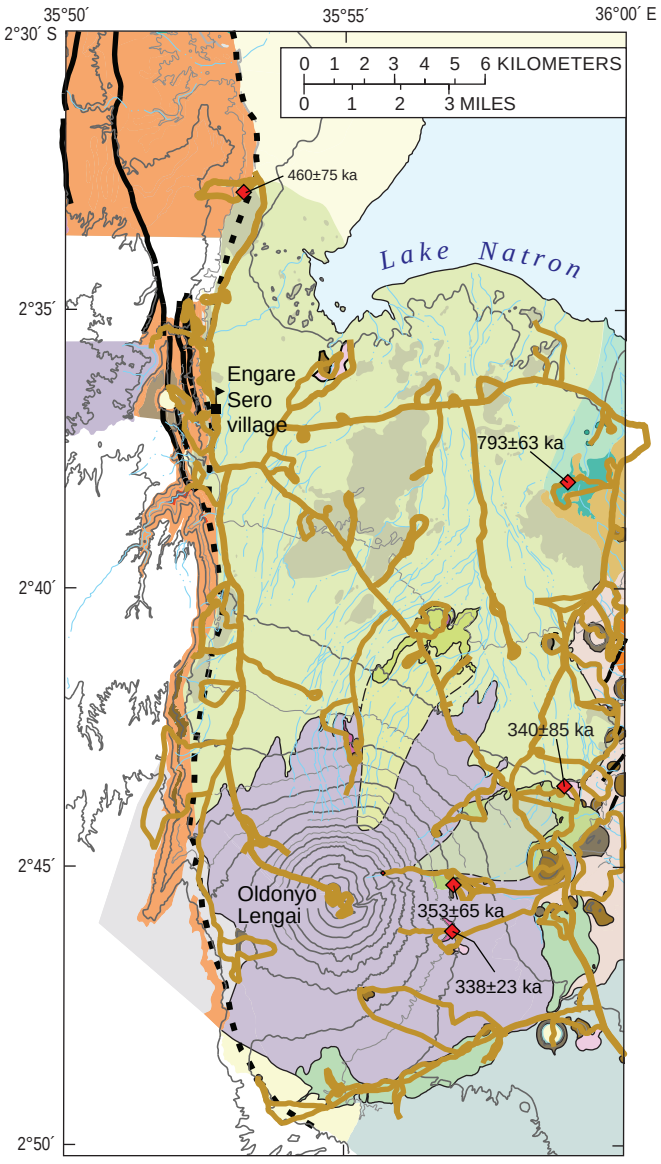

Figure 45. Traverse map compiled from each day's field work (brown lines). Red diamonds mark sample locations, showing age established by radiometric dating (see appendix 5).

Appendix 3. Whole-Rock Geochemistry

Major and trace element analyses for 48 samples were determined at Washington State University Geoanalytical Laboratories by X-ray fluorescence spectroscopy using an automated Thermo-ARL spectrometer. Analytical precision for major elements is better than 0.5 percent. For the trace elements, precision is better than 10 percent and commonly in the range 3–5 percent except for those elements in concentrations less than 10 ppm, in which case the precision may exceed 50 percent of reported value. Unlike spectrometers in use by the lab as recently as 2006, the Thermo-ARL produces quantitative values for all elements analyzed, including Sc, Th, La, Ce, and Nd.

An electronic database (spreadsheet) accompanying this publication includes the raw (nonnormalized) data and sample locations for all our analyses. Many of the results are also compiled within the explanatory pamphlet (tables 1, 4, 5–10, 12). Included in the tables are several previously published analyses of rocks from the map area, for comparison.

For comparative purposes, all analyses are reported normalized to 100 percent, volatile free. The alkali-rich, low-silica rocks that characterize the map area alter to clay more quickly than in other volcanic provinces where DRS has worked. This alteration shows in the analyses as low oxide totals, high loss on ignition, high water contents (H_2O^+), and sporadically high CO_2. Normalization is necessary to compare the analyses, but in the more highly altered rocks, the resulting recalculations

Table 13. Geographic place names used in text and map.

This map	Dawson (2008)	Keller and others (2006)	Mosonik topographic quadrangle	Oldonyo Lengai quad	Kitumbeine West quad	Mattsson and Tripoli (2011)	Johnson and others (1997)	Lake Natron East, Gelai Mountain quads
Geographic features								
Deeti	--	--	--	--	Unnamed	--	Deeti	--
Eastern Chasm	Eastern Chasm	--	--	--	--	--	--	--
Embalulu Kirurum	--	Kirurum crater	--	--	--	--	--	--
Embalulu Oltatwa	--	Oltatwa crater	--	--	--	--	--	--
Embalulu Sekenge	--	Sekenge crater	--	--	--	--	--	--
Enarok Kohoke	--	Black Belly (english equivalent)	--	--	--	Norok Nokoschoke	--	--
Esoit Ondulali	--	--	--	--	--	Essoite	--	--
Gelai	Gelai	--	--	--	--	--	--	Gelai Mountain
Ildonyo Loolmurwak	Oldoinyo Loolmurwak	Oldoinyo Loolmurwak	--	Loolmurwak	--	--	--	--
Kerimasi	Kerimasi	--	--	Karmassi	--	--	--	--
Kisitei	Kisitey	--	--	--	Kisitei	--	--	--
Lalarasi(name of tephra cone)	Lalarasi	Sinja Lalarasi	unnamed	Lalarasi	--	Lalarasi	--	--
Loluni	Loluni, Loluni crater	--	--	Loluni	--	--	--	--
Loolmurwak crater	Loolmurwak (Swallow) crater	Loolmurwak crater	--	--	--	Loolmurwak maar	--	--
Mosonik	Mosonik	--	Mosonik	--	--	--	--	--
Oldonyo Lengai	Oldoinyo Lengai	--	Oldonyo Lengai	--	--	--	--	--
Olmoiton	Armykon Hill	Armykon Hill	unnamed	--	--	Armykon Hill	--	--

Table 13. Geographic place names used in text and map.—Continued

This map	Dawson (2008)	Keller and others (2006)	Mosonik topographic quadrangle	Oldonyo Lengai quad	Kitumbeine West quad	Mattsson and Tripoli (2011)	Johnson and others (1997)	Lake Natron East, Gelai Mountain quads
Streams								
Engare Sero stream	--	--	Engare Sero	--	--	--	--	--
Leshuta stream	Leshuta River	--	unnamed	--	--	--	--	--
Sidan Indare	--	Sinja Ndare	Sinja Ndare, Sinji Ndare	--	--	--	--	--
Geologic/hydrologic features								
Nasira cones	--	Nasira cones	--	--	--	--	--	--
Natron-Engaruka volcanic field	Natron-Engaruka tuff-cone area	--	--	--	--	Lake Natron-Engaruka monogenetic volcanic field	--	--
	Engaruka Basin	--	--	--	--	--	--	--
	Natron Basin	--	--	--	--	--	--	--
Natron fault	Natron Basin boundary fault, boundary fault system	--	--	--	--	--	--	--
Natron escarpment		--	--	--	--	--	--	--
Sanjan fault	Sanjan Fault, fault segment	--	--	--	--	--	--	--
Infrastructure								
Engatoto village	--	--	--	unnamed	--	--	--	--
Engaruka-Loliondo road	Engaruka-Loliondo road	--	--	--	--	--	--	--

may distort the analysis so greatly as to render a comparison unwarranted. The reader should be alert to these difficulties.

(Excel spreadsheet file can be found at http://pubs.usgs.gov/of/2013/1306.)

Appendix 4. Previously Published Ages

Previously published radiometric ages for the Lake Natron basin and the adjacent fault escarpment are all within the range 0–4 Ma (table 2). Early-published ages predated the adoption of now widely accepted standards for isotopic abundance and decay rates (Steiger and Jäger, 1977). Therefore, table 2 shows recalculations which, as expected, are generally 2–3 percent older than ages described in the early publications. One age that lacks published analytical data (Bagdasaryan and others, 1973) was recalculated by the method of Dalrymple (1979), although this age was young enough that it remains unchanged at the reported precision of two significant figures.

Table 2 also brings to light some long-overlooked minor flaws in previously published results. A few of the early-published ages change substantially by recalculation, which indicates either incorrect data in the original publication, an error in the published calculation, or some other flaw. For example, No. 13a (table 2) had a reported age of 1.33 Ma, but recalculation yields a younger (not older) age of 1.19 Ma, about a 10 percent difference. Whether this discrepancy arises from a typographical error or incorrect age calculation in the source document is probably irreconcilable, given the lengthy delay between original publications and our discovery of the inconsistencies. We base our discussion on the recalculated ages. As a consequence, the ages preferred in our data compilation may differ from those in other compilations (Foster and others, 1997; or Dawson, 2008, his appendix 1). Finally, weighted mean ages are calculated for samples with two or more gas extractions, a commonly accepted practice in geochronology.

Locations for dated samples (table 14) are reported in decimal degrees (longitude and latitude) with precision to the fourth decimal place, which corresponds to about ±10 m on the ground in the map area. This level of precision matches the accuracy reported for our sample locations (obtained using handheld GPS receivers) and that of Foster and others (1997) or Dawson's new ages (2008, appendix 1b), which are the only samples with published geographic coordinates. For most other samples, we determined location by georegistering map illustrations found in the source publications and then reading coordinates of the sample-location symbols directly from a GIS. Precision by this method can range from tens of meters to several kilometers, depending on the craftsmanship and map scale of the original illustrations. For example, the small-scale map (1:6,000,000) of Bagdasaryan and others (1973) gives confidence of no better than ±4 km for sample locations measured from it. Ideally, poorly located sample coordinates should be reported with fewer significant figures to indicate greater uncertainty. Such tactics lack practicality, however, because users tend to treat all data similarly. For example, longitude 38.02° would likely appear as 38.0200° when compiled in a database with sample locations bearing greater precision. The net effect would be an unintended shift in geographic location away from our best estimate.

No geographic coordinates are offered for the samples dated by Isaac and Curtis (1974), which were described in broad geographic terms and illustrated only with regard to stratigraphic position (no location map).

Table 14. Sample locations for previously published ages in map area.

[Potassium-argon ages recalculated using modern decay constants, as described for table 2. Locations for samples dated by Foster and others (1997) were listed in the source publication and are likely accurate to within 20 m. All other locations were derived by georegistering sample-location maps and reading coordinates in a geographic information system. For those, location accuracy probably not better than ±1 km. The map of Bagdasaryan and others (1973) registered nicely but is of such small scale that location accuracy is no better than ±4 km]

Number in Table 2	Sample No.	Age and 1σ error, Ma	Latitude, WGS84	Longitude, WGS84	Reference	Geographic locality
1	11301	0.15±0.02	−2.7918	35.9935	Bagdasaryan and others, 1973	Near Oldonyo Lengai
2	105	0.15±0.12	−2.8008	35.9908	Macintyre and others, 1974	Ildonyo Loolmurwak
3	891	0.36±0.05	−2.7991	35.9799	Macintyre and others, 1974	Loolmurwak crater
4	3	0.37±0.11	−2.8216	36.0057	Macintyre and others, 1974	Kisetey crater
5	138	1.00±0.02	−2.6817	36.1017	Evans and others, 1971	Gelai
6	S9/6	1.45±1.45	−2.4593	35.8285	Foster and others, 1997	Top, Natron basin
7	S10/10	1.26±1.26	−2.4365	35.8914	Foster and others, 1997	100 m below top, Natron basin
8	KA1187	1.13±0.06	−2.4721	35.8831	Manega, 1993	Intra-Moinik lava flow
9	KA1186	1.41±0.04	−2.5367	35.8850	Manega, 1993	Intra-Moinik lava flow
10	BPT-NAT	1.26±0.04	−2.3040	35.9359	Manega, 1993	Birdprint tuff in Moinik Fm
11	S11/4	1.28±0.05	−2.5493	35.8817	Foster and others, 1997	Nephelinite lava flow in Moinik Fm
12	S11/6	1.31±0.26	−2.5313	35.8772	Foster and others, 1997	Nephelinite in upper Moinik, Natron basin
16	NAT90-07	1.7±0.02	−2.5035	35.8512	Manega, 1993	Basal Humbu tuff
17	S10/11	3.5±0.3	−2.4888	35.8861	Foster and others, 1997	Interbedded in lower Humbu, Natron basin
19	KA1185	2.99±0.09	−2.4934	35.7934	Manega, 1993	Beneath Humbu Fm
21	NATM89-07	3.53±0.06	−2.5637	35.8401	Manega, 1993	Mosonik(?) lava flow

Appendix 5. New $^{40}Ar/^{39}Ar$ Ages

Samples for radiometric dating were processed and dated by John Huard in the noble gas mass spectrometry laboratory in the College of Earth, Ocean, and Atmospheric Sciences at Oregon State University[5]. Whole-rock samples were crushed, sieved, washed, and dried, then passed through a Frantz magnetic separator. Samples collected as free phlogopite in the field received similar processing, except no magnetic separation was needed. For all samples, resulting material then underwent mild acid cleaning (HNO_3, HF), ultrasonic wash, drying, and a final hand-picking under binocular microscope. After irradiation, samples were heated incrementally and the extracted gas analyzed using a Mass Analyser Products model 215-50 rare-gas mass spectrometer. Laboratory dating standard is FCT-3 (biotite), which is assumed to have the same age as FCTs sanidine from the same rock, namely 28.03±0.18 Ma (Renne and others, 1994, cited here with 2σ error). Results (tables 3, 11) are shown as plateau and isochron ages (fig. 46). Locations are summarized in table 15.

An Age Too Old

A lava block (sample S10-L306) collected from a tuff breccia in the Eastern Chasm gave an age in excess of 1 Ma. Separate $^{40}Ar/^{39}Ar$ ages were obtained from a nepheline separate (1.68±0.04 Ma) and the glassy matrix (1.27±0.15 Ma) (fig. 47). The sampling site is labeled L306 in figure 19. We find it highly improbable that the upper part of the existing main cone has been intact for over 1 million years, so we discard the age.

[5](http://geochronology.coas.oregonstate.edu/).

(Appendix 6 begins page 62)

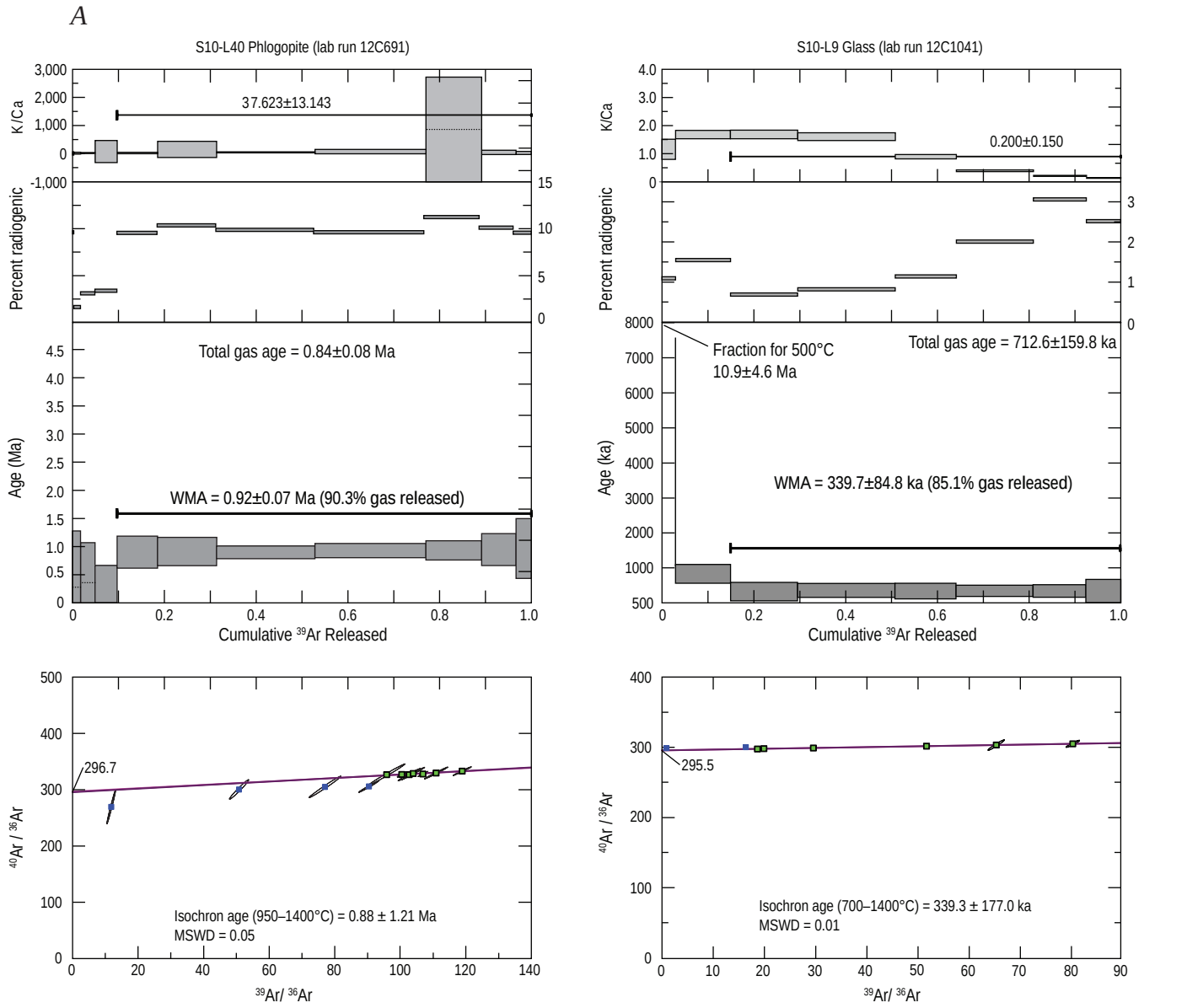

Figure 46. Argon plateau and isochron diagrams for dated samples in map area. John Huard, analyst. *A*, Samples from Loolmurwak crater and lava flow north of Lalarasi, which are part of the Natron-Engaruka volcanic field. Figures 46*B* and 46*C* on following pages.

Table 15. Sample locations for new ages on this map.

[Ages are plateau ages and 2σ error. If comparing, then double the 1σ error of previously published ages to get corresponding 2σ error. Altitude is orthometric altitude, meters above sea level, as determined by plotting handheld GPS location on topographic map and interpolating between contour lines, to nearest 10 m altitude]

Number in table 3 or 11	Sample No.	Age and 2σ error, Ma	Latitude, WGS84	Longitude, WGS84	Altitude, meters	Geographic locality
1 (table 3)	S10-L9	0.340±0.085	-2.7283	35.9829	820	Oremit, 1 mile north of Lalarasi
2 (table 3)	S10-L40	0.92±0.07	-2.7985	35.9798	1,020	Loolmurwak crater
1 (table 11)	S10-L103	0.338±0.023	-2.7718	35.9497	1,230	Phonolite lava, east flank Oldonyo Lengai
2 (table 11)	S10-L236B	0.353±0.065	-2.7579	35.9501	1,190	Tuff ring, east flank Oldonyo Lengai
3 (table 11)	S10-L136	0.460±0.075	-2.5507	35.8875	650	Block in debris avalanche, unit $Qoda_5$, north of Engare Sero village
4 (table 11)	S10-L65	0.793±0.063	-2.6373	35.9837	630	Block in debris avalanche, unit $Qoda_6$, near Gelai school

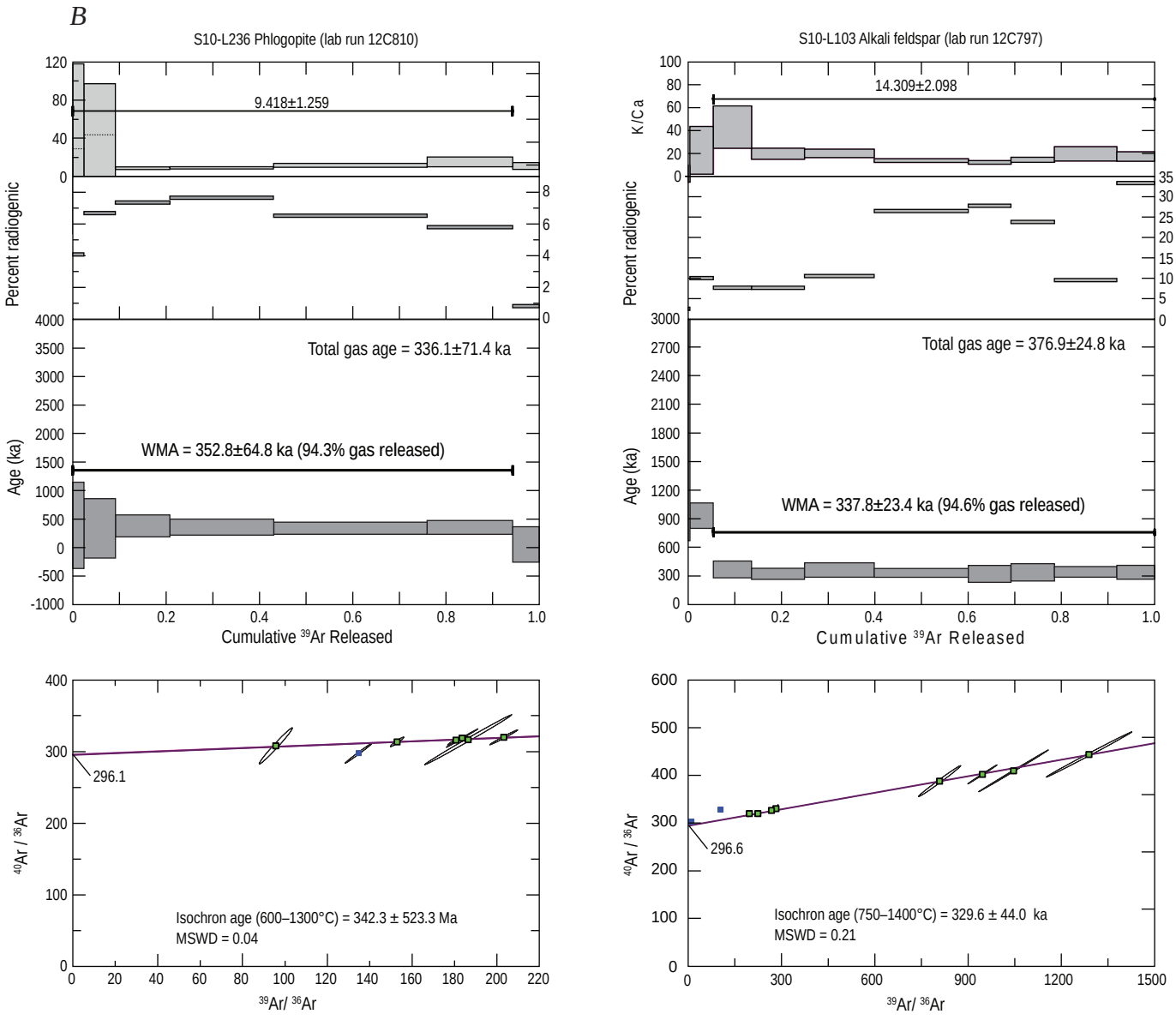

Figure 46—Continued. Argon plateau and isochron diagrams for dated samples in map area. *B*, Samples from east flank of Oldonyo Lengai, phonolite lava flow and Embalulu Oltatwa tuff ring, depicted on figure 19.

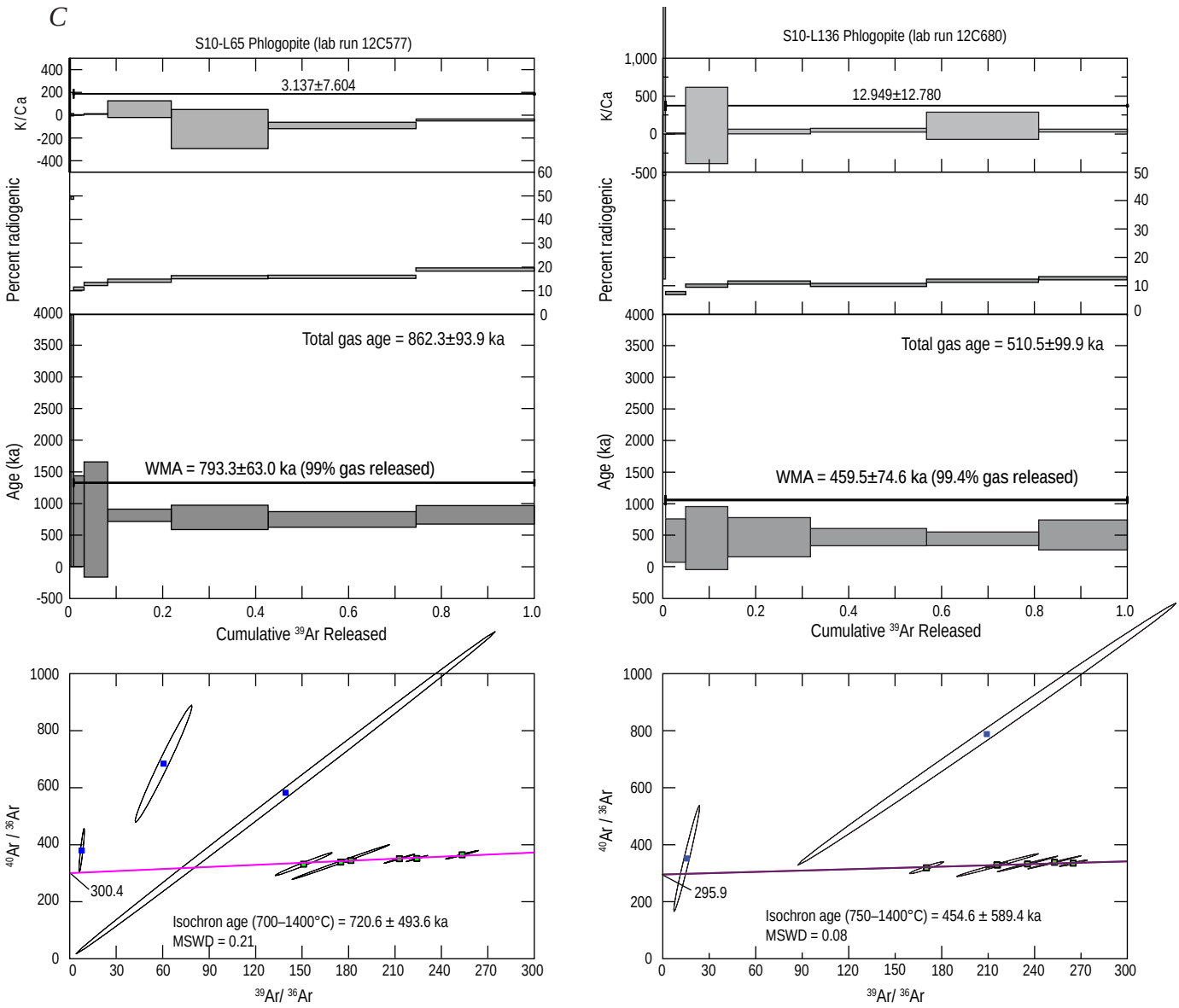

Figure 46—Continued. Argon plateau and isochron diagrams for dated samples in map area. *C*, Samples from debris-avalanche deposits.

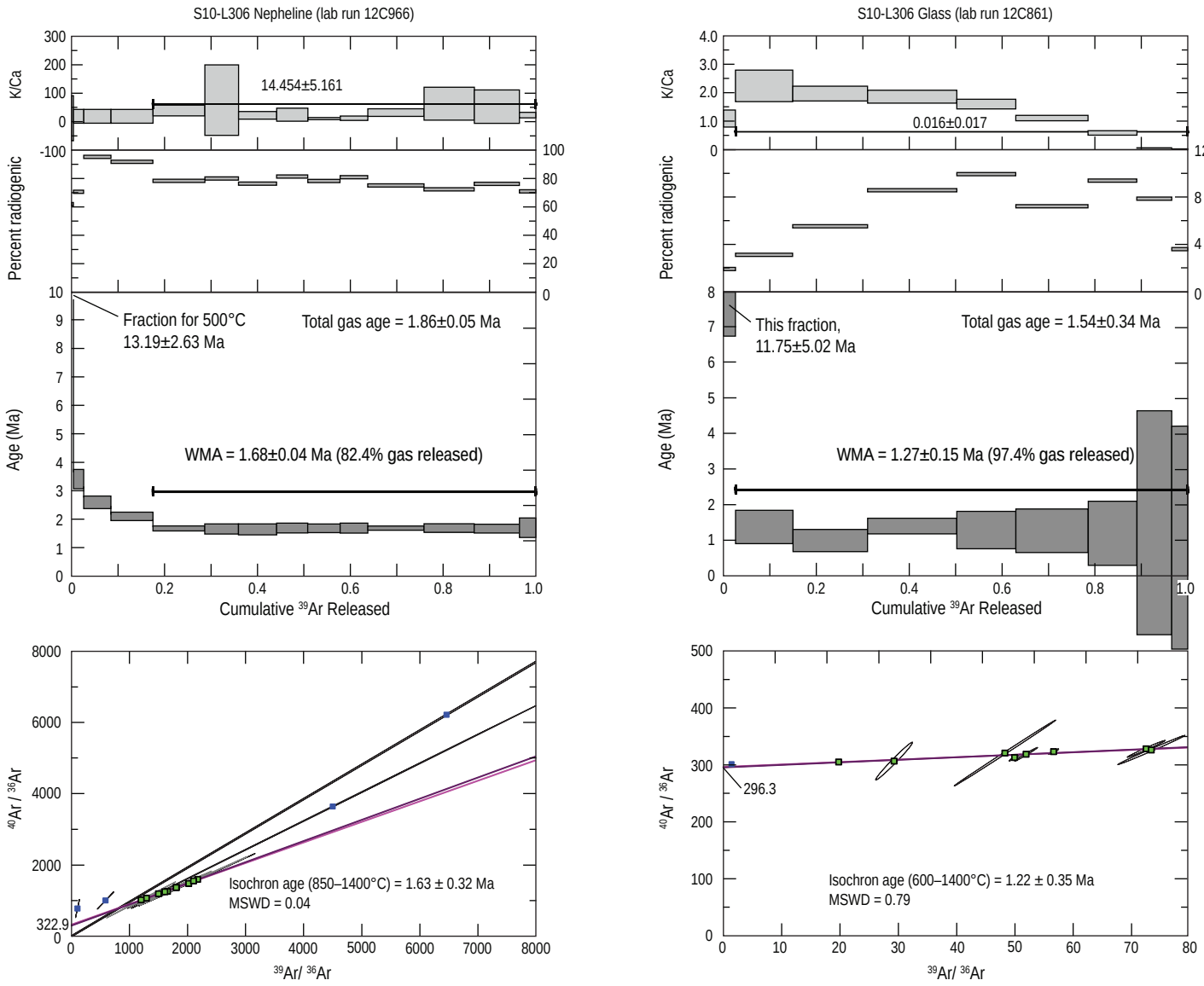

Figure 47. Argon plateau and isochron diagrams for glass and nepheline mineral separate from S10-L306, an age likely distorted by excess argon. Location, in Eastern Chasm of Oldonyo Lengai, is depicted in figure 19.

Appendix 6. Summit Volcanic Setting in March 2010

This appendix summarizes a trip report submitted to the Smithsonian Institution's Global Volcanism program in March 2010. Trip reports are used to compile monthly updates on active volcanoes of the world (Bulletin of the Global Volcanism Network, http://www.volcano.si.edu/reports/bulletin). The version herein has been shortened to avoid a repetition of discussions provided elsewhere in this map publication. Measurements of crater depth, diameter of crater rim and crater throat, and stratal dips or slope were made using compass, inclinometer, laser rangefinder, and handheld GPS receiver.

North Crater

Oldonyo Lengai's North Crater hosted a tephra cone when visited Friday, March 12, 2010. The cone's crater rim, approximately circular, ranged in diameter from 270 to 310 m (fig. 48). Crater depth was 110 to 122 m, two-thirds or more of which was the height of cliffs that rose directly from the crater floor to its throat, and the remainder the height of the sloping crater rim (fig. 49). If the crater had not deepened since June 2009, then a depth of 80 m reported by T. Fisher was an underestimate (Bulletin of Global Volcanism Network 34:08). From its rim, the crater mouth sloped inward 30°, descending at that pitch for 15–30 m before ending abruptly at the cliffs of the crater throat. Fine-grained pale gray or light-brownish gray ash, in part altered by weak solfataric steaming, mantled the upper slopes. A rockfall that occurred before April 2009 (A. Daneel's photos in Bulletin of Global Volcanism Network 34:05) had scalloped the northeast crater wall slope, leaving a shallow scar 70 m wide (figs. 50, 51). Outward-dipping beds of vent-building tephra, exposed by the scar, gave visual evidence that the overlying, mouth-coating ash was thin, only 30 cm or less in most places (fig. 51).

Figure 48. View north from summit of Oldonyo Lengai toward tephra cone built within North Crater. Top of Pearly Gates lava flow visible emerging from fog on west slope (left). Photo 8098, March 13, 2010.

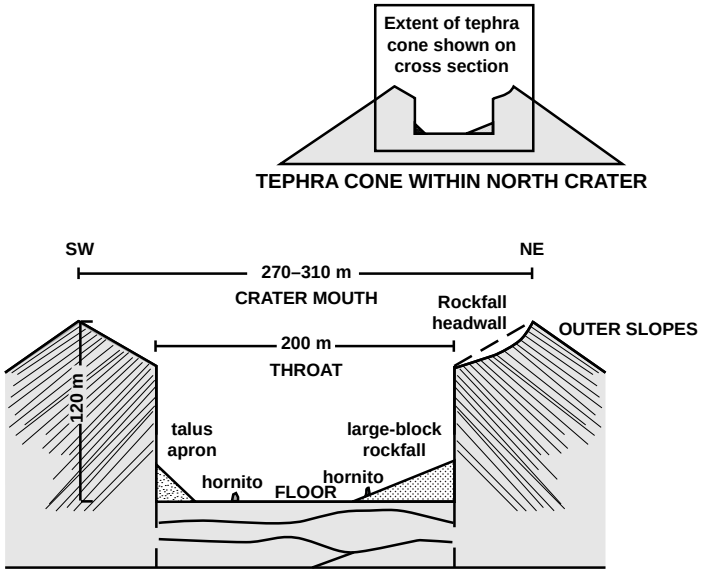

Figure 49. Cross section of tephra cone in North Crater of Oldonyo Lengai as observed on March 12, 2010.

The throat was about 200 m diameter. The crater floor had an area of 3.26 ha. It lay at an altitude slightly lower than the "Pearly Gates" traversed on the west-side climbers' route (fig. 52).

The setting of the crater floor on March 12 appeared largely or entirely unchanged from that appearing in photos taken one month earlier (February 2010); at that time, pāhoehoe covered nearly half of the crater floor. The smell of H_2S was weak, SO_2 smell was undetectable, and steam escaped from the few cracks that cut across the crater slopes. Neither steam nor fume were notable in the deeper part of the crater. Several volcanic and erosional events, listed next, were surmised from geologic relations on the crater floor, although none of the events is dated except by knowledge of their presence or absence during previously documented visitation. The recent lava flows and hornitos described below presumably are carbonatite, but none was sampled because they are inaccessible.

- (1) Globs of lava are spattered on the throat walls. The spatter and rock alteration obscure much of the layering of strata exposed in the cliff faces.
- (2) Rubble from wall collapses has formed talus cones that cover more than half the crater floor. The oldest of these talus deposits comprises large blocks from the rockfall that carved the east side of the crater slopes (pre-April 2009) (figs. 50, 51). This large-block rockfall has light brown ash on it, erupted from a 3–4-m wide pit blasted through the talus debris. Ash has also muted several smaller craters on the crater floor that appear in March and April 2009 photos (S. Lübben, posted on Fred Belton's website—http://oldoinyolengai.pbworks.com; and B. Wilhelmi, Bulletin of Global Volcanism Network 34:05). Nestled among the large-block talus field is a small hornito. It and the short pāhoehoe flows that issued from it are covered by the same brown ash that coats the talus. If the hornito is a product of June 2009 activity described and pictured in various reports, then the brown ash must postdate June 2009.

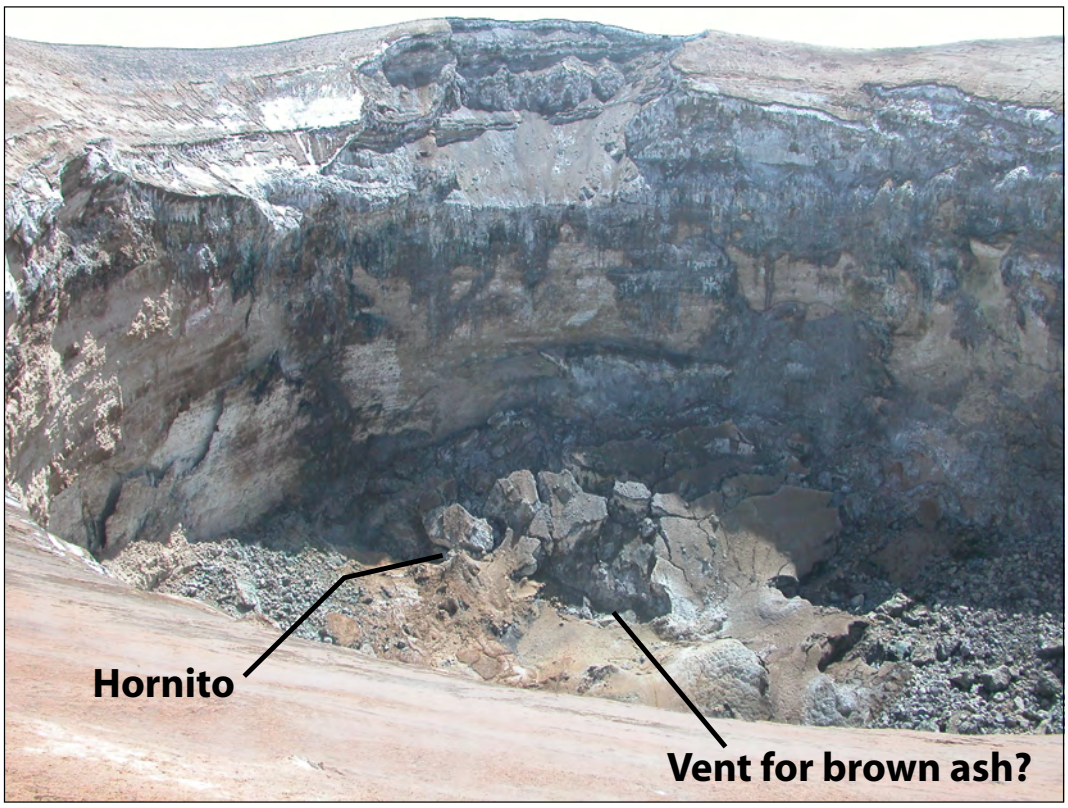

Figure 50. View northeast showing large-block rockfall on crater floor and resulting scar on northeast rim of tephra cone in North Crater. Photo 0002, March 13, 2010.

Figure 51. View north toward the rockfall scar on northeast rim. Photo 8022, March 12, 2010.

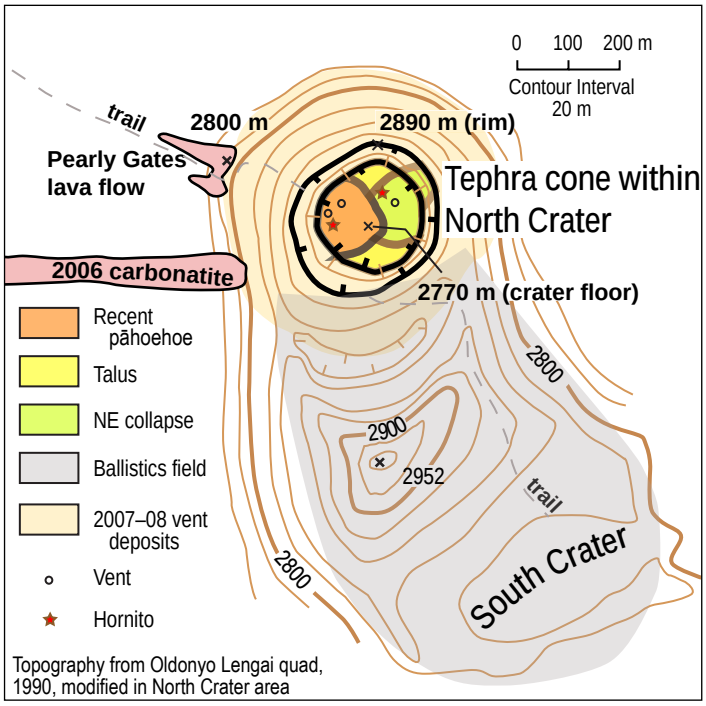

Figure 52. Map of summit area of Oldonyo Lengai as observed on March 12, 2010. Bold hachured lines show crater rim and boundary of crater floor for tephra cone within North Crater. Geographically, North Crater sweeps as far south as the volcano's summit, 2952 m, but the name is also commonly applied to the smaller crater within the tephra cone itself. North flank of tephra cone was at grade with volcano's north flank in March 2010.

- (3) Young gray pāhoehoe, lacking any ash cover, covers about 1.37 ha, or 40 percent of the crater floor (fig. 53). It issued from three vents near the north crater wall (scene essentially identical to that photographed by Frank Möckel in February 2010 (posted on Fred Belton's website and Bulletin of Global Volcanism Network 35:05). Within this field of pāhoehoe is the second of the two hornitos on the crater floor.

The faintest of noise could be heard from the area of the three vents in the North Crater. The sound was reminiscent of sloshing heard deep in pits on Kīlauea, although with more of a drumming percussion, like that of periodic gas release occurring every 3–10 seconds; but wind across the crater rim made it extremely difficult to resolve the crater sounds or their origin.

A nighttime visit to the rim from camp was made on March 13. At that time the crater and all vents within it were dark. No incandescence was seen.

South Crater

The South Crater, where we camped, is now dotted by ballistic craters, which presumably resulted from the eruptive events of 2007–08 (fig. 44). The shallow impact craters, as wide as 1.5 m diameter, chiefly or entirely postdate the ashfall that accompanied the 2007–08 eruptions, judging from crater preservation and the deformation of surface beds. Craters were sparse close to the vent, especially on steep slopes, so the distribution of ballistic craters may be an artifact of favorable summit slopes.

Figure 53. View northwest from the rim of tephra cone in Oldonyo Lengai's North Crater toward vent and young pāhoehoe on crater floor. Photo 8019, March 12, 2010.

Hazards

The chief hazard at the North Crater's tephra cone was crater rim stability during the quiescent conditions of March 2010. A faint footpath around the rim had been traced by the many visitors who wished to see as much of the crater floor as possible or who walked to the east rim on clear mornings for a better view of Mount Kilimanjaro, about 164 km east-southeast. It is unclear if rim-collapse hazard would diminish with time, as the rim materials become better cemented, or increase as ongoing alteration weakens otherwise stable rock. Those who walk the rim need to study adjacent slopes for traces of circumferential fractures and then judge where those fractures might transect the rim. The northeast rim seemed especially unstable in March 2010.

We detected no perceptible gas hazard during our visit. The summit area is well ventilated, and the smell of sulfide gas was weak. No CO_2 was indicated by a handheld field device[6] inserted into low-temperature steaming cracks at the summit. Null values were also obtained when placing the CO_2 monitor into shallow pits in the south crater where soil gas might percolate, but the holes were so shallow (<60 cm) that summit breezes probably prevent gas accumulation under nearly all conditions. Under March 2010 conditions, concentration of ground CO_2 was unlikely to pose a hazard for those in closed areas (tents?), given the wind across the summit area. The North Crater's cliff-lined walls precluded access to the only obvious topographic trap for CO_2.

[6]The device, Analox Corp.'s CO_2 Buddy, is specifically for personal protection and has default alarms at 0.5, 1.5, and 4 percent CO_2. The manufacturer specifies that it will read down to 0.01 percent, but low concentrations are not reported reliably and ambient concentrations typically read 0 percent.